POLITECNICO
MILANO 1863

SCUOLA DI INGEGNERIA INDUSTRIALE
E DELL'INFORMAZIONE

EXECUTIVE SUMMARY OF THE THESIS

Modelling of frequency control in hydroelectric power plants

TESI MAGISTRALE IN ELECTRICAL ENGINEERING – INGEGNERIA ELETTRICA

AUTHOR: ALESSIA SAGRIPANTI

ADVISOR: ALBERTO BERIZZI

ACADEMIC YEAR: 2021-2022

1. Introduction

The aim of the thesis is the realization of frequency regulation models for hydroelectric power plant participating to the thesis group project of Nuclear Section of DENG on modelling in Dymola, a software based on Modelica language. Dymola allows a multi-engineering approach and so is ideal to realize interconnected energy models; hence, it is possible to add other power plants to the frequency regulation models realized.
The hydroelectric adduction system is examined in linear and nonlinear models starting from the simple ideal case of inelastic penstock to more complex hypothesis: the presence of surge tank effect and the propagation of pressure waves.
The speed governor has been tuned through stability analysis in islanding operation, and frequency control with variation of electrical power has been realized.
The case study for all the models is the Susqueda power plant-reported in Table 4.

2. Linear model adduction system

The inelastic conduit of the penstock is identified by the water starting time T_w:

$$T_w \triangleq \frac{L}{gA_c}\frac{Q_0}{H_0} \quad (1)$$

The adduction transfer function $G_a(s)$ is the relation between mechanical power $\bar{P}_m$ and opening of gate $\bar{A}$. $G_a(s)$ in case of ideal and inelastic penstock is:

$$G_a(s) = \frac{\Delta\bar{P}_m}{\Delta\bar{A}} = \frac{1 - T_w s}{1 + \frac{1}{2}T_w s} \quad (2)$$

The time response of $\Delta\bar{P}_m$(Figure 1) for a step of 0.01 p.u. of $\Delta\bar{A}$ shows a negative behaviour due to the inertia of the water: when the valve is opened the water cannot instantaneously change the flow for its weight, and the pressure across the turbine is reduced so the mechanical power produced is lower.

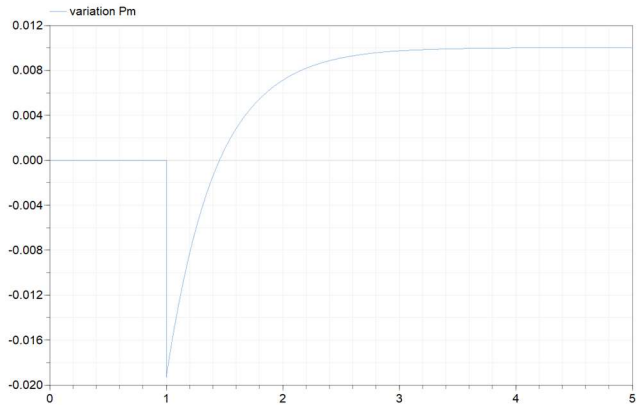

Figure 1- Mechanical power[p.u.] in time[s] case with inelastic penstock

The hydraulic response is shown in Figure 2: the volumetric flow $\bar{Q}$, unlike the mechanical power, has the same variation of valve section $\bar{A}$; the variation of the available head $\bar{H}$ is not relevant for the final steady state value of mechanical power, since its total variation is null.

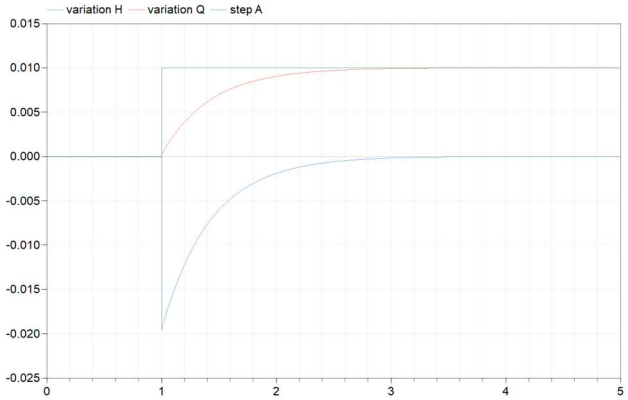

Figure 2 -Variation of hydraulic response[p.u.] in time[s]

For very long penstocks, the wave travel time of the water column becomes significant, and subsequentlty the dynamic should not rely only on T_w, but also the elastic time T_{ep}:

$$T_{ep} = \frac{L}{c} \tag{3}$$

The normalized impedance of the penstock Z_p is defined as:

$$Z_p = \frac{c}{gA_c} = \frac{T_w}{T_{ep}} \tag{4}$$

The transfer function $G_a(s)$ for ideal turbine considering the propagation of elastic waves becomes:

$$G_a(s) = \frac{\Delta\bar{P}_m}{\Delta\bar{A}} = \frac{1 - Z_p \tanh(sT_{ep})}{1 + \frac{1}{2} Z_p \tanh(sT_{ep})} \tag{5}$$

The hyperbolic tangent is represented by the distributed parameter theory as:

$$\tanh(T_{ep}s) = \frac{1 - e^{-2T_{ep}s}}{1 + e^{-2T_{ep}s}} = \frac{sT_{ep}\prod_{n=1}^{\infty}\left[1 + \left(\frac{sT_{ep}}{n\pi}\right)^2\right]}{\prod_{n=1}^{\infty}\left[1 + \left(\frac{2sT_{ep}}{(2n+1)\pi}\right)^2\right]} \tag{6}$$

The hyperbolic tangent can be approximated for power system with lumped parameter $n = 1$, which preserves the fundamental harmonic of water column.

The time response of the variation of the mechanical power $\Delta\bar{P}_m$ (Figure 3) has oscillations in the transient phase due to propagation of elastic waves.

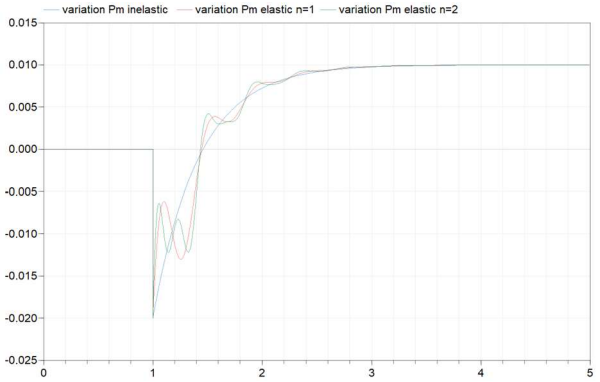

Figure 3-Mechanical power[p.u.] in time[s] with elastic penstock

The parameters of the circuit reserve-surge tank are:

- The water starting time of the tunnel T_{wc}

$$T_{wc} = \frac{L_t}{A_t g}\frac{Q_0}{H_0} T_{ec} \tag{7}$$

- The surge tank storage constant C_s

$$C_s = \frac{A_S}{Q_0} H_0 \tag{8}$$

In the first seconds, the time response of $\Delta\bar{P}_m$ is the same of the case without surge tank effect. In the long term there are oscillations (Figure 4) because the water level in the surge tank begins to oscillate following a change in the turbine flow with the natural period T_S:

$$T_S = 2\,\pi\sqrt{T_{wc}C_s} \tag{9}$$

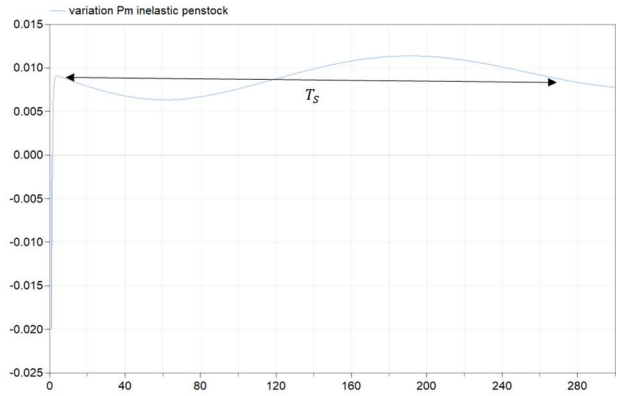

Figure 4-Mechanical power oscillations[p.u.] in time[s]

3. Nonlinear model of adduction

The linear model is useful for its simplicity to obtain insights into the basic characteristics of hydraulic system, and it is acceptable to represent small signal performance, but inadequate for studies of large variation in frequency and power output, hence a nonlinear model is necessary.
The following parameters are introduced:

- Turbine gain A_t is the relation between the real and the ideal gate

$$A_t = \frac{1}{\bar{g}_{FL} - \bar{g}_{NL}} \quad (10)$$

The ideal gain G is based on having 1 p.u. as change from no load to full load, while the real gate opening g is based on having 1 p.u. as change from the fully closed ($\bar{g}_{NL}$) to the fully open position ($\bar{g}_{FL}$)

- Losses due to no load speed $\bar{U}_{NL}$, defined as

$$\bar{U}_{NL} = A_t \bar{g}_{NL} (\bar{H}_0)^{\frac{1}{2}} \quad (11)$$

In the present study, the nonlinear models of IEEE have been realized. Figure 5 shows the nonlinear model with only the dynamics of the penstock.

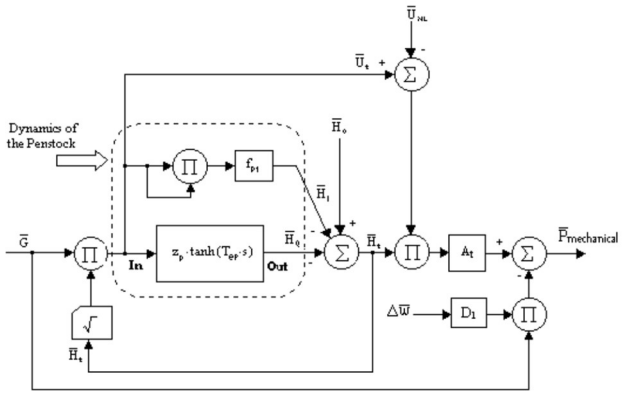

Figure 5-Nonlinear model of IEEE only penstock dynamic

The value of hyperbolic tangent has been approximated with lumped parameter in the three cases of n=0,1,2.
The time response of mechanical power $\bar{P}_m$ (Figure 6) has been studied having as input a step variation of the gate from 0.5 to 0.51 p.u. at time 1 s.

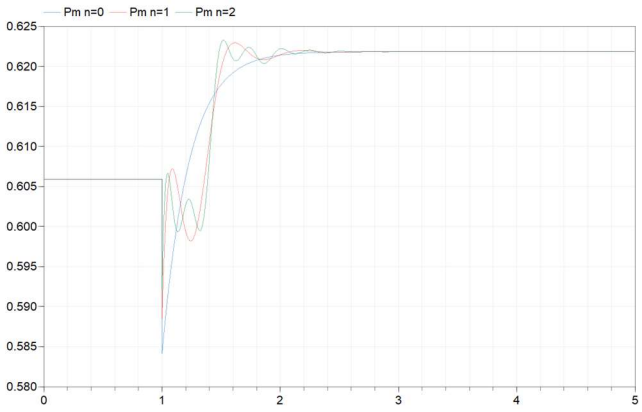

Figure 6-Mechanical power[p.u.] in time[s] nonlinear model without surge tank effect

It is important to initialize the transfer functions for the initial steady states. The expression of the speed in turbine at steady state U_{tss} is:

$$U_{tss} = \sqrt{\frac{1}{\frac{1}{\bar{g}^2} + f_{p1}}} \quad (12)$$

For the case study the values of steady state speed of water flow in turbine $\bar{U}_{tss}$, head in turbine $\bar{H}_{tss}$ and mechanical power $\bar{P}_{mec}$ are reported in Table 1.

Table 1-Values of steady state model without surge tank effect

$\bar{g}$[p.u.]	$\bar{U}_{tss}$[p.u.]	$\bar{H}_{tss}$[p.u.]	$\bar{P}_{mec}$[p.u.]
0.5	0.4971	0.9883	0.6058
0.51	0.5069	0.9878	0.6217

Figure 7 is the IEEE nonlinear model that deals with penstock, surge tank, tunnel dynamics, and losses.

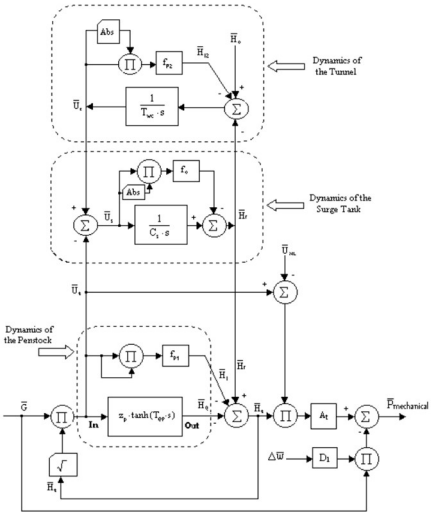

Figure 7-Nonlinear model of IEEE with surge tank effect

The equations of steady state value of the head at the risers of surge tank $\bar{H}_{rss}$, the speed of water flow in turbine $\bar{U}_{tss}$ and the respective head $\bar{H}_{tss}$ are:

$$\bar{H}_{rss} = \frac{\phi_p + \frac{1}{\bar{g}^2}}{\phi_c + \phi_p + \frac{1}{\bar{g}^2}} \qquad (13)$$

$$\bar{U}_{tss} = \sqrt{\frac{\bar{g}^2}{1 + \bar{g}^2(\phi_p + \phi_c)}}$$

$$\bar{H}_{tss} = \frac{\bar{U}_{tss}^2}{\bar{g}^2}$$

For the case study the steady state values are reported in Table 2.

Table 2-Values of steady state model without surge tank effect

$\bar{g}[p.u.]$	$\bar{U}_{tss}[p.u.]$	$\bar{H}_{tss}$[p.u.]	$\bar{H}_{rss}$[p.u.]
0.5	0.4970	0.9880	0.9998
0.51	0.5068	0.9875	0.9997

The mechanical power $\bar{P}_m$ in the first instants is equal to the model without surge tank effect, but in long term Figure 8 shows oscillations of $\bar{P}_m$ around the steady state value of 0.6217 p.u..

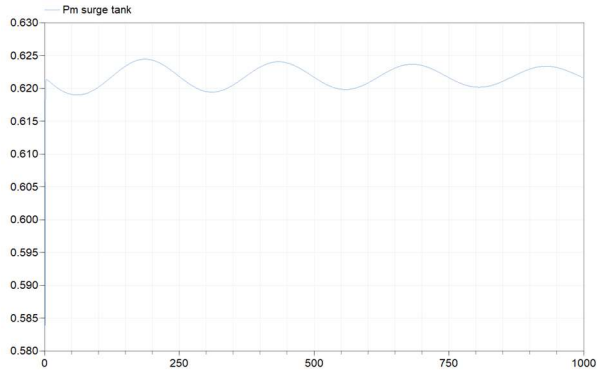

Figure 8-Mechanical power oscillations[p.u.] in time[s]

Indeed, the water mass oscillates inside the surge tank as shown by the time response of head riser of the surge tank $\bar{H}_r$ (Figure 9).

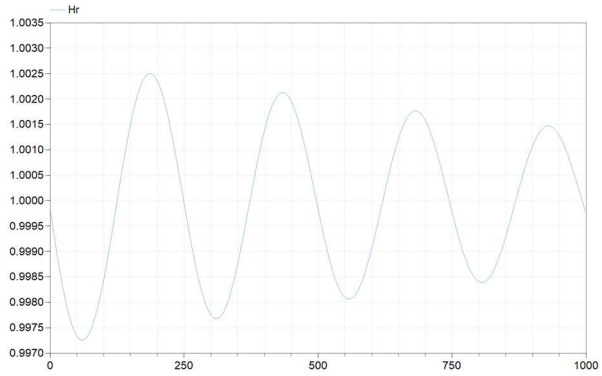

Figure 9-Head riser of surge tank oscillations [p.u.] in time[s]

4. Tuning PID speed governor

The stability analysis for the power plant in islanding (scheme in Figure 10) with inelastic penstock has been realized to choose the PID speed governor, with only proportional effect equal to the reverse of permanent droop.

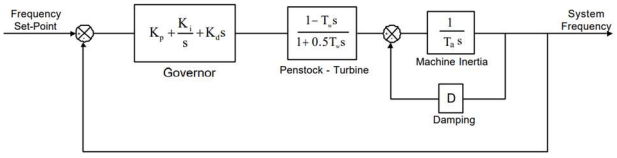

Figure 10-Frequency loop in islanding

The permanent droops and their respective poles are reported in Figure 11 and Table 3 for the cases: undamped, critically damped, unstable and underdamped.

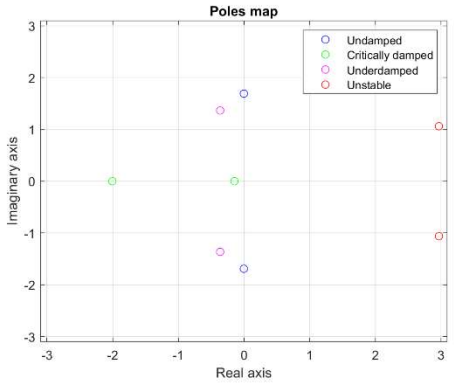

Figure 11-Poles map

Table 3-Permanent droops and poles

Cases:	$b_p[p.u./p.u.]$	Poles
Undamped	0.1395	[1.6896i , -1.6896i]
Critically damped	1.3809	[-2.0042, -0.1439]

Underdamped	0.2000	[-0.3614 + 1.3640i ,-0.3614 - 1.3640i]
Unstable	0.0400	[2.9719 + 1.0601i, 2.9719 - 1.0601i]

5. Frequency control

The effects of water starting time T_w and mechanical starting time T_a in regulation have been studied:

- Increasing T_w, the delayed flow has more effects on hydraulic turbine and enhances the oscillations of the mechanical power and of the frequency of the system;
- Increasing T_a, the mechanical power and the frequency of the system reduce deviation, but the time to reach the steady state increases.

The frequency control after a variation of power load, represented in Figure 12, has been analyzed.

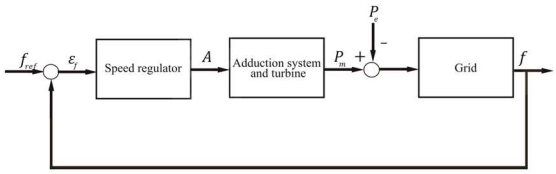

Figure 12-Control loop for frequency regulation

The transfer function representing the grid is:

$$G_{grid} = \frac{1}{sT_a + D} \quad (13)$$

The load damping coefficient D is assumed null and T_a has as reference the Italian grid in the blackout of 2003 (Table 5).

This analysis has considered only the proportional effect of the PID speed governor. The transfer function of speed regulator $G_r(s)$ is a gain with value equal to the reverse of the permanent droop $b_p$of 0.20 p.u. as the underdamped case in islanding (Table 3).

The frequency variation f and mechanical power $\bar{P}_{mec}$ have been analyzed adding gradually more complex dynamics of the adduction system.

The power load variation $\bar{P}_e$ is a step from 0 to 0.01 p.u. at time 1 s; the time response of the frequency (Figure 13) has been studied for cases: negligible adduction system with $G_a(s)$ as unit function, penstock inelastic, penstock elatic with grade n=1 and n=2. f decreases until the minimum value of 49.90 Hz (0.998 p.u.)-as expected from the chosen droop:

$$b_p = \frac{\Delta\bar{f}}{\Delta\bar{P}} \rightarrow \Delta\bar{f} = b_p \cdot \Delta\bar{P} = 2 \cdot 10^{-3}\,\text{p.u.} \quad (14)$$
$$\bar{f} = 1\,\text{p.u.} - \Delta\bar{f} = 0.998\,\text{p.u.}$$

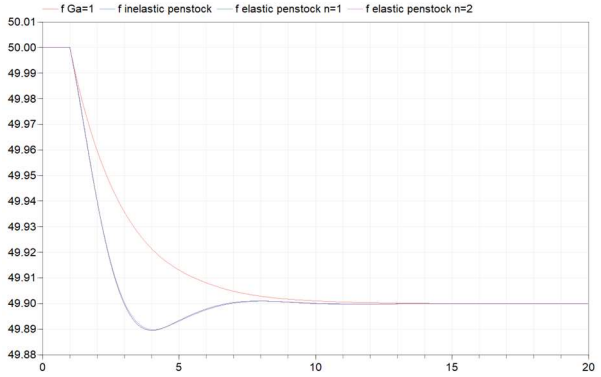

Figure 13-Frequency variation[Hz] in time [s]

In case of surge tank, frequency oscillates in the long term as shown by Figure 14.

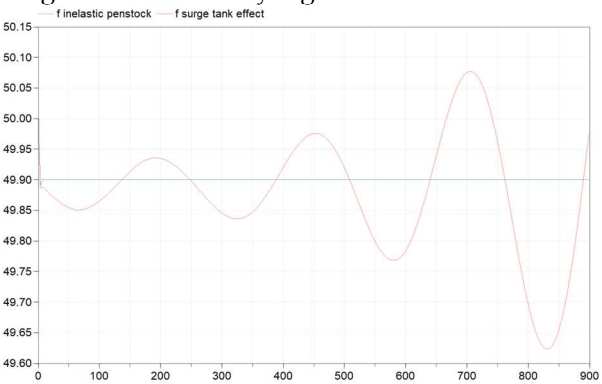

Figure 14-Frequency[Hz] in time[s] with surge tank effect

For nonlinear models, the frequency has similar behavior, but the steady state value is not 49.90 Hz but 49.937 Hz, hence nonlinearity does not satisfy the value expected for the frequency from droop computation (14).

The frequency regulation of the hydroelectric powerplant has been studied also in presence of baseload nuclear power in the grid.

The nuclear power is realized by IRIS (Figure 15), a SMR reactor able to produce 335 MW of electrical power.

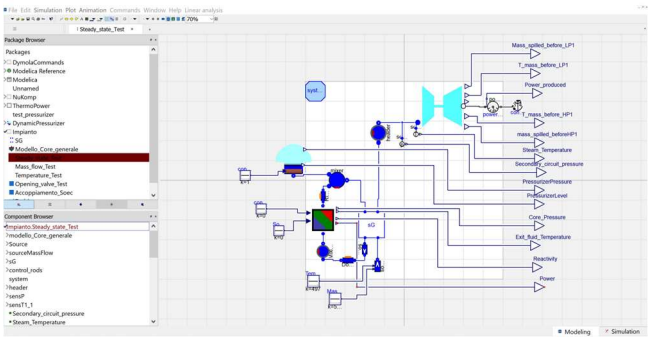

Figure 15-Dymola model of IRIS

The frequency regulation has been studied for 1 MW variation of power load in the grid at time 300 s. The mechanical power $\bar{P}_{mec}$ (Figure 16) oscillates before and after the disturbance for the surge tank effect, and after 300 s increases its value from 0.6058 p.u. to 0.6175 p.u.- equivalent to 52.5 MW. The frequency of the grid (Figure 17) is oscillating around 50 Hz before the disturbance, then decreases and oscillates around 49.925 Hz.

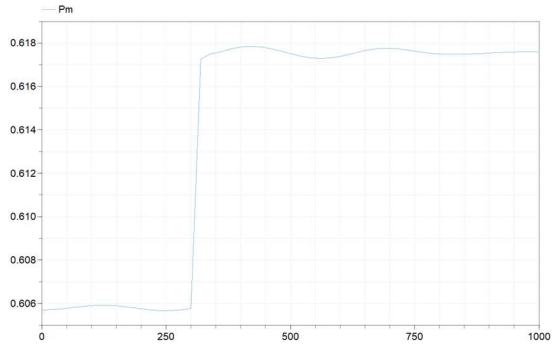

Figure 16-Mechanical power[p.u.] in time[s] of hydro unit

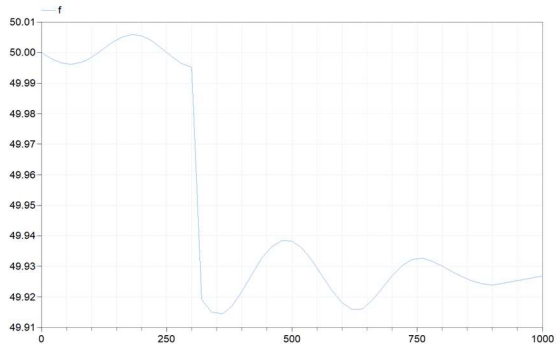

Figure 17-Frequency of the grid[Hz] in time[s]

6. Conclusions

The Dymola models of the hydroelectric power plant in frequency regulation have been realized taking singularly the dynamics of adduction system, speed regulator and grid, and are all consistent with a progressive increase of accuracy.

Some suggestions to increase the accuracy of regulation models are: the adoption of a speed regulator with transient droop, the addition of frequency dependency of the load and of secondary regulation.

7. Bibliography

[1] Ó. D. Quiroga, «Modelling and nonlinear control of voltage frequency of hydroelectric power plants,» 2000.

[2] Kundur, Power System Stability and Control, McGraw-Hill Education, 1994.

[3] R. Marconato, Electric power systems vol.2 Steady-state behaviour controls, short circuits and protection systems, CEI, 2004.

[4] P. Croce, «Master degree thesis "Preliminary simulations for nuclear power plant cogeneration",» 2020-2021.

[5] M. Giangi, «Master thesis "Dynamic Modelling of Virtual and Real Inertia Systems in Green Microgrids",» 2021.

Table 4-Susqueda power plant

	Parameter	Value
Penstock	Length $[L]$	250 m
	Initial diameter $[d_{ic}]$	4.3 m
	Final diameter $[d_{fc}]$	3.3 m
	Average section $[A_c]$	11.34 m^2
	Pressure wave velocity $[c]$	1200 m/s
	Friction coefficient $[\phi_p]$	0.0475
Tunnel	Diameter $[d_t]$	4.3 m
	Section $[A_t]$	14.52 m^2
	Length $[L_t]$	3500 m
	Friction coefficient $[\phi_c]$	0.0010112
Surge tank	Diameter $[d_s]$	9 m
	Section $[A_s]$	63.61 m^2
	Length $[L_s]$	100 m
Turbine	Rated mechanical power $[P_m]$	86 MW
	Rated discharge $[Q_0]$	65 m^3/s
	Total head $[H_0]$	174.41 m

Table 5-Grid block

	Parameter	Value
Grid	Mechanical starting time $[T_a]$	9.72 s

Politecnico di Milano

SCHOOL OF INDUSTRIAL AND INFORMATION ENGINEERING

Master of Science – Electrical Engineering

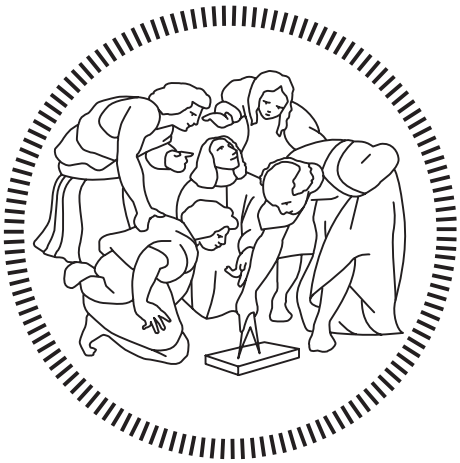

Modelling of frequency control in hydroelectric power plants

Supervisor

Prof. Alberto Berizzi

Co-Supervisor

Prof. Stefano Lorenzi

PhD. Stud. Andrea Vicario

Candidate

Alessia Sagripanti – 1752480

Academic Year 2021 – 2022

List of contents

Abstract

The aim of the thesis is the realization of frequency regulation models for hydroelectric power plant participating to thesis group project of Nuclear Section of DENG on modelling in Dymola, a software based on Modelica language. Dymola allows a multi-engineering approach and so is ideal to realize interconnected energy models; hence, it is possible to add other power plants to the frequency regulation models realized.

The identification of all Dymola models has been performed for Susqueda power plant, hydroelectric generating unit of Endesa Group in Spain.

The models have been realized starting from the simplest case, and then more complex dynamics have been considered. The adduction system was, at first, ideally approximated with only penstock, then, model by model, the effects of surge tank, friction, propagation of elastic waves and nonlinearity were added.

The first chapter deals on the theory of frequency regulation and explains the control loop scheme that has been used in the models. The second and third chapter discuss the theoretical background of, respectively, linear and nonlinear model of the hydroelectric adduction system. Chapter four explains speed regulators and their role in frequency regulation, along with how to realize a stability analysis for hydroelectric power plant in islanding operation.

Dymola software is briefly analyzed in chapter five. Each one of adduction system models is examined in chapter six, through the analysis of time response of the mechanical power after variation of gate in turbine.

The last chapter combines the models of frequency regulation and adduction system of hydroelectric powerplant; furthermore, the model of frequency regulation has been connected with the Dymola model of nuclear power plant. It presents the results for stability analysis of the case study, and analyzes the results of frequency regulation of hydro unit after power load variation through the time response of mechanical power and frequency of the grid.

Estratto

Lo scopo della tesi è quello di realizzare modelli di regolazione di frequenza di un impianto idroelettrico partecipando ad un progetto di tesi del dipartimento nucleare DENG di modellizzazione su Dymola, software con linguaggio Modelica. Dymola permette di avere un approccio multi-ingegneristico e quindi ben si presta a realizzare modelli energetici interconnettibili tra di loro; è dunque possibile aggiungere altri impianti di generazione ai modelli di regolazione di frequenza realizzati.

Nel compimento di tutti i modelli è stato preso in considerazione l'impianto idroelettrico Susqueda in Spagna appartenente al Gruppo Endesa.

I modelli sono stati realizzati partendo da prime semplificazioni, per poi tener conto di dinamiche più complesse. Il sistema di adduzione, infatti, è stato prima semplificato idealmente con solo la condotta forzata, per poi aggiungere di modello in modello l'effetto del pozzo piezometrico, di attriti, di propagazione di onde elastiche e non linearità.

Nel primo capitolo è esposta la teoria alla base della regolazione di frequenza, ed è spiegato lo schema di regolazione successivamente realizzato nei modelli. Il secondo e terzo capitolo trattano la teoria alla base dei modelli, rispettivamente, lineare e non lineare del sistema di adduzione dell'impianto idroelettrico. Mentre nel quarto capitolo vengono trattati i regolatori di velocità e il loro ruolo in regolazione, insieme alla realizzazione di un'analisi di stabilità per un impianto idroelettrico in modalità islanding.

L'ambiente di Dymola è sintetizzato nel quinto capitolo. I risultati dei modelli di adduzione vengono analizzati separatamente nel capitolo sei, con l'analisi delle risposte in potenza meccanica nel tempo a seguito di variazioni alla valvola in turbina.

Nell'ultimo capitolo si fondono i modelli di regolazione e dei sistemi di adduzione dell'impianto idroelettrico, inoltre è mostrato un modello combinato di regolazione dell'idroelettrico con un impianto nucleare in rete. Sono esposti i risultati dell'analisi di stabilità svolta sul case study e i risultati della regolazione dell'impianto idroelettrico a seguito di una variazione di potenza dei carichi tramite l'analisi della risposta nel tempo di potenza meccanica e frequenza di rete.

List of Figures

List of Tables

Chapter 1
Frequency control

This first chapter recalls some bases on frequency control and its importance. The main approach proposed in this thesis work, which is the frequency loop control of a single generating unit, will be presented and discusses in later paragraphs.

1.1 Fundamentals of frequency control

The frequency regulation consists in limiting the frequency oscillations of the grid to the nominal value, which for Italian grid is 50 Hz.

The frequency value is continuously perturbed by load disconnection and connection throughout the day, variations of power absorption and tripping of generators due to faults: hence the power system industry implemented three hierarchical levels of frequency regulation schemes. [1]

In reality, the electrical system is “elastic”: there are electromechanical transients between the rotors, hence the electrical speed of the rotating groups is not unique. The electrical grid is assumed to be “rigid”: the period of electromechanical transients is considered fast enough compared to the time of frequency regulation. Therefore, the machines are deemed to move in synchronous to a frequency, named “the frequency of the system”. [2]

The problem of frequency control is traduced in problem of speed control of turbine-alternator; indeed, the mechanical rotational speed ω_m corresponds to frequency:

$$f = \frac{\omega_m p}{2\pi} \tag{1.1}$$

With p number of pole pairs.

The fundamental equation in power system stability analysis is the Swing equation: the effect of imbalance between the electrical and mechanical torques of the machines results in a variation of the mechanical speed of the rotor.

$$J\frac{d\omega_m}{dt} = T_m - T_e \tag{1.2}$$

Where:

- J is the combined moment of inertia of generator and turbine $[kg \cdot m^2]$, it depends on rotor structure and material;
- ω_m is the mechanical rotational speed $[\frac{rad}{s}]$ and it is the derivative of mechanical angle $\theta_m[rad]$, $\omega_m = \frac{d\theta_m}{dt}$;
- T_m is the mechanical torque given by the turbine to the electrical machine $[N \cdot m]$;
- T_e is the electrical torque generated by machine $[N \cdot m]$.

$T_m - T_e$ is the accelerating torque:

- $T_m > T_e$ determines a positive accelerating torque, resulting in an increase of rotor speed and electrical frequency;
- $T_m < T_e$ determines a negative accelerating torque, resulting in a decrease of rotor speed and electrical frequency;
- $T_m = T_e$ determines a null accelerating torque, and the electrical frequency and rotor speed result constant.

Equation (1.2) is more useful expressed in terms of power:

$$J\omega_m\frac{d\omega_m}{dt} = P_m - P_e \tag{1.3}$$

Where:

- P_m is the mechanical power in input to the shaft [W];
- P_e is the electrical power output generated by the machine [W].

It is possible to introduce the mechanical starting time T_a, which is the time required for the rated torque to accelerate the rotor from null speed to rated speed $\omega_{m,n}$. The mechanical starting time is function of nominal power of generator S_n, inertia J and the type of prime mover:

$$T_a \triangleq \frac{J\omega_{m,n}^2}{S_n} \tag{1.4}$$

As consequence, the factor M can be defined as:

$$M \triangleq \frac{T_a S_n}{\omega_{m,n}} \tag{1.5}$$

1.2 Frequency regulation

The Italian grid is a synchronous area of continental Europe that is part of European Network of Transmission System operator (ENTSO-E).

The ENTSO-E has established three hierarchical levels: primary, secondary, and tertiary regulation. It has also provided Time control with the aim of correcting the average value of frequency in the long term. [3]

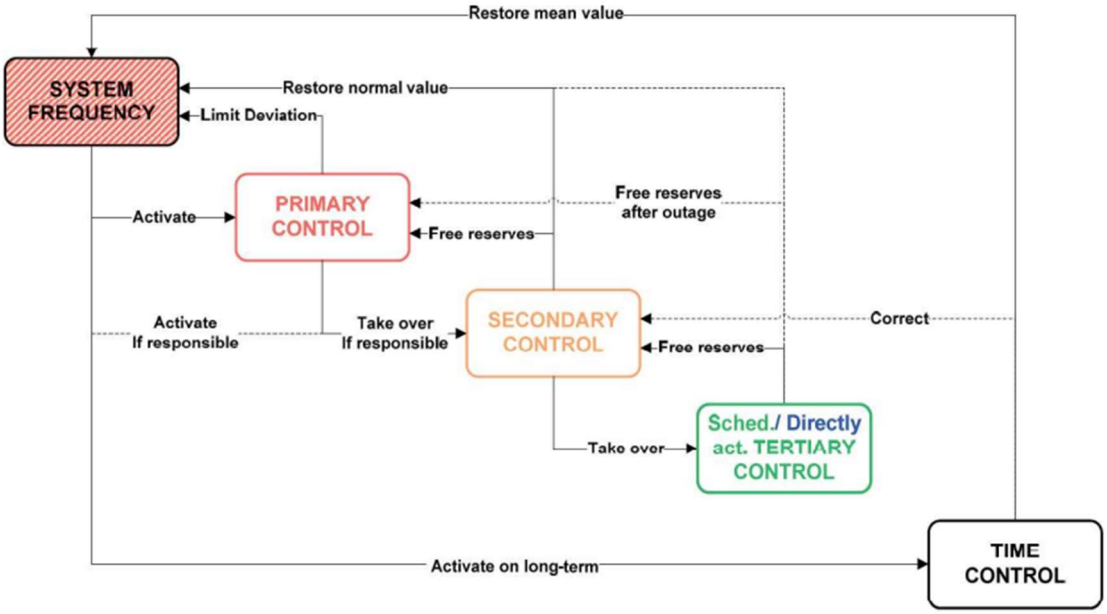

Figure 1-1 Operations of ENTSO-E for frequency (entsoe.eu/)

1.2.1 Primary regulation

The frequency is not immediately restored at the nominal value in the new permanent regime: the speed regulators asses the frequency to a value near the nominal one, because the need is to restore the balance of electrical and mechanical power.

This first part of control, called primary regulation, occurs in $0 \div 30$ seconds and the goals are:

- Establish the equilibrium between absorbed power and the generated one;
- Limit the value of frequency overshooting;

- Arrive to the new value of frequency with strongly damped transient oscillations;
- Allow the various synchronous generators to cover the increase of load by sharing it among themselves.

Of course, the new steady-state value for frequency should not be so low as to cause damage in final users, turbines, and electrical machines.

The primary regulation is realized by local speed governors, which must act very quickly. The generators participating to the primary regulation are large synchronous generators that constitute the primary reserve-also called the "spinning reserve".

The permanent regulating droop-or statism of generation unit- is defined as the relation of variation of frequency (maximum frequency f_{max} and nominal f_n) and power (nominal power P_n and minimum P_{min}):

$$b_p = \frac{\frac{f_{max} - f_n}{f_n}}{\frac{P_n - P_{min}}{P_n}} \tag{1.6}$$

The droop $b_p[\text{p.u.}/\text{p.u.}]$ is a value in the range between 2% and 7%.

Another important parameter to introduce is the permanent regulating energy $E_p[\frac{MW}{Hz}]$ that is correlated to the droop:

$$E_p = \frac{1}{b_p}\frac{P_n}{f_n} \tag{1.7}$$

E_p represents the variation of power due to a frequency variation of 1 Hz.

The static characteristic of speed regulator, illustrated in Figure 1-2, shows how the frequency-and so speed- varies in function of the mechanical power that the machine supplies. [4]

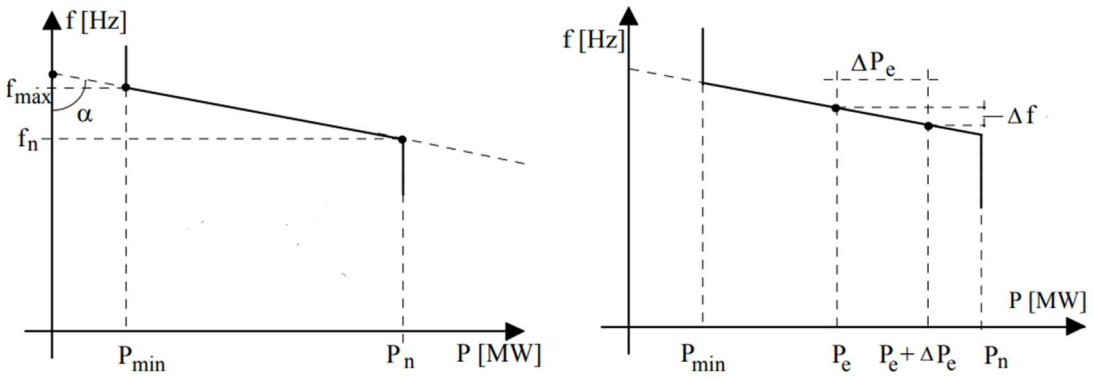

Figure 1-2 The static characteristic of speed regulator [4]

The slope of frequency is negative because to a variation of power required by the load ΔP_e there is a variation of frequency. The expression of frequency variation Δf is:

$$\Delta f = -b_p \frac{f_n}{P_n} \Delta P_e \tag{1.8}$$

1.2.2 Secondary regulation

The secondary regulation is done by the system regulator, placed in the Central Dispatching Centre, that sends a level signal to speed regulators of secondary reserve to adjust the power generation.

The Figure 1-3 shows how the increase of load ΔP_e determines a decrease of frequency, which is equal to f_1 at the end of primary regulation frequency. Via the level signal Y_e the secondary regulation allows the translation of the static characteristic of the frequency to the nominal value f_n.

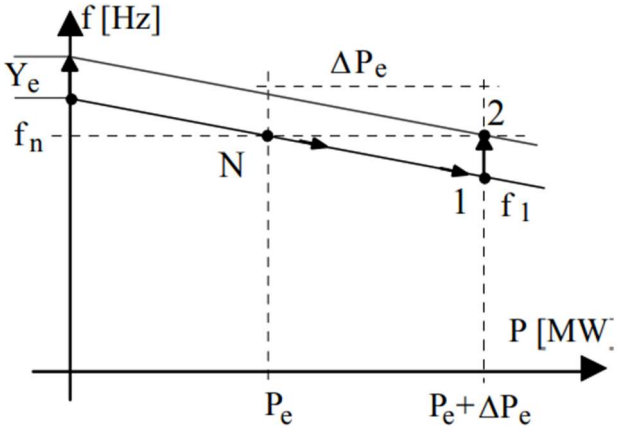

Figure 1-3 Secondary regulation

In comparison with the primary regulation, it is worth noting that the secondary regulation is a frequency regulation and is slower, centralized and digital, while the primary regulation is a speed regulation done by local regulators.

1.2.3 Tertiary regulation

The tertiary regulation concerns only real power and, differently from the previous ones, is activated manually and not automatically by the TSO.

Its main goals are to restore the secondary reserve and adjust the power generation to the requirements of economic dispatch generation (currents, voltage, N-1 security).

The tertiary power intervention can be represented as power ramp and has maximum time of activation equal to 15 minutes.

Figure 1-4 shows how the different control reserves cover different time frames. It illustrates in case of large frequency drop (the dotted line beginning before activation of Primary Control shows the principle plot of the frequency deviation) how the activation of primary control reserve (activated within seconds) is followed up by secondary controlled reserve (activated within minutes) that is supported and followed up by tertiary control reserve. [3]

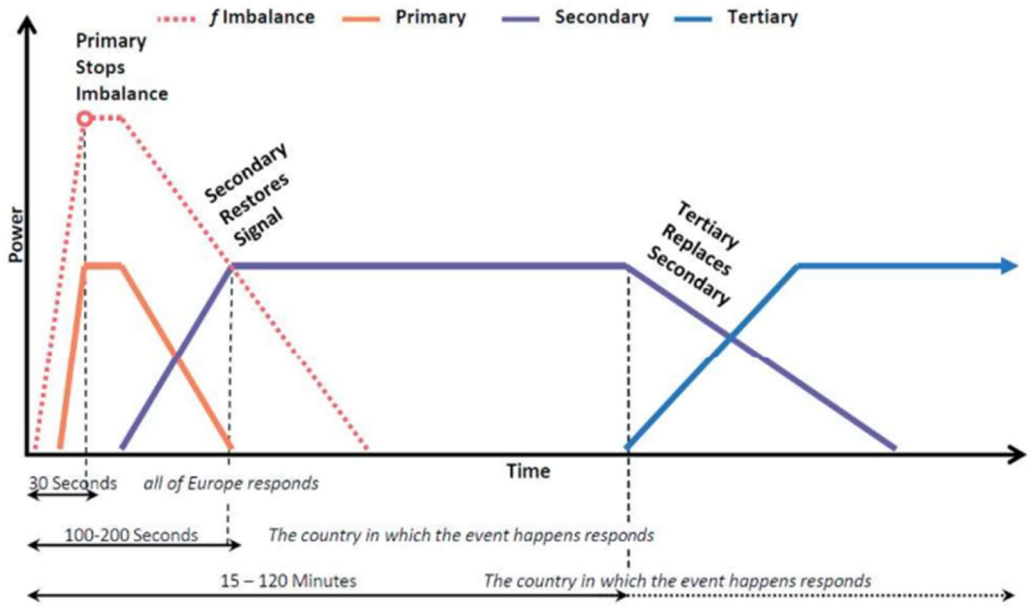

Figure 1-4 Tertiary regulation (entsoe.eu/)

1.3 Speed regulation of a generating unit in isolated operation

A first approach of control frequency consists in analyzing the case of a single generating unit in charge of speed regulation, shown in Figure 1-5. The generation is analyzed considering separately the speed regulator, the valve system, and the adduction system with the turbine.

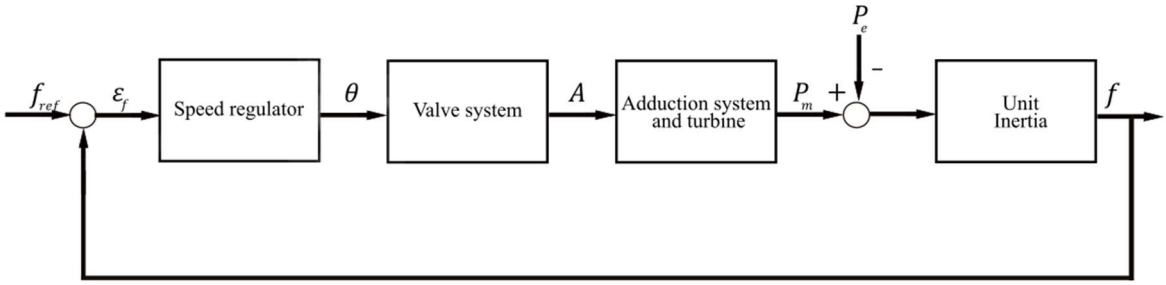

Figure 1-5 Control loop for a single generating unit

The frequency error is

$$\varepsilon_f = f_{ref} - f \tag{1.9}$$

Where f and f_{ref} are the measured frequency and the reference frequency.

Figure 1-6 shows the linearized block diagram of speed regulation for a generating unit: the closed loop control determines the restoration of frequency after the disturbance caused by load variation ΔP_L. The closed loop is constituted by the transfer function of speed governor $G_r(s)$, valve control system $G_v(s)$, turbine $G_a(s)$ and the unit inertia block. [1]

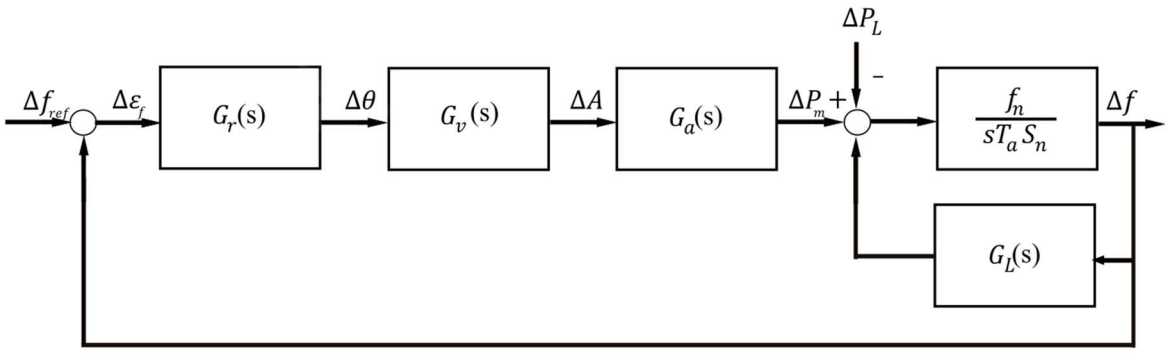

Figure 1-6 Control loop for a single generating unit

The generating unit is represented by the inertia block after the balance of mechanical power from the generating unit and electrical power by the load.
The inertia block comes by the swing equation in term of power:

$$\frac{df}{dt} = \frac{f_n}{T_a S_n}[P_m - P_e] \tag{1.10}$$

In LaPlace domain:

$$\Delta f = \frac{1}{s}\frac{f_n}{T_a S_n}[\Delta P_m - \Delta P_e] \tag{1.11}$$

The electrical power can be expressed as the sum of load variation ΔP_L and load dependence of frequency ΔP_C:

$$\Delta P_e = \Delta P_L + \Delta P_C = \Delta P_L + G_L(s)\Delta f \cong \Delta P_L + D\Delta f \tag{1.12}$$

Where G_L is the transfer function that takes in account the dependency of the load on frequency and is usually approximated to pure gain, the load damping coefficient D.

Hence the frequency variation is:

$$\Delta f = \frac{1}{s}\frac{f_n}{T_a S_n}\left[\Delta P_m - \Delta P_L - G_L\,\Delta f\right] \tag{1.13}$$

The transfer function $G_f(s)$ is the main transfer function: it is the cascade of speed governor, valve control system and supply system and turbine transfer function.

$$G_f(s) \triangleq G_r(s)G_a(s)G_v(s) \tag{1.14}$$

Where:

- The transfer function for the speed governor $G_r(s)$ has as input the error in frequency $\Delta\varepsilon_f$ and as output the opening of regulating servomotor $\Delta\theta$, so $G_r(s) \triangleq \frac{\Delta\theta}{\Delta\varepsilon_f}$;
- The transfer function for the valve control system $G_v(s)$ has as input the opening of regulating servomotor $\Delta\theta$ and as output the opening of the turbine admission valve ΔA, so $G_v(s) \triangleq \frac{\Delta A}{\Delta\theta}$;
- The transfer function for the supply system and the turbine $G_a(s)$ has as input the opening of the turbine admission valve ΔA and output regulating power ΔP_r, so $G_a(s) \triangleq \frac{\Delta P_r}{\Delta A}$.

The shape of the transfer function $G_f(s)$ is in the following form:

$$G_f(s) = K_f T_1 \frac{1 + sT_2}{1 + sT_1} \tag{1.15}$$

With time constant T_1 and T_2 and constant of proportionality K_f.

The static value of the transfer function $G_f(s)$ is the ratio between the change in regulating energy and the corresponding frequency variation:

$$G_f(0) = K_f T_1 = \frac{\Delta P_r}{\Delta \varepsilon_f}(0) = \left[-\frac{\Delta P_r}{\Delta f}(0)\right]_{\Delta f_{ref}=0} \tag{1.16}$$

(1.16) corresponds to the permanent regulating energy E_p defined in (1.7), so

$$G_f(0) = E_p \tag{1.17}$$

Similarly, the transient gain of the transfer function $G_f(s)$ is computed:

$$G_f(\infty) = K_f T_2 = \frac{\Delta P_r}{\Delta \varepsilon_f}(\infty) = \left[-\frac{\Delta P_r}{\Delta f}(\infty)\right]_{\Delta f_{ref}=0} \tag{1.18}$$

And $G_f(\infty)$ is identified as the transient regulating energy E_t

$$E_t \triangleq G_f(\infty) \tag{1.19}$$

Moreover, it is possible to introduce the transient regulating droop b_t

$$b_t \triangleq \left[-\frac{\frac{\Delta f}{f_n}}{\frac{\Delta P_r}{P_n}}(\infty)\right]_{\Delta f_{ref}=0} = \frac{P_n}{f_n K_f T_2} \tag{1.20}$$

The $G_f(s)$ can be put in form of energy regulating

$$G_f(s) = E_p \frac{1 + sT_2}{1 + sT_1} = E_t + \frac{E_p - E_t}{1 + sT_1} \tag{1.21}$$

$$G_f(s) = \frac{P_n}{f_n b_p}\frac{1+sT_2}{1+sT_1} = \frac{P_n}{f_n}\left[\frac{1}{b_t} + \frac{\frac{1}{b_p} - \frac{1}{bt}}{1+sT_1}\right] \tag{1.22}$$

Figure 1-6 shows the bode diagram of $G_f(s)$: the regulating energy in the first instants after the load variation is equal to the transient regulating energy E_t, which is a lower value; then it increases until it reaches the permanent regulating energy E_p. [1]

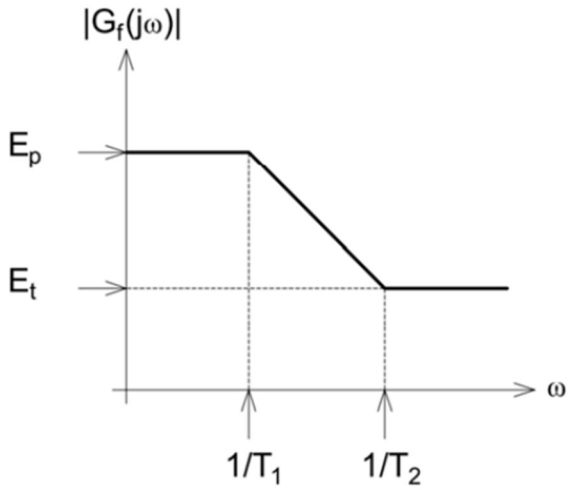

Figure 1-7 Bode diagram of $G_f(s)$

Chapter 2
Hydroelectric system

This chapter concerns the linearization of the model of hydroelectric system, that is mainly constituted by the adduction system and the turbine.

The adduction system is the part of the hydro power plant engaged in feeding the water from the intake to the powerhouse. It is constituted of pressure tunnels, surge tank and penstocks.

The hydraulic turbine converts the stored energy of water as hydraulic fluid into mechanical energy.

The hydroelectric adduction system is examined starting from the simple ideal case of inelastic condition to more complex hypothesis, like the presence of surge tank and water hammer effect. The first subdivision is power plant with and without the effect of the surge tank.

2.1 Power plant without surge tank effect

The effect of the power plant upstream the penstocks is considered negligible in the first approach, because the dynamic influence of pressure tunnels and surge tank is assumed to be very low: the adduction system in this first analysis is simply represented by the penstock only. [1]

2.1.1 Inelastic Penstock

In the first considerations the losses for friction are assumed negligible, the model in analysis is characterized by a penstock considered as cylindric pipe with section A_c, length L and β angle of inclination represented in Figure 2-1.

The other fundamental parameters are the total energy per unit of weight H_t referred to the terminal section of the penstock and volumetric flow Q.

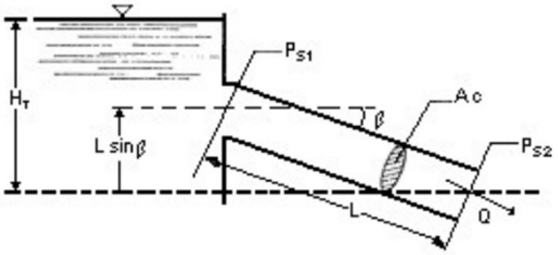

Figure 2-1 Adduction system

With the following conditions, it is possible to write the Bernoulli equation:

$$z + \frac{p_s}{\gamma} + \frac{u^2}{2g} = constant \tag{2.1}$$

Where:

- γ is the specific weight of water $[\frac{N}{m^3}]$;
- p_s is the average pressure in the section $[Pa]$;
- z is the height $[m]$;
- u is the speed$[\frac{m}{s}]$.

Taking in consideration a high head power plant, the energy from speed is assumed to be negligible $z + \frac{p_s}{\gamma} \gg \frac{u^2}{2g}$.

So, the total energy H_t is expressed as:

$$H_t = \frac{p_{s1}}{\gamma} + L \sin \beta \tag{2.2}$$

with p_{s1} the average pressure at the initial section of the penstock.

H is the total energy at the outtake of penstock per unit of weight and it is expressed as:

$$H = \frac{p_{s2}}{\gamma} \tag{2.3}$$

with p_{s2} the average pressure at the terminal of the penstock.

The difference between the energy associated to the two sections

$$H_t - H = \frac{p_{s1} - p_{s2}}{\gamma} + L \sin \beta \tag{2.4}$$

leads to an accelerating force $(H_t - H)\gamma A_c$ acting on water column of mass $\frac{\gamma L A_c}{g}$ and speed $\frac{Q}{A_c}$. Hence it is possible to express the second Newton rule of motion as:

$$(H_t - H)\gamma A_c = \frac{\gamma L A_c}{g} \cdot \frac{d\left(\frac{Q}{A_c}\right)}{dt} \tag{2.5}$$

Once the inertia of penstock $J_c[\frac{s^2}{m^2}]$ is defined:

$$J_c \triangleq \frac{L}{A_c g} \tag{2.6}$$

The expression (2.5) is expressed as:

$$\frac{dQ}{dt} = \frac{H_t - H}{J_c} \tag{2.7}$$

It shows how the energy H is dynamically related to the volumetric flow Q.

The (2.7), assuming H_t constant, can be written in LaPlace domain for small displacement around the operating point as

$$\Delta H = -Z_w(s)\Delta Q \tag{2.8}$$

Where the subscript Δ denotes small deviations and $Z_w(s)$ the impedance of penstock defined as

$$Z_w(s) \triangleq sJ_c = \frac{sL}{gA_c} \tag{2.9}$$

Another important variable is the water starting time T_w, defined in the same way of mechanical starting time of a power group T_a: T_w is equal to the ratio of the twice the kinetic

energy of water in penstock with speed $\frac{Q_0}{A_c}$ and the hydraulic power of water jet with volumetric flow Q_0 and energy H_0. [1]

$$T_w \triangleq \frac{\frac{\gamma}{g} L A_c \left(\frac{Q_0}{A_c}\right)^2}{\gamma Q_0 H_0} = \frac{L}{g A_c} \frac{Q_0}{H_0} = J_c \frac{Q_0}{H_0} \tag{2.10}$$

where the subscript "0" denotes initial steady state values.

T_w is not constant but varies with load: with the same energy of operation H_0, the time constant of penstock T_w is proportional to the volumetric flow Q_0

$$T_w = T_{wn} \frac{Q_0}{Q_n} \tag{2.11}$$

Where Q_n is the nominal volumetric flow and T_{wn} is the nominal water starting time defined as

$$T_{wn} \triangleq \frac{L}{g A_c} \frac{Q_n}{H_0} \tag{2.12}$$

The water starting time T_{wn} at full load lies in the range of $0.5 \div 4.0\ s$. [5]

2.1.2 Effect of friction

The losses for friction H_{l1} in the penstock are taken in account through the friction loss coefficient ϕ_p

$$H_{l1} = \phi_p |Q| Q \tag{2.13}$$

ϕ_p is approximated with the following formula

$$\phi_p = \frac{\rho L}{D_c^5} \tag{2.14}$$

Where:

- the resistance coefficient ρ is defined as

$$\rho = \frac{64}{\pi^2 \Sigma^2} \tag{2.15}$$

  in which Σ is Chézy's coefficient;

- D_c and L are respectively the diameter and the length of the penstock

The dynamic relation between the head and the flow is rewritten as

$$H_t - H = J_c \frac{dQ}{dt} + \phi_p |Q| Q \tag{2.16}$$

2.1.3 Elastic Penstock

For very long penstocks, the wave travel time of the water column becomes significant, and the reflected pressure waves in the water column cause the preceding treatment of water start time to be no longer valid. When the wave travel time approaches 25% of the water starting time T_w, the dynamic should not rely on T_w, and the performance of the turbine governing system should be evaluated by considering the effects of both the water starting time and the wave travel time, also defined as elastic time T_e. [6]

The traveling wave speed c for a circular section is computed as function of the speed of sound in in water C (value around 1245 m/s), the compression ratio ε, the Young's modulus of elasticity E, the geometrical parameter of the penstock (diameter D_c and the thickness e)

$$c = \frac{C}{\sqrt{\left(1 + \frac{\varepsilon}{E}\frac{D_c}{e}\right)}} \tag{2.17}$$

The value of c in penstock is around 700-1200 m/s.

The elastic time of penstock T_{ep} is defined as the

$$T_{ep} = \frac{L}{c} \tag{2.18}$$

Taking in consideration propagation effect and friction, the impedance of penstock Z_w is expressed as

$$Z_w(s) \triangleq Z_p \tanh(\theta_c) \tag{2.19}$$

with Z_p the normalized impedance of the penstock and elastic phase θ_c:

$$Z_p = \frac{c}{gA_c}\sqrt{1 + \frac{2\phi_p Q_0 g A_c}{sL}} \tag{2.20}$$

$$\theta_c = \frac{sL}{c}\sqrt{1 + \frac{2\phi_p Q_0 g A_c}{sL}} \tag{2.21}$$

Neglecting friction losses, through a null value of coefficient ϕ_p. (2.20) and (2.21) become

$$Z_p = \frac{c}{gA_c} \tag{2.22}$$

$$\theta_c = \frac{sL}{c} = sT_{ep} \tag{2.23}$$

It is worth noticing the relation between the water starting time and elastic time is given in no friction case by the normalized impedance:

$$Z_p = \frac{T_w}{T_{ep}} \tag{2.24}$$

In the later models, for the sake of simplicity the friction coefficient is taken into account separately by the normalized impedance Z_p, hence (2.24) results always valid.

2.1.4 Turbine

The hydraulic turbines are machines that transform the potential energy of water in rotational kinetic energy. The mechanical power depends on the hydraulic power in input to the turbine, that is modulated acting on the inlet valve placed at the end of the penstock: changing the opening of inlet valve varies the water in turbine and so the power.

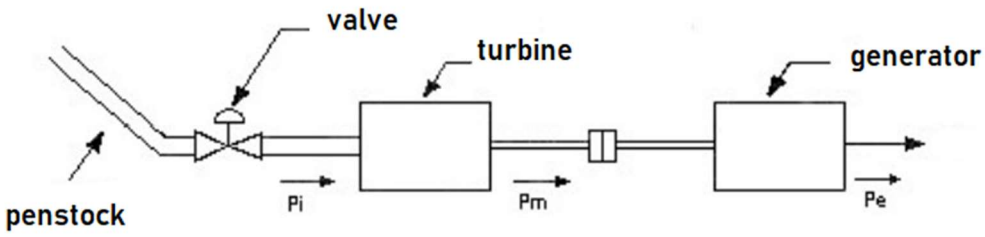

Figure 2-2 Transformation of hydraulic power in electrical power

Therefore, the dynamic relation is between the opening gate and the mechanical power of turbine P_m.

There are two main types of hydraulic turbine: impulse turbine (Pelton turbine) and reaction turbine (Francis and Kaplan turbine). The impulse turbine obtains the resulting thrust on the runner blades by changing direction of the speed, while reaction turbine changes only the speed magnitude; hence, reaction turbines also modify pressure while impulse-type has no impact on pressure.

The hydraulic power at the inlet of turbine is:

$$P_i = \gamma Q H \tag{2.25}$$

Where the head H for Pelton turbine can be expressed in function of the cross-sectional area of discharge A as

$$H = \frac{Q^2}{2gA^2} \tag{2.26}$$

while for Francis turbine, the reaction degree α is introduced

$$H = \frac{Q^2}{2gA^2} + \alpha H \tag{2.27}$$

The hydraulic power is transformed in mechanical power taking care of efficiency coefficient η:

$$P_m = \eta\gamma QH \tag{2.28}$$

η takes care of the following considerations:

- losses due to water speed left at the outlet;
- losses because the water flow has changes in direction;
- not all the points of the water jet have the same speed;
- the water jet leaves the blade in a different point respect the point of incidence.

The expression is linearized around the operating point, indicated with subscript "0", to obtain the turbine transfer function:

$$\Delta P_m = (\gamma\eta_0 H_0)\Delta Q + (\gamma\eta_0 Q_0)\Delta H + (\gamma Q_0 H_0)\Delta\eta \tag{2.29}$$

Dividing by $P_{m_0} = \gamma\eta_0 Q_0 H_0$, the expression becomes

$$\frac{\Delta P_m}{P_{m_0}} = \frac{\Delta Q}{Q_0} + \frac{\Delta H}{H_0} + \frac{\Delta\eta}{\eta_0} \tag{2.30}$$

The efficiency of turbine η is function of opening of inlet valve A, hence

$$\frac{\Delta\eta}{\eta_0} = k_{\eta A}\frac{\Delta A}{A_0} \tag{2.31}$$

With $k_{\eta A} = \frac{A_0}{\eta_0}(\frac{d\eta}{dA})^o$ depending on the gradient of function $\eta = \eta(A)$; only in the ideal case, the coefficient $k_{\eta A}$ is considered null.

The volumetric flow Q for Pelton turbine is $Q = A\sqrt{2gH}$. Rewriting (2.27), the linearization is

$$\Delta Q = \left(\frac{\partial Q}{\partial A}\right)^0 \Delta A + \left(\frac{\partial Q}{\partial H}\right)^0 \Delta H \tag{2.32}$$

In which the partial derivatives are

$$\begin{cases} \left(\frac{\partial Q}{\partial A}\right)^0 = \left[\sqrt{2gH}\right]^0 = \frac{Q_0}{A_0} \\ \left(\frac{\partial Q}{\partial H}\right)^0 = \left[\frac{1}{2}A(2gH)^{-\frac{1}{2}}2g\right]^0 = \frac{1}{2}\frac{Q_0}{A_0} \end{cases} \tag{2.33}$$

Hence the linearization of volumetric flow Q (2.32) can be written:

$$\frac{\Delta Q}{Q_0} = \frac{\Delta A}{A_0} + \frac{1}{2}\frac{\Delta H}{H_0} \tag{2.34}$$

The linearization of mechanical power (2.30) can be rewritten with (2.34) and (2.31) as

$$\frac{\Delta P_m}{P_{m_0}} = \left(1 + k_{\eta A}\right)\frac{\Delta A}{A_0} + \frac{3}{2}\frac{\Delta H}{H_0} \tag{2.35}$$

Defining $k_{pA} = 1 + k_{\eta A}$, which is equal to 1 in ideal case because $k_{\eta A}$ is null. So, in the ideal case normalizing the variable it is obtained:

$$\Delta \bar{P}_m = \Delta \bar{A} + \frac{3}{2}\Delta \bar{H} \tag{2.36}$$

It can be also expressed through the variation of volumetric flow instead of head with the equation $\Delta \bar{Q} = \Delta \bar{A} + \frac{1}{2}\Delta \bar{H}$ (2.34)

$$\Delta \bar{P}_m = 3\Delta \bar{Q} - 2\Delta \bar{A} \tag{2.37}$$

2.1.5 Transfer function of the adduction system with ideal turbine

The acceleration of water column due to change in head at turbine is expressed by the Newton's second law of motion:

$$\rho L \frac{d\Delta Q}{dt} = -\rho g \Delta H A \tag{2.38}$$

With ρ water density and $\rho g \Delta H$ incremental change in pressure at turbine gate. [5]

Dividing both side for $\rho g H_0 Q_0$ and normalizing it is obtained:

$$T_w \frac{d\Delta \bar{Q}}{dt} = -\Delta \bar{H} \tag{2.39}$$

Substituting with the equation of (2.34), the dynamic relation between the cross-sectional area of discharge A and the volumetric flow Q is obtained in LaPlace domain:

$$T_w \Delta \bar{Q} s = 2(\Delta \bar{A} + \Delta \bar{Q}) \tag{2.40}$$

That can be expressed as

$$\Delta \bar{Q} = \frac{1}{1 + \frac{1}{2} T_w s} \Delta \bar{A} \tag{2.41}$$

The relation between the variation cross-sectional area of discharge A and the variation of mechanical power P_m determines the adduction transfer function $G_a(s)$. Through (2.41) and (2.37) the adduction transfer function for the ideal case is:

$$G_a(s) = \frac{\Delta \bar{P}_m}{\Delta \bar{A}} = \frac{1 - T_w s}{1 + \frac{1}{2} T_w s} \tag{2.42}$$

2.1.6 Transfer function of the adduction system with non-ideal turbine

In case of non-ideal turbine, the transfer function can be expressed by the following:

$$G_a(s) = \frac{\Delta \bar{P}_m}{\Delta \bar{A}} = \frac{a_{23} + (a_{11}a_{23} - a_{13}a_{21})\, T_w s}{1 + a_{11} T_w s} \tag{2.43}$$

Where the coefficients a_{11} and a_{13} are partial derivatives of water flow with the respect to head and gate opening, and the coefficients a_{21} and a_{23} are partial derivatives of turbine power with respect to head and gate opening. [5]

The values of coefficients for a 40 MW Francis turbine in different working conditions are shown in Table 2-1.

Table 2-1 Coefficients for a 40 MW Francis turbine

Coefficient	Ideal lossless	Typical at full load	Typical at no load
a_{11}	0.5	0.58	0.57
a_{13}	1.0	1.1	1.1
a_{21}	1.5	1.4	1.18
a_{23}	1.0	1.5	1.5

2.1.7 Transfer function with elastic penstock

The transfer function $G_a(s)$ for ideal turbine taking into consideration the propagation phenomena is:

$$G_a(s) = \frac{\Delta \bar{P}_m}{\Delta \bar{A}} = \frac{1 - Z_p \tanh\,(sT_{ep})}{1 + \frac{1}{2} Z_p \tanh\,(sT_{ep})} \tag{2.44}$$

Taking into consideration also the friction coefficient in the penstock, $G_a(s)$ is:

$$G_a(s) = \frac{1 - Z_p \tanh(sT_{ep}) - \phi_p}{1 + \frac{1}{2} Z_p \tanh\,(sT_{ep})} \tag{2.45}$$

The hyperbolic tangent is defined using distributed-parameter theory:

$$\tanh(T_{ep}s) = \frac{1 - e^{-2T_{ep}s}}{1 + e^{-2T_{ep}s}} = \frac{sT_{ep} \prod_{n=1}^{\infty} \left[1 + \left(\frac{sT_{ep}}{n\pi}\right)^2\right]}{\prod_{n=1}^{\infty} \left[1 + \left(\frac{2sT_{ep}}{(2n+1)\pi}\right)^2\right]} \tag{2.46}$$

The infinite product is required to preserve all the characteristics of the transfer function, anyway it is possible to approximate lumped parameter equivalent maintaining a certain accuracy.

In case of $n = 0$, the value of hyperbolic tangent $\tanh(sT_{ep})$ is equal to sT_{ep}. $G_a(s)$ becomes:

$$G_a(s) = \frac{1 - Z_p(sT_{ep})}{1 + \frac{1}{2} Z_p(sT_{ep})} \tag{2.47}$$

In this way the transfer function has the same approximation of inelastic case, indeed (2.47) through (2.24) is:

$$G_a(s) = \frac{1 - \mathrm{T_w} s}{1 + \frac{1}{2} T_w s} \tag{2.48}$$

With $n = 1$ the first pole and the zero of hyperbolic function are preserved, which represent the fundamental harmonic of water column:

$$Z_P \tanh(T_{ep} s) \approx \frac{s T_{wp} \left[1 + s^2 \left(\frac{T_{ep}}{\pi}\right)^2\right]}{\left[1 + s^2 \left(\frac{2T_{ep}}{\pi}\right)^2\right]} \tag{2.49}$$

In most cases, the simplification with n=1 for power system stability is enough. [5]

2.2 Power plant with surge tank effect

The surge tank is an open standpipe to the conduit of hydroelectric power plant, the top is typical open to atmosphere. The conduit between the reservoir and the surge tank is referred as pressure tunnel, and only the one between surge tank and powerhouse is the penstock.

The role of surge tank is of paramount importance because it improves regulation of hydraulic turbine: it reduces the length of power conduit determining reduction of water starting time T_w. The oscillations in surge tank are slow, so the approximation with lumped parameter n=0 is often accurate. [7]

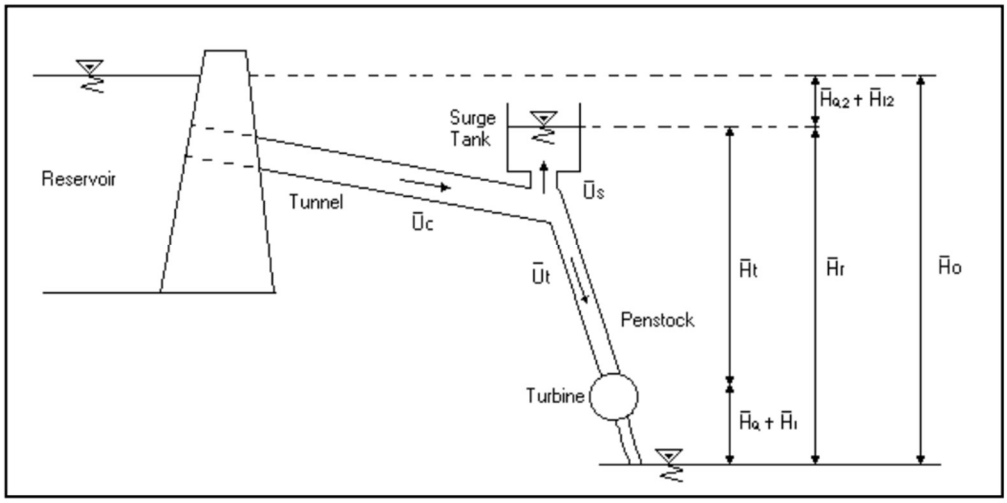

Figure 2-3 Surge tank hydraulic scheme

The water starting time of the tunnel T_{wc}, is defined i.e. the time required to accelerate the flow from zero to the rated flow of tunnel under the base head.

$$T_{wc} = \frac{L_t}{A_t g}\frac{Q_0}{H_0}T_{ec} = Z_t T_{ec} \tag{2.50}$$

Where L_t and A_t are the length and the section of tunnel, Z_t and T_{ec} are the normalized impedance and the time elasticity of tunnel.

For the surge tank the storage constant C_s is introduced:

$$C_s = \frac{A_S}{Q_0}H_0 \tag{2.51}$$

Where A_S is the section of surge tank.

In addition, the water level in the surge tank begins to oscillate following a change in the turbine flow with the natural period T_S:

$$T_S = 2\,\pi\sqrt{T_{wc}C_s} \tag{2.52}$$

The amplitude of these oscillations may increase or decrease in time depending upon the system parameters and the magnitude and time variation of the flow change. The oscillations are defined: “stable” if they dampen to the final steady state in a reasonable time, and “unstable” if their magnitude increases with time. [7]

2.2.1 Dynamic equations

The Newton second law, mentioned in (2.38), is rewritten in function of speed of the water flow U. Taking infinitesimally small values of space Δx, time Δt and ΔU: [5]

$$\frac{\partial U}{\partial t} = -g\frac{\partial H}{\partial x} \tag{2.53}$$

The speed of water flow U is proportional to the flow Q and inversely proportional to the section of conduit A:

$$U = \frac{Q}{A} \tag{2.54}$$

The increase in volume of the conduit walls due to compressibility of the water is described by another differential equation:

$$\frac{\partial U}{\partial x} = -\beta\frac{\partial H}{\partial t} \tag{2.55}$$

With the auxiliar variable β in function the geometric parameters (diameter D and thickness e) and elasticity parameter (compression ratio ε and modulus of elasticity of Young E):

$$\beta = \rho g \left(\frac{1}{\varepsilon} + \frac{D}{Ee}\right) \tag{2.56}$$

The solution of the two differential equations (2.53) and (2.55):

$$H_2 = H_1\, sech(T_e s) - Z_0 Q_2 tanh\,(T_e s) \tag{2.57}$$

$$Q_1 = Q_2\, cosh(T_e s) - \frac{1}{Z_0} H_2 sinh\,(T_e s) \tag{2.58}$$

Where Z_0 is the hydraulic surge impedance.

These equations allow to identify the dynamics separately in tunnel, surge tank and penstock. [8]

In the tunnel:

$$\bar{H}_r = \bar{H}_0 - \bar{H}_{l2} - \bar{H}_{Q2} \tag{2.59}$$

Where:

- $\bar{H}_r$ is the head of the riser of the surge tank.
- The initial steady state value of $\bar{H}_0$ is assumed 1.0 p.u.
- The head loss in tunnel $\bar{H}_{l2}$ is in function of the speed of the water flow in the tunnel $\bar{U}_c$ and head loss coefficient f_{p2}

$$\bar{H}_{l2} = f_{p2}\bar{U}_c|\bar{U}_c| \tag{2.60}$$

f_{p2} is assumed to be equal to the friction coefficient ϕ_c.

- The head $\bar{H}_{Q2}$ due to the water flow in the tunnel is in function of water starting time of tunnel

$$\bar{H}_{Q2} = T_{wc}\frac{d\bar{U}_c}{dt} \tag{2.61}$$

In the surge tank:

$$\bar{H}_r = \frac{1}{C_S}\int \bar{U}_S dt - f_0\bar{U}_S|\bar{U}_S| \tag{2.62}$$

With f_0 as surge tank orifice head loss coefficient and $\bar{U}_S$ as speed in the surge tank. Indeed, many surge tanks include an orifice which dissipates the energy of hydraulic oscillations and produces damping.

In the penstock:

$$\bar{H}_t = \bar{H}_r - \bar{H}_l - \bar{H}_Q \tag{2.63}$$

Where:

- $\bar{H}_t$ and $\bar{U}_t$ are the head and the speed in turbine;
- $\bar{H}_l$ is the head due to losses in turbine

$$\bar{H}_l = f_{p1}\bar{U}_t^2 \tag{2.64}$$

Where the head loss coefficient in the penstock $f_{p1}$is assumed equal to the friction coefficient ϕ_p.

- The head due to water flow in turbine $\bar{H}_Q$:

$$\bar{H}_Q = Z_p \tanh\,(T_{ep}s)\bar{U}_t \tag{2.65}$$

2.2.2 Transfer function

The auxiliary transfer function $G(s)$ defines the relations in the circuit Surge Tank-Penstock [8]:

$$G(s) = \frac{\bar{H}_0 - \bar{H}_S}{\bar{U}_p - \bar{U}_0} = \frac{\phi_c + Z_c \tanh(T_{ec}s)}{1 + sC_s\phi_c + Z_c \tanh(T_{ec}s)\, sC_S} \tag{2.66}$$

Where:

- $\bar{U}_p$ is the upper penstock water velocity;
- $\bar{U}_0$ is the initial steady state of water speed;
- $\bar{H}_0$ is the initial steady state of head;
- $\bar{H}_S$ is the surge tank head.

For the circuit surge tank-tunnel the expansion of the hyperbolic tangent with n=0 has been considered, (2.66) becomes:

$$G(s) = \frac{\phi_c + sT_{wc}}{1 + sC_s\phi_c + s^2C_ST_{wc}} \tag{2.67}$$

The transfer function $F(s)$ relates penstock speed and head and for elastic water column in penstock is:

$$F(s) = \frac{\bar{U}_t - \bar{U}_0}{\bar{H}_t - \bar{H}_0} = -\frac{1 + \frac{G(s)}{Z_p}\tanh(T_{ep}s)}{\phi_p + G(s) + Z_p \tanh(T_{ep}s)} \tag{2.68}$$

For inelastic water column:

$$F(s) = \frac{\bar{U}_t - \bar{U}_0}{\bar{H}_t - \bar{H}_0} = -\frac{1 + \frac{G(s)}{Z_p}T_{ep}s}{\phi_p + G(s) + Z_p T_{ep}s} \tag{2.69}$$

The adduction transfer function is computed starting from the formula of linearization of mechanical power (2.37) and the function $F(s)$; in case of an elastic water column in the penstock and non-elastic water column in the tunnel $G_a(s)$ is:

$$G_a(s) = \frac{1 - \phi_p - Z_P \tanh(T_{ep}s) + \frac{G(s)}{Z_p}\tanh(T_{ep}s) - G(s)}{1 + \frac{1}{2}\phi_p + \frac{1}{2}Z_p T_{ep}s + \frac{1}{2}G(s) + \frac{G(s)}{Z_p}\tanh(T_{ep}s)} \tag{2.70}$$

In case of inelastic water column in the penstock, $G_a(s)$ becomes:

$$G_a(s) = \frac{1 - \phi_p - Z_p T_{ep}s + \frac{G(s)}{Z_p}T_{ep}s - G(s)}{1 + \frac{1}{2}\phi_p + \frac{1}{2}Z_p T_{ep}s + \frac{1}{2}G(s) + \frac{G(s)}{Z_p}T_{ep}s} \tag{2.71}$$

Chapter 3
Nonlinear model

The linear model is useful for its simplicity to obtain insight into the basic characteristics of hydraulic system, and it is acceptable to represent small signal performance, but it is inadequate for studies of large variation in frequency and power output, hence a nonlinear model is necessary.

The discussion of nonlinearity starts with models realized by P. Kundur, to more models of IEEE. As for Chapter 2, the first subdivision is nonlinear models with and without surge tank effect.

3.1 General considerations

In a nonlinear system the response of perturbation of finite duration depends on initial condition and the kind of perturbation, so it is not possible to apply the overlap of the effects. Furthermore, the analysis of stability is not valid for all the points of equilibrium of the system, all the points of equilibrium have different stability features.

The ideal gain G is based on having 1 p.u. as change from no load to full load, while the real gate opening g is based on having 1 p.u. as change from the fully closed to the fully open position. [5]

The relation between the real and the ideal gate is given by the turbine gain A_t:

$$A_t = \frac{1}{\bar{g}_{FL} - \bar{g}_{NL}} \tag{3.1}$$

With $\bar{g}_{FL}$ full load gate and $\bar{g}_{NL}$ no load gate.

These considerations are shown in Figure 3-1.

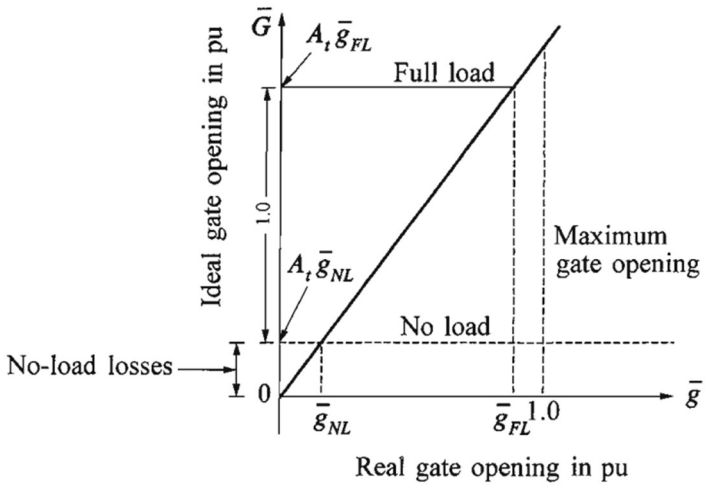

Figure 3-1 Real gate g and ideal gate G

The mechanical power output of turbine P_m is obtained by the difference between the turbine power and the losses.

$$P_m = P - P_{Losses} \tag{3.2}$$

In which the losses are given by

$$P_{Losses} = \overline{U}_{NL}\overline{H} \tag{3.3}$$

Where $\overline{U}_{NL}$is the no load water speed:

$$\overline{U}_{NL} = A_t\bar{g}_{NL}(\overline{H}_0)^{\frac{1}{2}} \tag{3.4}$$

The expression of mechanical power P_m is:

$$\bar{P}_m = (\bar{U} - \bar{U}_{NL})\bar{H} \tag{3.5}$$

3.2 Kundur models

The nonlinear model realized by Kundur is represented Figure 3-2.

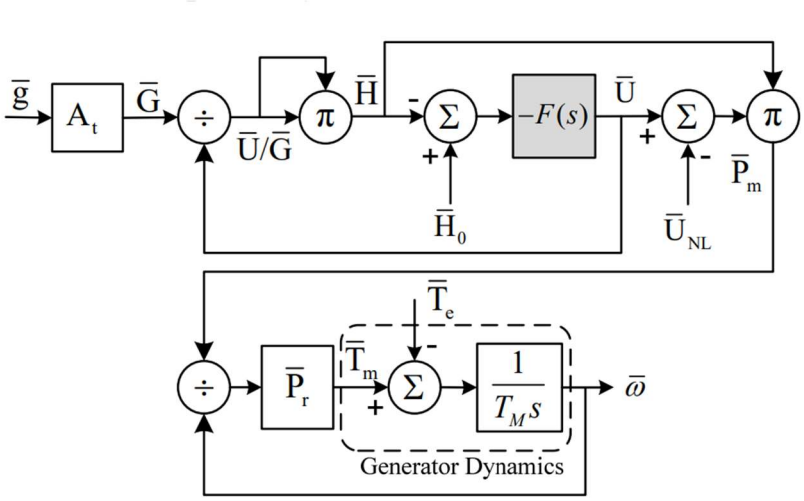

Figure 3-2 Nonlinear model Kundur

The transfer function $F(s)$, as asserted in Chapter 2, is the relation between the variation of water speed in turbine u_t and the variation of head h_t:

$$F(s) = \frac{\bar{U}_t - \bar{U}_0}{\bar{H}_t - \bar{H}_0} = \frac{u_t}{h_t} \tag{3.6}$$

The transfer function $F(s)$ depends on the kind of assumptions taken.

3.2.1 Power plant without surge tank effect

The dynamics of the penstock in a power plant without surge tank are written through (2.57):

$$\bar{H}_t = \bar{H}_0 - \bar{H}_l - \bar{H}_Q \tag{3.7}$$

Where:

- $\bar{H}_l$ is the head due to losses defined as (2.64);
- $\bar{H}_Q$ head to water flow without considering propagation effect is:

$$\bar{H}_Q = T_w \frac{d\bar{U}_t}{dt} \tag{3.8}$$

The head in turbine $\bar{H}_t$ can be rewritten in function of $\bar{U}_t$ through

$$\bar{U}_t = \bar{G}(\bar{H}_t)^{\frac{1}{2}} \tag{3.9}$$

hence it is possible to rewrite the dynamics (3.8) as a differential equation of $\bar{U}_t$:

$$\frac{d\bar{U}_t}{dt} = \frac{1}{T_w}\left(1 - \frac{\bar{U}_t^{\,2}}{\bar{G}} - f_{p1}\bar{U}_t^2\right) \tag{3.10}$$

Neglecting the friction coefficient

$$\frac{d\bar{U}_t}{dt} = \frac{1}{T_w}\left(1 - \frac{\bar{U}_t}{\bar{G}}^2\right) = -\frac{1}{T_w}(\bar{H}_t - \bar{H}_0) \tag{3.11}$$

$F(s)$ is defined only by the water starting time T_w and it is found rewriting (3.11) in LaPlace domain:

$$F(s) = \frac{\bar{U}_t}{\bar{H}_t - \bar{H}_0} = -\frac{1}{T_w s} \tag{3.12}$$

Taking in considerations the propagation of waves, the transfer function becomes in function of the normalized impedance of the penstock Z_p and the elastic time T_{ep}

$$F(s) = \frac{-1}{Z_p \tanh(T_{ep}s)} \tag{3.13}$$

Also considering friction losses through coefficient ϕ_p

$$F(s) = \frac{-1}{\phi_p + Z_p \tanh(T_{ep}s)} \tag{3.14}$$

The expression (3.14) can be simplified with lumped parameter:

- taking n=0 the expression $\tanh(T_{ep}s) \approx T_{ep}s$, the transfer function is so

$$F(s) = \frac{-1}{\phi_p + Z_p T_{ep} s} = \frac{-1}{\phi_p + T_w s} \tag{3.15}$$

Neglecting the friction, this expression is equivalent to the inelastic case of (3.12).

- with n=1 the first pole and the zero of the tanh function are maintained and they represent the fundamental harmonic of water column, $F(s)$ becomes

$$F(s) = \frac{-1}{\phi_p + F_2(s)} \tag{3.16}$$

With

$$F_2(s) = Z_p \tanh\left(T_{ep}s\right) \approx \frac{sT_{Wp}\left[1 + s^2\left(\frac{T_{ep}}{\pi}\right)^2\right]}{\left[1 + s^2\left(\frac{2T_{ep}}{\pi}\right)^2\right]} \tag{3.17}$$

The transfer function $F(s)$ must be initialized for steady state output, therefore there is the need to compute the steady state speed of water flow in turbine $\bar{U}_{tss}$.

The steady state value U_{tss} is found nulling the derivative term $\frac{d\bar{U}_t}{dt}$ in (3.10): [8]

$$U_{tss} = \sqrt{\frac{1}{\frac{1}{\bar{G}^2} + f_{p1}}} \tag{3.18}$$

3.2.2 Power plant with surge tank effect

The dynamics of power plant with surge tank have been already described taking separately penstock, pressure tunnel and surge tank by (2.59-2.65). [8]

The additional transfer function $G(s)$ (2.67) has been introduced to describe the relation between the circuit tunnel-surge tank with the penstock in section (2.2.9).

The $F(s)$for elastic water column in the penstock and inelastic pressure tunnel is (2.68) while in case of inelastic water column in penstock is (2.69).

Starting from dynamics equations (2.59-2.65) the following differential equations have been analyzed:

$$\frac{d\bar{U}_t}{dt} = \frac{1}{T_w}\bar{H}_r - \left(\frac{1}{T_w\bar{G}^2} + \frac{f_{p1}}{T_w}\right)\bar{U}_t^2 \tag{3.19}$$

$$\frac{d\bar{H}_r}{dt} = \frac{\bar{U}_c}{C_s} - \frac{\bar{U}_t}{C_s} \tag{3.20}$$

$$\frac{d\bar{U}_c}{dt} = \frac{1}{T_{wc}} - \frac{\bar{H}_r}{T_{wc}} - \frac{f_{p2}}{T_{wc}}\bar{U}_c^2 \tag{3.21}$$

The aim is to find the steady state values of the water flow of turbine $\bar{U}_t$, the water flow in tunnel $\bar{U}_c$ and the head of riser of surge tank $\bar{H}_r$:

$$0 = \frac{1}{T_w}\bar{H}_{rss} - \left(\frac{1}{T_w\bar{G}^2} + \frac{f_{p1}}{T_w}\right)\bar{U}_{tss}^2 \tag{3.22}$$

$$0 = \frac{\bar{U}_{css}}{C_s} - \frac{\bar{U}_{tss}}{C_s} \tag{3.23}$$

$$0 = \frac{1}{T_{wc}} - \frac{\bar{H}_{rss}}{T_{wc}} - \frac{f_{p2}}{T_{wc}}\bar{U}_{css}^2 \tag{3.24}$$

The solutions are:

$$\bar{H}_{rss} = \left(\frac{1}{\bar{G}^2} + f_{p1}\right)\bar{U}_{tss}^2 \tag{3.25}$$

$$\bar{U}_{tss}^2 = \frac{1}{f_{p2}} - \frac{\bar{H}_{rss}}{f_{p2}} \tag{3.26}$$

$$\bar{U}_{tss} = \bar{U}_{css} \tag{3.27}$$

The solutions for $\bar{H}_{rss}$ and $\bar{U}_{tss}$ are function of the ideal gate opening $\bar{G}$ and head losses coefficient f_{p1} and f_{p2}, that are supposed equal to friction coefficient ϕ_p and ϕ_c:

$$\bar{H}_{rss} = \frac{f_{p1} + \frac{1}{\bar{G}^2}}{f_{p2} + f_{p1} + \frac{1}{\bar{G}^2}} \tag{3.28}$$

$$\bar{U}_{tss} = \bar{U}_{css} = \sqrt{\frac{\bar{G}^2}{1 + \bar{G}^2\left(f_{p1} + f_{p2}\right)}} \tag{3.29}$$

The computation of $\bar{U}_0$ starts from the solution for head of dynamics equations (2.57) for the surge tank-penstock-turbine circuit:

$$\bar{H}_t - \bar{H}_0 = (\bar{H}_r - \bar{H}_0)\,\mathrm{sech}\left(T_{ep}s\right) - (Z_p \tanh\left(T_{ep}s\right) + \phi_p)(\bar{U}_t - \bar{U}_0) \tag{3.30}$$

At the steady state it becomes

$$\bar{H}_{tss} = \bar{H}_{rss} - \phi_p(\bar{U}_{tss} - \bar{U}_0) \tag{3.31}$$

The same process is done for the circuit reservoir-tunnel-surge tank to find the value of $\overline{H}_{rss}$. The solution of dynamic equations is:

$$\overline{H}_r - \overline{H}_0 = (\overline{H}_w - \overline{H}_0)\,\mathrm{sech}(T_{ec}s) - (Z_c \tanh(T_{ec}s) + \phi_c)(\overline{U}_c - \overline{U}_0) \tag{3.32}$$

That at the steady state gives:

$$\overline{H}_{rss} = \overline{H}_0 - \phi_c(\overline{U}_{tss} - \overline{U}_0) \tag{3.33}$$

Replacing the result of the steady state head at the riser of surge tank $\overline{H}_{rss}$ in the equation of steady state head at turbine $\overline{H}_{tss}$ (3.31), $\overline{U}_0$ is found:

$$\overline{U}_0 = \overline{U}_{tss} + \frac{\frac{\overline{U}_{tss}^2}{\bar{G}^2} - \overline{H}_0}{\phi_p + \phi_c} \tag{3.34}$$

The value $\overline{U}_0$ is depends on the gate opening $\bar{G}$, the dependency is shown in Figure 3-3 for Susqueda power plant (Table 6-1).

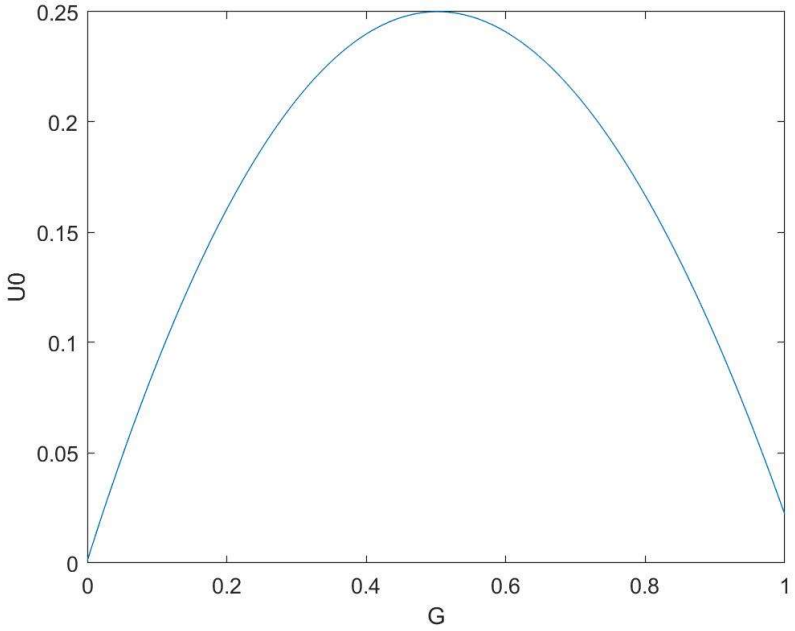

Figure 3-3 Variation of initial steady state $\overline{U}_0$ on the ideal gate $\bar{G}$

3.3 IEEE models

3.3.1 Power plant without surge tank effect

IEEE working group of 1992 has developed the nonlinear model in Figure 3-4 expliciting the dynamic equations of penstock (3.8)-(3.11).

In addition, this model considers includes a turbine self-regulation gain term (D_t), which depends on both speed variation $\Delta\overline{w}$) and flow: [9]

$$\overline{\mathrm{P}}_t = D_t \bar{G} \Delta\overline{w} \tag{3.35}$$

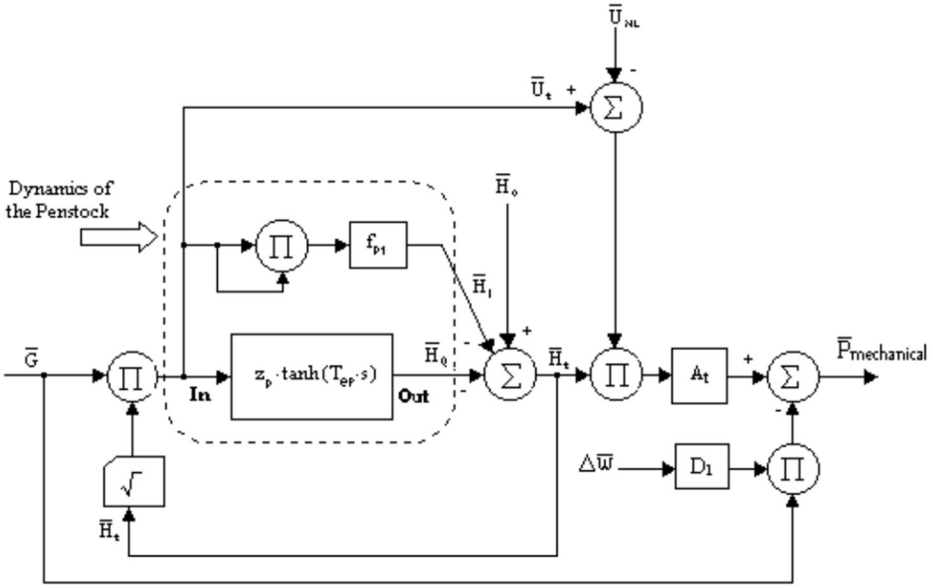

Figure 3-4 Model of IEEE without surge tank effect

The computations of U_{tss} is (3.18) but with real gate $\bar{g}$, because the turbine gain is afterward.

3.3.2 Power plant with surge tank effect

The nonlinear model with surge tank effect of IEEE working group the in Figure 3-5 iincludes the representation of:

- penstock dynamics,
- surge chamber dynamics,
- tunnel dynamics,
- penstock, tunnel, and surge chamber orifice losses [10]

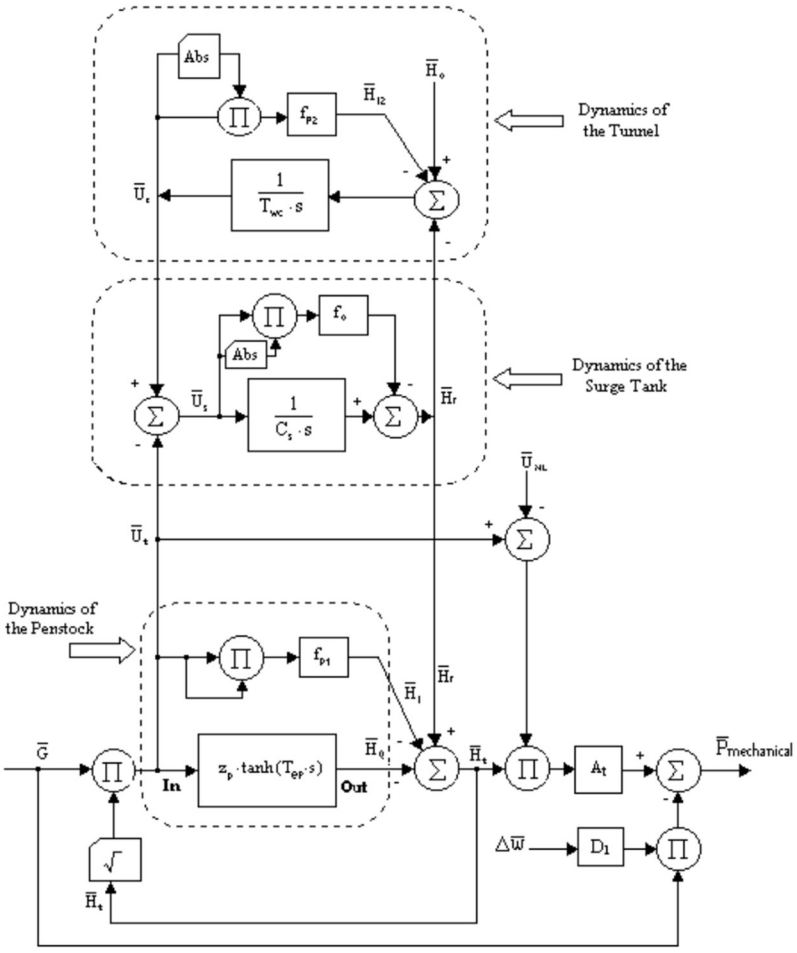

Figure 3-5 Model of IEEE with surge tank effect

The computations of H_{rss} and U_{tss} are respectively (3.28) and (3.29) but with real gate $\overline{g}$.

Chapter 4
Speed regulators

The speed regulators are constituted by a speed transducer, with one or more error amplifiers and servomotors. In the past, there was a large use of hydraulic type, while nowadays they are electrical or electronic. [1]

The block diagram of regulation is shown in Figure 4-1: the input of the speed regulator is the frequency error, and the output is the opening of servomotor θ, that acts on the valve of distribution in turbine by changing the area of outflow A.

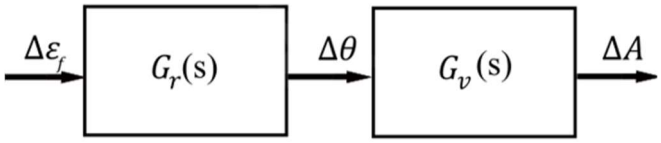

Figure 4-1 Speed regulator and valve system block control

The following chapter discusses theoretical and general form of speed regulator with at first the distinction into two main groups, tacho-accelerometer and transient feedback, and then more specific speed regulators for hydroelectric power plant.

4.1 General form

A preliminary general form for the speed regulator transfer function is achievable through the desired form of the main transfer function G_f , that has been already computed in the first chapter:

$$G_f = \frac{P_n}{f_n b_P}\frac{1+sT_2}{1+sT_1} = \frac{P_n}{f_n}\frac{1+sT_2}{b_P+sT_2 b_t} \tag{4.1}$$

$$G_f = G_a(s)G_v(s)\, G_r(s) \tag{4.2}$$

The control system of valve is the dependency of A on θ, and the transfer function is

$$G_v = \frac{K_v}{1 + sT_v} \tag{4.3}$$

The static dependency (A ,θ) is nonlinear with gain K_v

$$K_v \triangleq \left(\frac{dA}{d\theta}\right)^o \tag{4.4}$$

And the time constant T_v is around 0.1÷0.5 seconds

In first approximation, the transfer function of valve system and the one of the adduction system are assumed pure gains, so $G_v = K_v$ and $G_A = K_A$.

Hence the transfer function of speed regulator becomes

$$G_r = \frac{G_f(s)}{G_a(s)G_v(s)} = \frac{P_n}{f_n b_P K_A K_V} \frac{1 + sT_2}{1 + sT_1} \tag{4.5}$$

Defining the permanent opening droop b_P' and the transient opening droop $b_t{}'$:

$$b_t{}' \triangleq \frac{b_t(\theta_n K_V K_a)}{P_n} \tag{4.6}$$

$$b_p{}' \triangleq \frac{b_p(\theta_n K_V K_a)}{P_n} \tag{4.7}$$

The final formula for speed regulator transfer function is:

$$G_r(s) = \frac{\theta_n}{f_n} \frac{1 + sT_2}{b_P^{'} + sT_2 b_t{}'} \tag{4.8}$$

(4.8) in per unit is:

$$g_r(s) = \frac{\frac{\Delta\theta}{\theta_n}}{\frac{\Delta\varepsilon_f}{f_n}} = \frac{1 + sT_2}{b_P^{'} + sT_2 b_t{}'} \tag{4.9}$$

There are two solutions to obtain a transfer function like (4.9): speed regulator with tacho-accelerometer and speed regulator with transient feedback. [1]

4.1.1 Speed regulator with tacho-accelerometer

The Figure 4-2 shows the block diagram for tacho-accelerometer speed governor. [1]

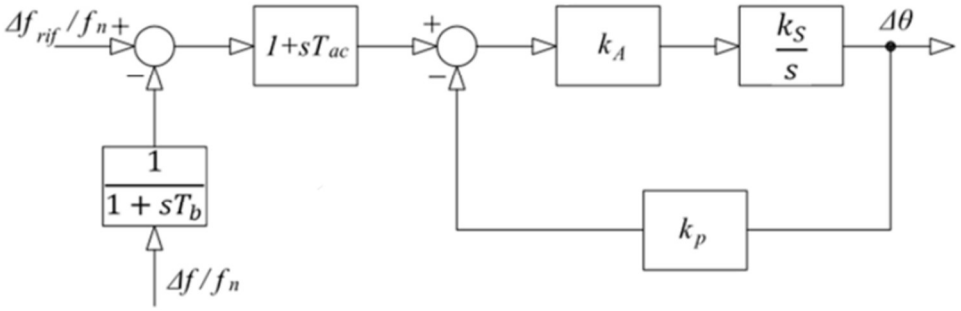

Figure 4-2 speed governor with tacho-accelerometer

The transfer function of speed regulator $g_r(s)$ is:

$$g_r(s) = \frac{1 + sT_{ac}}{1 + sT_b} \frac{1}{k_P + \frac{s}{k_A k_s}} = \frac{1}{k_p} \frac{1 + sT_{ac}}{1 + sT_b} \frac{1}{1 + \frac{s}{k_A k_S k_P}} \tag{4.10}$$

Where:

- T_{ac} is the time constant of accelerometric regulator;
- T_b is the time constant of speedometer;
- $k_A$is the booster gain;
- k_P is the constant gain of permanent feedback;
- k_S is the constant of servomotor.

The delay due to speedometer T_b is usually very low, thus is assumed negligible. The requirements to obtain (4.10) equal to the ideal case of (4.9) are:

$$\begin{cases} b'_p = k_p \\ T_1 = \dfrac{1}{k_A k_S k_P} \\ T_2 = T_{ac} \end{cases} \tag{4.11}$$

4.1.2 Speed regulator with transient feedback

The Figure 4-3 is the block diagram of speed regulator with transient feedback. [1]

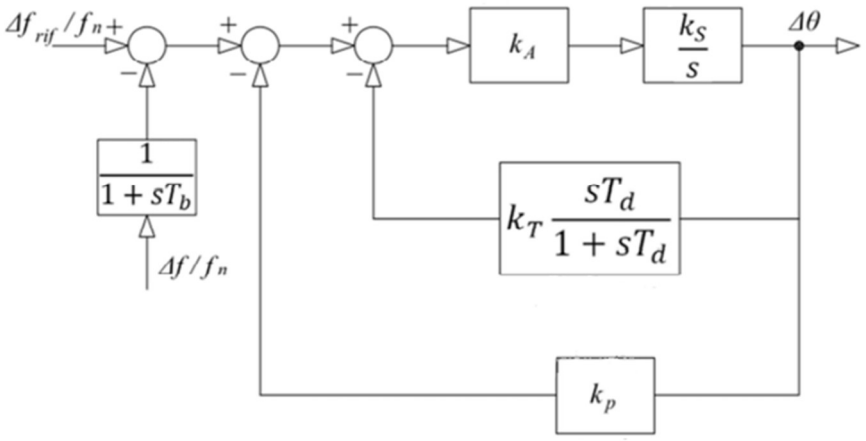

Figure 4-3 Speed regulator with transient feedback

In this case the transfer function neglecting T_b is:

$$g_r(s) = \frac{k_A k_S (1 + sT_d)}{k_A k_S k_P + s[1 + k_A k_S (k_P + k_T) T_d] + s^2 T_s} \tag{4.12}$$

Taking the following value

$$\begin{cases} k_A k_S k_T \gg \dfrac{1}{T_d} \\ k_T \gg k_P \end{cases} \tag{4.13}$$

The following expression of $g_r(s)$ is obtained:

$$g_r(s) = \frac{1 + sT_d}{k_P + s(k_P + k_T) T_d} \frac{1}{1 + sT_3} \tag{4.14}$$

In which T_3 is same order of T_b and can be neglected. The ideal $g_r(s)$ of (4.9) is obtained with these conditions:

$$\begin{cases} b'_p = k_p \\ T_1 = \dfrac{T_d (k_P + k_T)}{k_p} \\ T_2 = T_d \\ b'_t = k_P + k_T > k_T \end{cases} \tag{4.15}$$

4.2 Speed governor for Hydroelectric power plant

The hydro turbines have an initial reverse response in power due to water inertia and thus they require a large transient droop and long resetting time to obtain stable control. The final governor implies a high droop (so low gain) for fast deviation in frequency, while low droop (so high gain) and low deviation operation in frequency for steady state. [5]

4.2.1 Hydraulic-Mechanical turbine governor

The main elements of hydraulic governor are pilot valve, main servo, dashpot time constant and temporary droop.

The model of Hydro-Turbine Governor is represented in Figure 4-4 where:

- T_P is the pilot valve and servo motor time constant;
- K_S is the servo gain;
- T_G is the main servo time constant;
- R_P is the permanent droop;
- R_T is the temporary droop;
- T_R is the reset time or dashpot time constant.

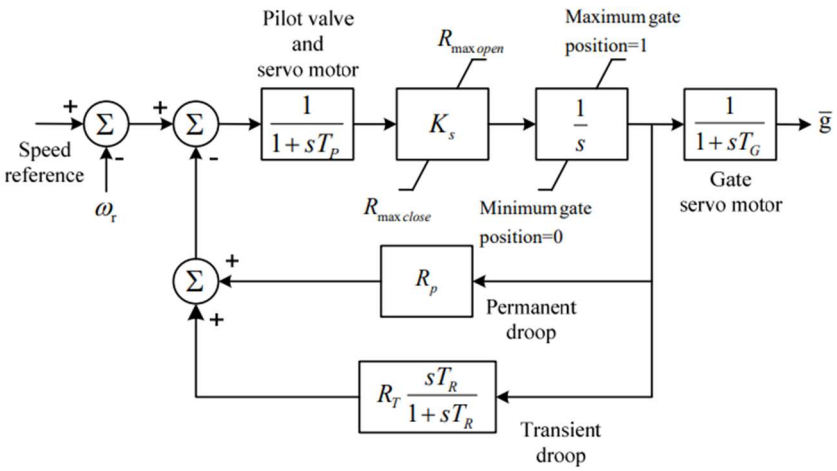

Figure 4-4 Speed regulator with transient drop

4.2.2 Electrohydraulic (PID) Governors

Nowadays, the most used speed governors for hydro turbine are electrohydraulic systems because they guarantee a greater flexibility and performance.

Electrohydraulic systems, shown in Figure 4-5, are generally formed by PID controller: the proportional term deals with the present error, the integral term with the past error and the derivate with the future error.

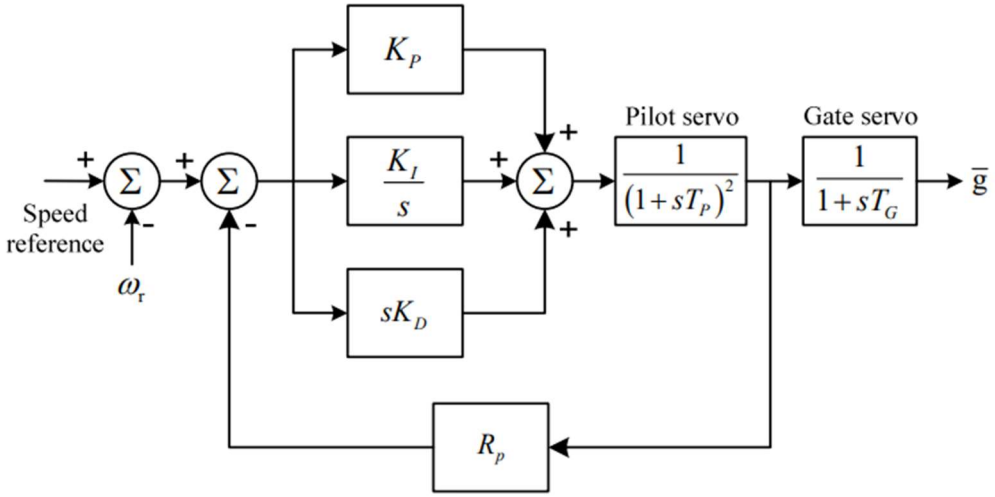

Figure 4-5 Block diagram of PID governor for hydraulic turbine

It is possible to consider only PI governor (PID without derivative part) because having high derivative term determines oscillations. In this case, the scheme results equivalent to hydromechanical governor.

4.3 Tuning of Hydro Governors

This section illustrates the basis for selection of hydraulic turbine governor settings. The stability analysis for unit in isolated operation is first presented examining linear and nonlinear model.

4.3.1 Stability of the Unit in Isolated Operation with PID governor

One of the most important considerations in selecting governor settings is having stable operation during islanding condition.

Figure 4-6 shows isolated unit of hydro power plant with the hydroelectric power plant approximated as inelastic penstock. The generator is represented by mechanical starting time T_a and the load is represented as constant power model, and the relation with frequency is given by (1.12). [5]

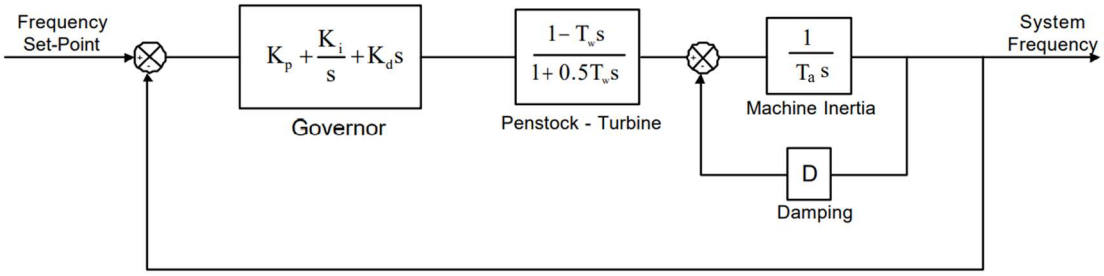

Figure 4-6 Block diagram of isolated operation

The system transfer function is:

$$G(s) = \frac{(K_p s + K_i + K_d s^2)(1 - T_w s)}{s(1 + 0.5 T_w s)(T_a s + D)} \tag{4.16}$$

The transient response of a linear closed-loop system is determined by the position of the poles of closed loop in the complex plane.

Figure 4-7 shows the response of second order system. A stable system has the necessary and sufficient condition that the transfer function has poles with no positive real part, otherwise the system is unstable.

The stable systems are divided in:

- Underdamped system, with poles with imaginary part not null and real part negative;
- Critically damped or overdamped system, with poles with imaginary part null;

- Undamped system, with poles that lay in the Imaginary axis.

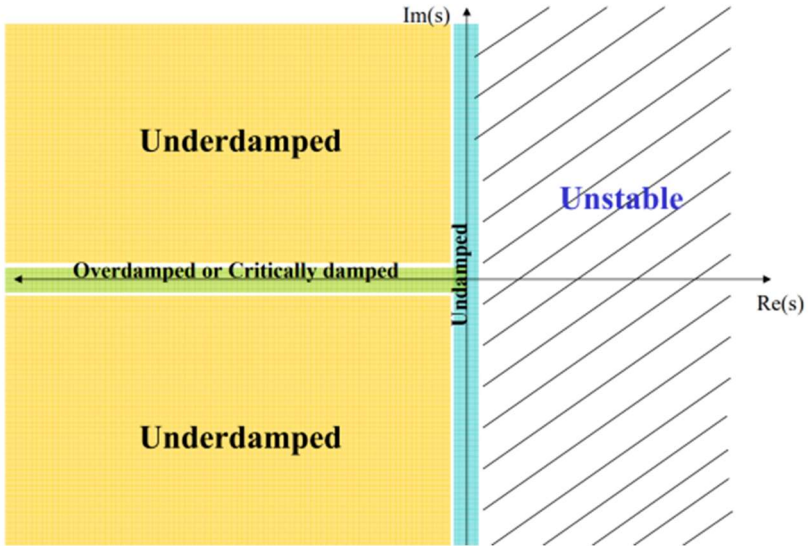

Figure 4-7 Second order system response

The research of poles is given solving in case of negative feedback loop:

$$1 + G(s)H(s) = 0 \tag{4.17}$$

with $G(s)$ the system function and $H(s)$ the feedback function.

(4.17) for the hydroelectric unit in isolated operation is rewritten as

$$\left[K_p + K_d s + \frac{K_i}{s}\right]\frac{\Delta\overline{P}_m}{\Delta\overline{G}}\left[\frac{1}{T_a s + D}\right] + 1 = \left[K_p + K_d s + \frac{K_i}{s}\right]\left[\frac{1 - T_w s}{1 + 0.5T_w s}\right]\left[\frac{1}{T_a s + D}\right] + 1 = 0 \tag{4.18}$$

4.3.2 Linearization of nonlinear model

Conventional PID governors are usually tuned using linear control theory tools. To use these methods, the turbine-penstock model has to be linear. Therefore, nonlinear models must be

linearized around the operating point, this is possible using first order Taylor series expansion. [11]

Starting from (3.9):

$$\bar{U}_0 + \Delta\bar{U} = (\bar{G}_0 + \Delta\bar{G})\sqrt{\bar{H}_0 + \Delta\bar{H}} \tag{4.19}$$

Solving for $\Delta\bar{U}$:

$$\Delta\bar{U} = \Delta\bar{G}\sqrt{\bar{H}_0} + \bar{G}_0\sqrt{\bar{H}_0}\frac{\Delta\bar{H}}{2\bar{H}_0} \tag{4.20}$$

The same is done for mechanical power:

$$\Delta\bar{P}_m = \bar{U}_0\Delta\bar{H} + \Delta\bar{U}\bar{H}_0 \tag{4.21}$$

The value $\Delta\bar{U}$ is taken by (4.20) while the value $\Delta\bar{H}$ depends on $F(s)$.

Selecting the power plant without surge tank, (3.12) is rewritten as:

$$F(s) = \frac{\Delta\bar{U}}{\Delta\bar{H}} = -\frac{B}{Z_p T_{ep} A s} \tag{4.22}$$

Where with the approximation of lumped parameter of the hyperbolic tangent:

(4.23)

- With $n = 0 \rightarrow A = 1,\ B = 1$

(4.24)

- With $n = 1 \rightarrow A = 1 + s^2\left(\frac{T_{ep}}{\pi}\right)^2,\ B = 1 + 4s^2\left(\frac{T_{ep}}{\pi}\right)^2$

(4.25)

- With $n = 2 \rightarrow \begin{cases} A = 1 + \frac{5}{4}s^2\left(\frac{T_{ep}}{\pi}\right)^2 + \frac{1}{4}s^4\left(\frac{T_{ep}}{\pi}\right)^4 \\ B = 1 + \frac{40}{9}s^2\left(\frac{T_{ep}}{\pi}\right)^2 + \frac{16}{9}s^4\left(\frac{T_{ep}}{\pi}\right)^4 \end{cases}$

The adduction transfer G_a function for linearization nonlinear model is obtained:

$$\frac{\Delta\bar{P}_m}{\Delta\bar{G}} = \frac{\Delta\bar{P}_m}{\Delta\bar{U}}\frac{\Delta\bar{U}}{\Delta\bar{G}} = \frac{2\bar{H}_0^{\frac{3}{2}}\left(\bar{H}_0 B - \bar{U}_0 T_w A s\right)}{2\bar{H}_0 B + \bar{U}_0 T_w A s} \tag{4.26}$$

The stability analysis and the selection of parameter is realized substituting the adduction transfer function (4.26) in (4.18).

4.3.3 Hydromechanical governor requirements

The transient gain has not to exceed the limit $\frac{1}{R_t} \leq 1.5\frac{H}{T_w}$ to have accettable stability in the speed regulator. The value of transient droop can be chosen following the guidelines: [10]

- The following formula

$$R_t = \frac{T_w}{H}[1.15 - (T_w - 1)0.075] \tag{4.27}$$

Where H is the inertia constant equal to two times the mechanical starting time T_a.

- Values of the ratio of $\frac{T_W}{H}$.

While the value of rest time T_R - or dashpot time constant- is suggested to be chosen with these two possible guidelines:

- T_R equal to 5 or 4 times T_W;
- Following the experimental formula

$$T_R = T_w[5 - (T_w - 1)0.5] \tag{4.28}$$

The above considerations are done when the unit is at full load supplying an isolated load, the most severe requirements. For loading and unloading, during normal interconnected system operation, the response is too slow with the previous settings: the reset time should be very low in this case, T_R less than 1.0 s; otherwise, an alternative arrangement is to bypass the dashpot in not islanding condition. [5]

The servomotor gain K_S should be set as high as possible to achieve good performance: it results in an improvement in damping and rate of response. Figure 4-8 shows the influence of servo gain constant: increasing K_S, it is obtained a higher region of stability for value R_t and T_R.

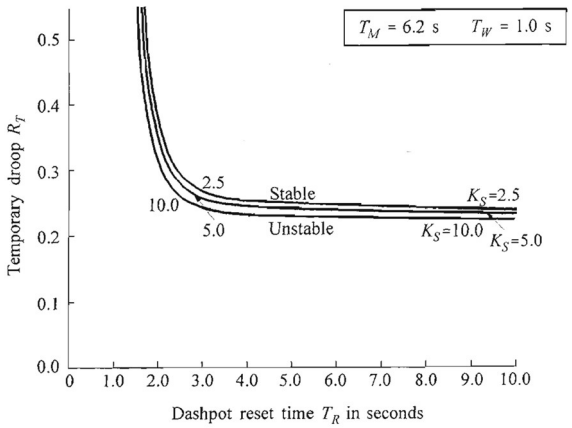

Figure 4-8 The effect of servo gain constant

Chapter 5
Dymola software

The development of models has been carried out using Dymola software based on the Modelica language.

Dymola adopts a new modeling methodology based on object orientation and equations, and the advantage of this approach is the possibility to use an acausal approach. Other highlights of Dymola that have been useful in this thesis work are:

• Handling of large, complex multi-engineering models.

• Faster modeling by graphical model composition.

• Faster simulation – symbolic pre-processing.

•Real-time simulations

5.1 Architecture of Dymola

Figure 5-1 shows the architecture of Dymola:

- it has a powerful graphic editor for composing models;
- it can also import other data and graphics files;
- Dymola contains a symbolic translator for Modelica equations generating C-code for simulation;
- the C-code can be exported to Simulink and hardware-in-the-loop platform.

[12]

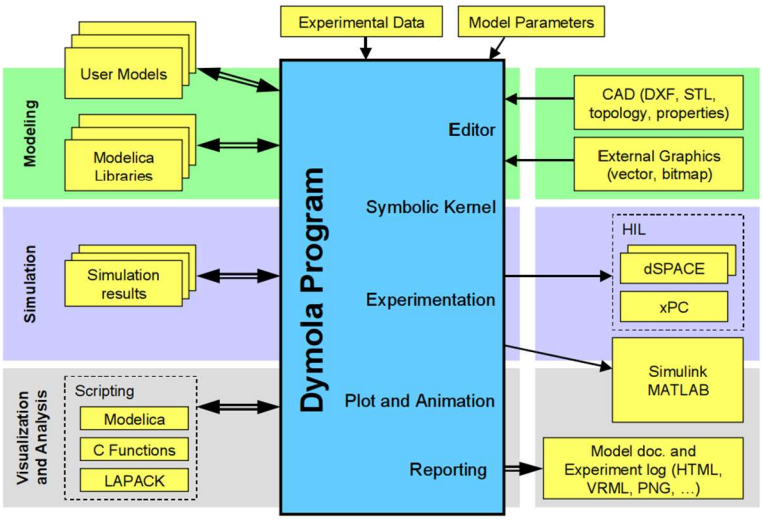

Figure 5-1 Dymola Architecture

5.2 Building models

The windows of Dymola are Main window and Library window.

The Main window can operate in one of two modes:

- Modelling mode, that is used to realize models and model components;
- Simulation mode, that is used to plot results and animate the behaviour of the models.

In the Library window there is the Modelica Standard Library, that includes the following:

- **Blocks**, that contains continuous and discrete input/output blocks such as transfer functions, filters, and sources.

- **Constants**, that provides constants from mathematics, machine dependent constants and constants from nature.

- **Electrical**, that provides electric and electronic components such as resistor, diode, MOS and BJT transistor.

- **Icons**, that provides common graphical layouts (used in the Modelica Standard Library).

- **Math**, that gives access to mathematical functions such as sine, cosine, and logarithm.

- **Mechanics**, that includes one-dimensional translational and rotational components such as inertia, gearbox, planetary gear, bearing friction and clutch.

- **SIunits**, that includes definitions with units, such as Angle, Voltage, and Inertia.

- **Thermal**, that provides models for heat-transfer.

The dynamics of hydropower plant and grid are represented by operations with transfer functions as explained in the theoretical background chapters (1,2,3 and 4). The Dymola models of this thesis work have been realized through the libraries Blocks: Math (Table 5-1) and Continuous (Table 5-2).

Table 5-1 Block Math library description / build.openmodelica.org

Name	Description
UnitConversions	Conversion blocks to convert between SI and non-SI unit signals
InverseBlockConstraints	Constructs inverse model by requiring that two inputs and two outputs are identical
Gain	Output the product of a gain value with the input signal
MatrixGain	Output the product of a gain matrix with the input signal vector
MultiSum	Sum of Reals: y = k[1]*u[1] + k[2]*u[2] + ... + k[n]*u[n]
MultiProduct	Product of Reals: y = u[1]*u[2]* ... *u[n]
MultiSwitch	Set Real expression that is associated with the first active input signal
Sum	Output the sum of the elements of the input vector
Feedback	Output difference between commanded and feedback input
Add	Output the sum of the two inputs
Add3	Output the sum of the three inputs

Product	Output product of the two inputs
Division	Output first input divided by second input
Abs	Output the absolute value of the input
Sign	Output the sign of the input
Sqrt	Output the square root of the input (input >= 0 required)
Sin	Output the sine of the input
Cos	Output the cosine of the input
Tan	Output the tangent of the input
Asin	Output the arc sine of the input
Acos	Output the arc cosine of the input
Atan	Output the arc tangent of the input
Atan2	Output atan(u1/u2) of the inputs u1 and u2
Sinh	Output the hyperbolic sine of the input
Cosh	Output the hyperbolic cosine of the input
Tanh	Output the hyperbolic tangent of the input
Exp	Output the exponential (base e) of the input
Power	Output the power to a base of the input
Log	Output the logarithm (default base e) of the input (input > 0 required)
Log10	Output the base 10 logarithm of the input (input > 0 required)
WrapAngle	Wrap angle to interval]-pi,pi] or [0,2*pi[

RealToInteger	Converts Real to Integer signal
IntegerToReal	Converts Integer to Real signals
BooleanToReal	Converts Boolean to Real signal
BooleanToInteger	Converts Boolean to Integer signal
RealToBoolean	Converts Real to Boolean signal
IntegerToBoolean	Converts Integer to Boolean signal
RectangularToPolar	Converts rectangular coordinates to polar coordinates
PolarToRectangular	Converts polar coordinates to rectangular coordinates
Mean	Calculates mean over period 1/f
RectifiedMean	Calculates rectified mean over period 1/f
ContinuousMean	Calculates the empirical expectation (mean) value of its input signal
RootMeanSquare	Calculates root mean square over period 1/f
Variance	Calculates the empirical variance of its input signal
StandardDeviation	Calculates the empirical standard deviation of its input signal
Harmonic	Calculates harmonic over period 1/f
TotalHarmonicDistortion	Output the total harmonic distortion (THD)
RealFFT	Sampling and FFT of input u
Pythagoras	Determines the hypotenuse or leg of a right triangle
Max	Passes through the largest signal
Min	Passes through the smallest signal

MinMax	Output the minimum and the maximum element of the input vector
LinearDependency	Output a linear combination of the two inputs
Edge	Indicates rising edge of Boolean signal
BooleanChange	Indicates Boolean signal changing
IntegerChange	Indicates integer signal changing

Table 5-2 Library Block in continuous/ build.openmodelica.org

Name	Description
CriticalDamping	Output the input signal filtered with an n-th order filter with critical damping
Der	Derivative of input (= analytic differentiations)
Derivative	Approximated derivative block
Filter	Continuous low pass, high pass, band pass or band stop IIR-filter of type CriticalDamping, Bessel, Butterworth or ChebyshevI
FirstOrder	First order transfer function block (= 1 pole)
Integrator	Output the integral of the input signal with optional reset
Internal …	Internal utility functions and blocks that should not be directly utilized by the user
LimIntegrator	Integrator with limited value of the output and optional reset
LimPID	P, PI, PD, and PID controller with limited output, anti-windup compensation, setpoint weighting and optional feed-forward
LowpassButterworth	Output the input signal filtered with a low pass Butterworth filter of any order

PI	Proportional-Integral controller
PID	PID-controller in additive description form
SecondOrder	Second order transfer function block (= 2 poles)
StateSpace	Linear state space system
TransferFunction	Linear transfer function

5.2.1 Initialization of models

A dynamic model describes how the states evolve in time; the states represent the memory of the model. When starting a simulation, the states need to be initialized.

Dymola allows to assume that the system is in steady state, which means that, in continuous time, the derivative shall be zero. Due to the flexibility in defining initialization equations in Modelica, it is possible to formulate more general initial conditions: a mixture of initial states and initial state derivatives is defined.

The linear models realized in thesis work have assumed steady state conditions, while for nonlinear models the state of initial output or input have been computed. [12]

Chapter 6
Dymola models of adduction system

This chapter shows the results of Dymola models regarding the adduction system of the hydroelectric power plant, which have been explained in theoretic details in Chapters 2 and 3.

The identification has been performed for the Susqueda power plant, that is a hydroelectric plant of Endesa Group in Spain described in Table 6-1. [8]

Table 6-1 Susqueda Hydroelectric Power Station parameters [8]

	Parameter:	Value:
Penstock	Length $[L]$	250 m
	Initial diameter $[d_{ic}]$	4.3 m
	Final diameter $[d_{fc}]$	3.3 m
	Average section $[A_c]$	11.34 m^2
	Pressure wave velocity $[c]$	1200 m/s
	Friction coefficient $[\phi_p]$	0.0475
Tunnel	Diameter $[d_t]$	4.3 m
	Section $[A_t]$	14.52 m^2
	Length $[L_t]$	3500 m
	Friction coefficient $[\phi_c]$	0.0010112
Surge tank	Diameter $[d_s]$	9 m

	Section $[A_s]$	63.61 m^2
	Length $[L_s]$	100 m
Turbine	Rated mechanical power $[P_m]$	86 MW
	Rated discharge $[Q_0]$	65 m^3/s
	Total head $[H_0]$	174.41 m

6.1 Linear model without surge tank effect

This section shows the results for linear models in which the surge tank effect has been assumed negligible.

6.1.1 Inelastic penstock

The transfer function of the adduction system $G_a(s)$ in case of inelasticity of the penstock and assuming no friction losses is represented as a block diagram in Figure 6-1:

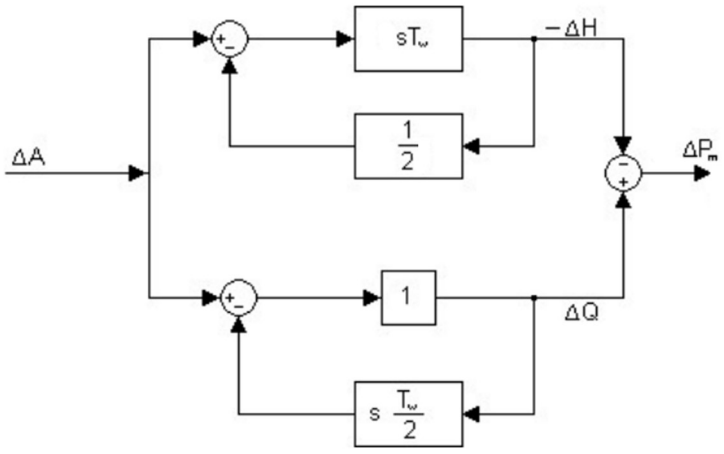

Figure 6-1 Adduction system and turbine control block

The parameter that represents the dynamics of the penstock is the water starting time T_w:

$$T_w = \frac{LQ_0}{gA_cH_0} = 0.837\ s \tag{6.1}$$

The transfer function of adduction system $G_a(s)$ is:

$$G_a(s) = \frac{\Delta\bar{P}_m}{\Delta\bar{A}} = \frac{1 - T_w s}{1 + \frac{1}{2}T_w s} = \frac{1 - 0.837s}{1 + 0.4185s} \tag{6.2}$$

Figure 6-2 shows the time response of mechanical power variation $\Delta\bar{P}_m$ after a step variation at the opening of the valve $\Delta\bar{A}$ of 0.01 p.u. at time 1 second.

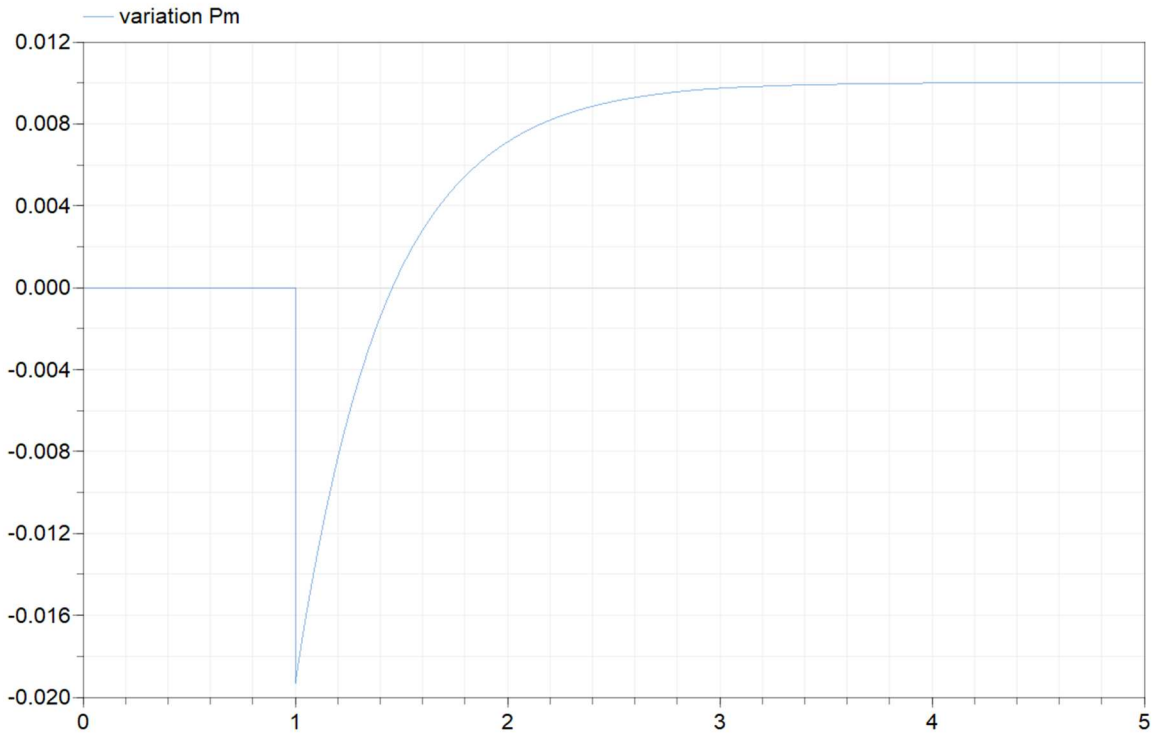

Figure 6-2 Mechanical power variation[p.u.] in time [s] after step variation of amplitude A

The mechanical power shows a transient behavior: the moment the valve opens $\Delta\bar{P}_m$ instantaneously decreases of two times the value of step variation $\Delta\bar{A}$, then increases to the value of $\Delta\bar{A}$ at steady state. Indeed, the initial value theorem gives for a step change $\Delta\bar{A}$ of 0.01 p.u.:

$$\Delta\bar{P}_m(0) = \lim_{s\to\infty} s\frac{0.01}{s}\frac{1 - T_w s}{1 + 0.5T_w s} = -0.02 \tag{6.3}$$

And the final value theorem gives

$$\Delta\bar{P}_m(\infty) = \lim_{s\to 0} s\frac{0.01}{s}\frac{1 - T_w s}{1 + 0.5T_w s} = 0.01 \tag{6.4}$$

The negative behavior of $\bar{P}_m$ is due to the inertia of the water: when the valve is opened the water cannot instantaneously change the flow due to its weight, and consequently the pressure across the turbine is reduced so the mechanical power produced is lower. [5]

The time response of mechanical power $\Delta\bar{P}_m(t)$ is represented by the following expression:

$$\Delta\bar{P}_m(t) = [1 - 3e^{-\left(\frac{2}{T_w}\right)t}]\Delta\bar{A} \tag{6.5}$$

Figure 6-3 represents the variation of the volumetric flow $\bar{Q}$ and available head $\bar{H}$. The volumetric flow $\bar{Q}$, unlike the mechanical power, has the same variation of amplitude $\bar{A}$: an increase of 0.01 p.u. of $\bar{A}$ corresponds to a rise of 0.01 p.u. of $\bar{Q}$. The variation of the available head $\bar{H}$ is not relevant for the final value of mechanical power, since its total variation is null: the $\bar{H}$ decreases instantaneously of 0.02 p.u. at time 1 s for the effect of water inertia, then restores its initial value. [5]

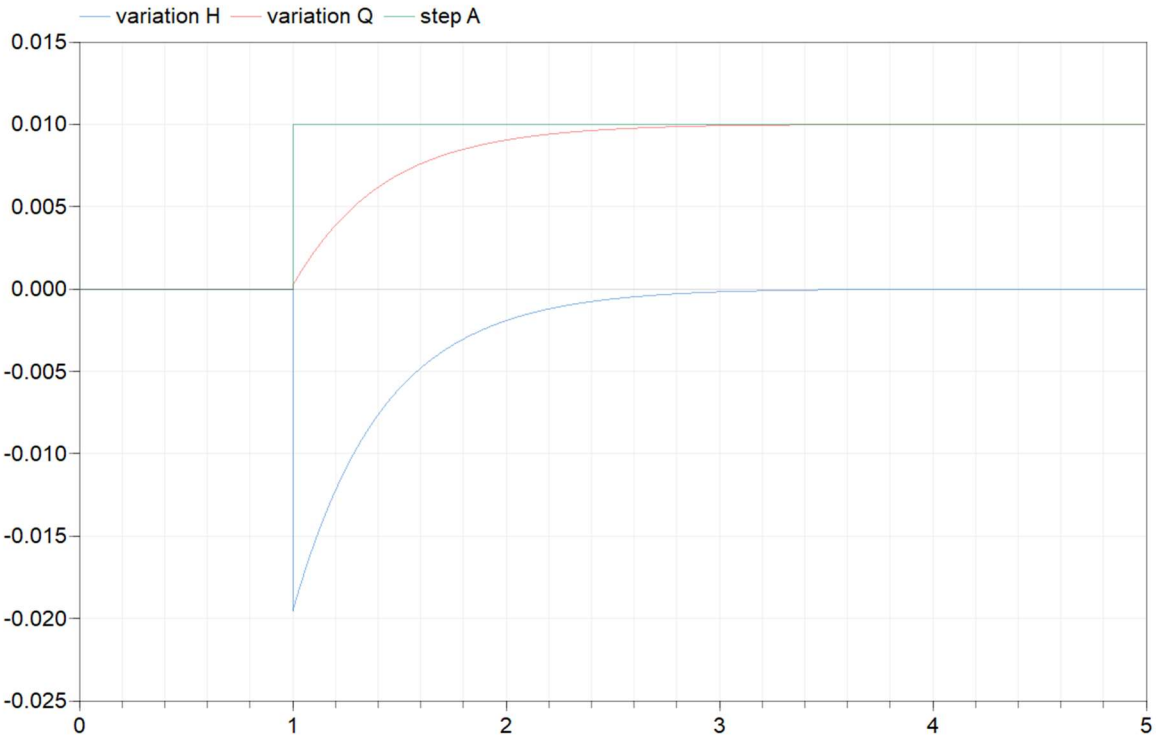

Figure 6-3 Variation of $\overline{H}$ and $\overline{Q}$ [p.u.] in time[s] for step variation of amplitude $\overline{A}$ in case of inelastic penstock

The same linear model is tested for a negative ramp of 0.01 p.u. with time duration of 1 s at time 1 s, Figure 6-4 shows the hydraulic response. Analogously to the previous case, the volumetric flow $\bar{Q}$ follows the behaviour of the amplitude $\bar{A}$: $\bar{Q}$ decreases until reaching -0.01 p.u. as steady state value. The time response of the head $\overline{H}$ starts with a ramp up with same duration of the ramp of $\bar{A}$, and then decreases restoring the initial steady state value, therefore $\overline{H}$ shows null variation. [5]

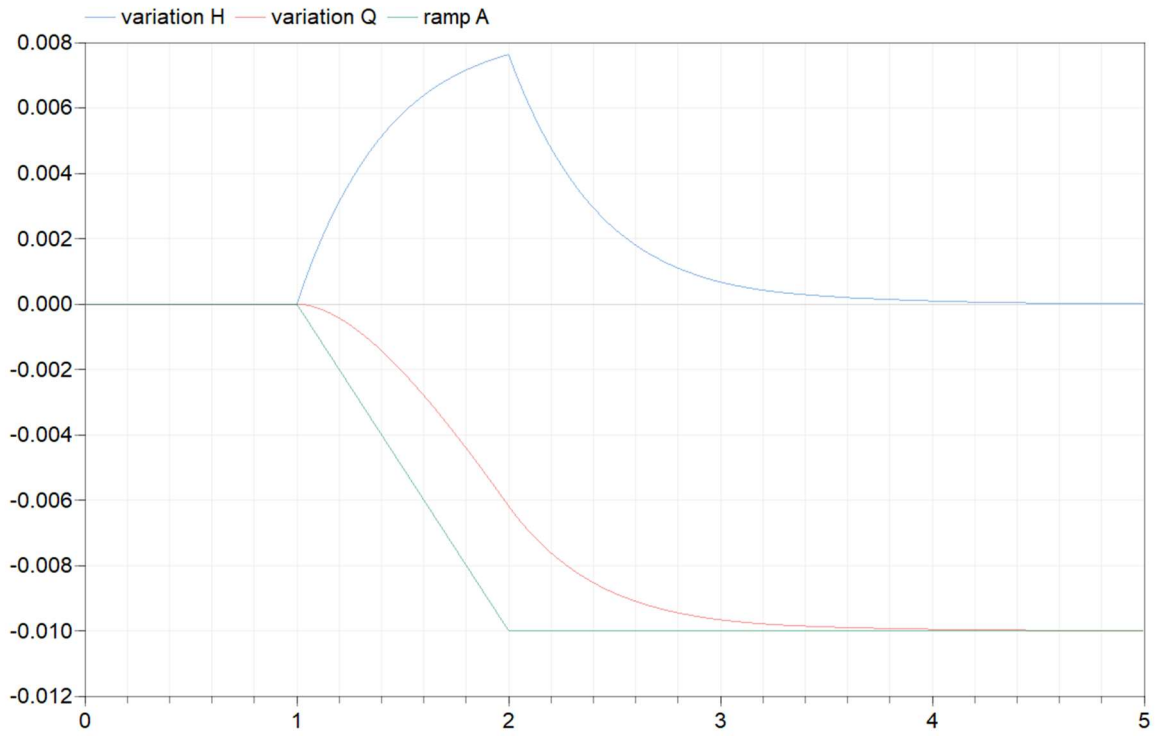

Figure 6-4 Variation of $\bar{H}$and $\bar{Q}$ [p.u.] in time[s] for ramp variation of $\bar{A}$ in case of inelastic penstock

The response of mechanical power $\Delta\bar{P}_m$in Figure 6-5 shows again the effect of water inertia: $\Delta\bar{P}_m$ increases in the transient phase instead of immediately decreasing to 0.01 p.u., but in this case the ramp variation, being less impulsive, allows not to reach the high value of two times the variation of $\bar{A}$.

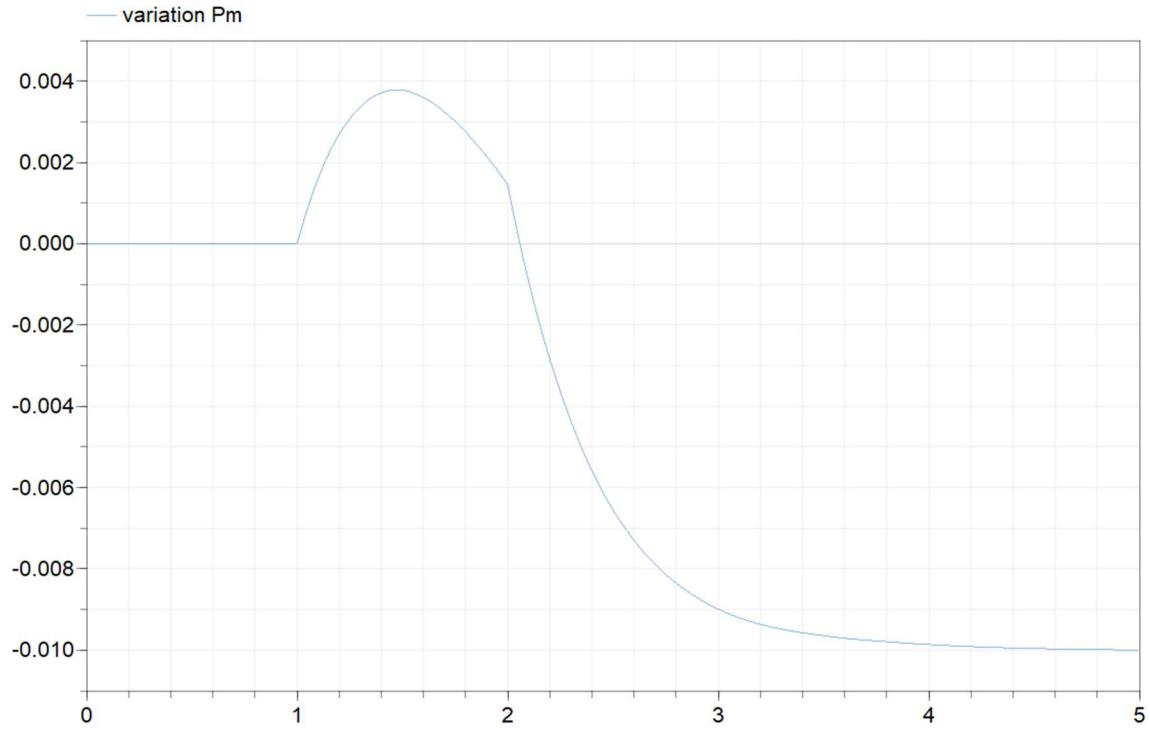

Figure 6-5 Variation of mechanical power[p.u.] in time[s] for ramp variation of $\overline{A}$ in case of inelastic penstock

6.1.2 Elastic penstock

The inelastic penstock has only one parameter-the water starting time T_w-while in the elastic penstock there is the necessity to also regard the elastic time constant T_{ep}:

$$T_{ep} = \frac{L}{c} = 0.208\ s \tag{6.6}$$

And the normalized impedance of the penstock Z_p:

$$Z_p = \frac{T_w}{T_{ep}} = 4.019\ p.u. \tag{6.7}$$

The adduction transfer function $G_a(s)$ becomes:

$$G_a(s) = \frac{\Delta\bar{P}_m}{\Delta\bar{A}} = \frac{1 - Z_p \tanh(sT_{ep})}{1 + \frac{1}{2} Z_p \tanh(sT_{ep})} = \frac{1 - 4.019 \tanh(0.208s)}{1 + 2.0095 \tanh(0.208s)} \quad (6.8)$$

$G_a(s)$ has been approximated with lumped parameter with n=1 and n=2 [1]following the formula:

$$\tanh(T_{ep}s) = \frac{1 - e^{-2T_{ep}s}}{1 + e^{-2T_{ep}s}} = \frac{sT_{ep} \prod_{n=1}^{\infty} \left[1 + \left(\frac{sT_{ep}}{n\pi}\right)^2\right]}{\prod_{n=1}^{\infty} \left[1 + \left(\frac{2sT_{ep}}{(2n+1)\pi}\right)^2\right]} \quad (6.9)$$

Figure 6-6 shows the mechanical power time response of $\Delta\bar{P}_m$ for a step at the opening of the valve of 0.01 p.u. at time 1 second for lumped parameter approximation with n=1 and n=2, which are compared with the case of inelastic penstock corresponding to the approximation n=0.

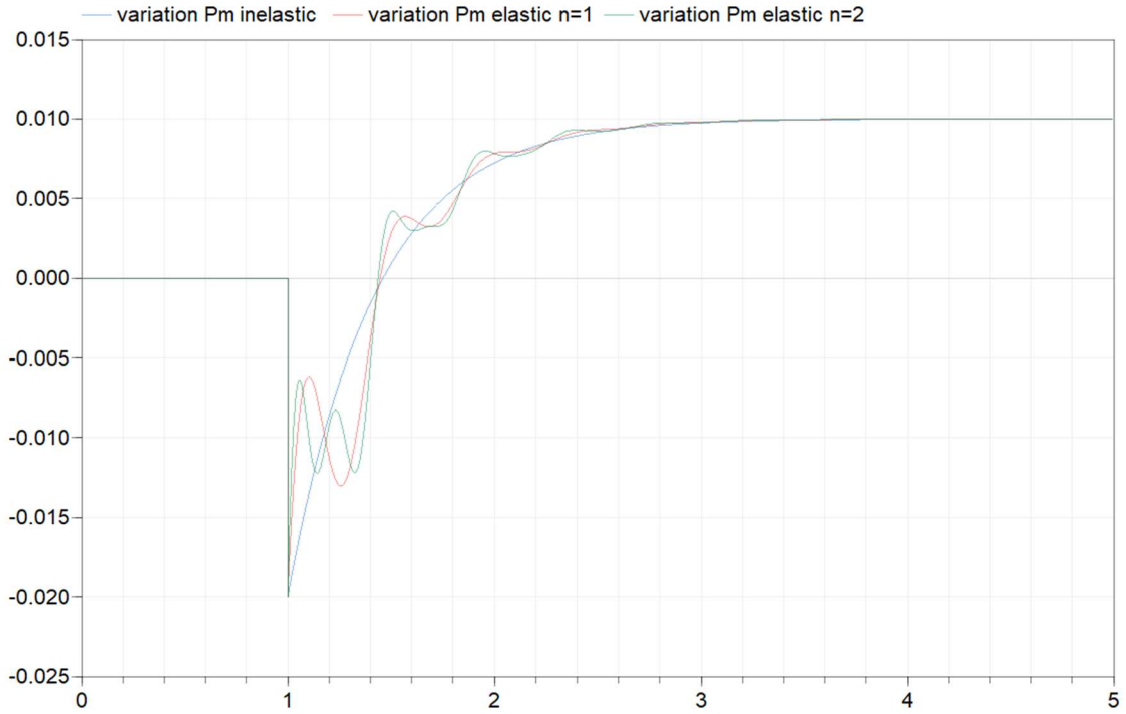

Figure 6-6 Variation of mechanical power[p.u.] in time[s] for step variation of amplitude $\bar{A}$ in case of elastic penstock

[1] The adduction transfer function for n=1 and n=2 is written in Appendix [1] and [2].

The mechanical power has the same trend of the inelastic case but has oscillations in the transient phase. Indeed, the initial value theorem and the final value theorem show the same results of (6.3) and (6.4):

$$\Delta P_m(0) = \lim_{s\to\infty} s\frac{0.01}{s}\frac{1 - Z_p\tanh\left(sT_{ep}\right)}{1 + \frac{1}{2}Z_p\tanh\left(sT_{ep}\right)} = -0.02 \tag{6.10}$$

$$\Delta P_m(\infty) = \lim_{s\to 0} s\frac{0.01}{s}\frac{1 - Z_p\tanh\left(sT_{ep}\right)}{1 + \frac{1}{2}Z_p\tanh\left(sT_{ep}\right)} = 0.01 \tag{6.11}$$

Also, the volumetric flow $\bar{Q}$ and available head $\bar{H}$[2] deviation have the same trend of the inelastic case with oscillations due to propagation effect. In Figure 6-7 the time response of $\bar{Q}$ and $\bar{H}$,using for hyperbolic tangent the approximation with lumped parameter n=1, is shown.

[2] The transfer function of the volumetric flow $\bar{Q}$ and available head $\bar{H}$ are transposed respectively in Appendix [3] and [4]

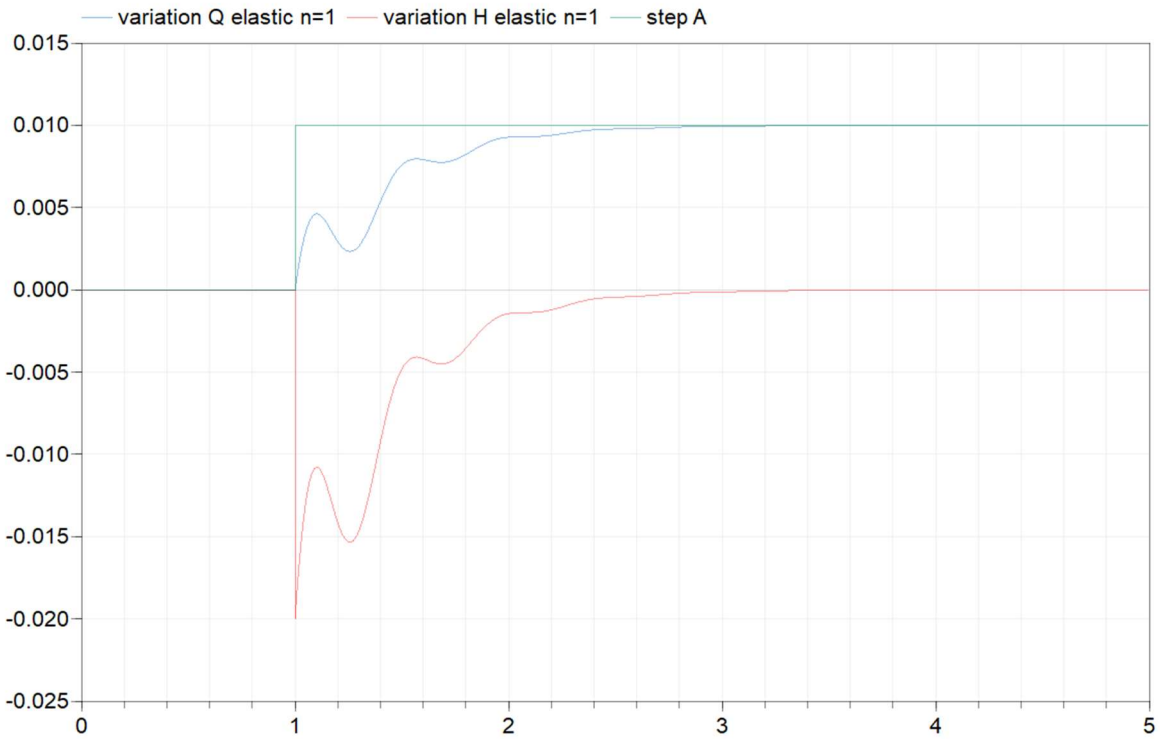

Figure 6-7 Variation of $\bar{H}$ and $\bar{Q}$ [p.u.] in time[s] for step variation of amplitude $\bar{A}$ in case of elastic penstock

6.1.3 Friction losses

The complete linear model of adduction system also takes in account also the friction losses through the friction coefficient ϕ_p. $G_a(s)$ becomes:

$$G_a(s) = \frac{1 - Z_p \tanh(sT_{ep}) - \phi_p}{1 + \frac{1}{2} Z_p \tanh(sT_{ep})} = \frac{1 - 4.019 \tanh(0.208s) - 0.0475}{1 + 2.0095 \tanh(0.208s)} \quad (6.12)$$

Figure 6-8 shows the time response of mechanical power $\Delta\bar{P}_m$ considering friction. The water column of penstock is presented in two cases: inelastic and elastic with lumped parameter approximation n=1[3]. It is worth to notice that the final value of $\Delta\bar{P}_m$ at the steady state is lower than the case without friction, while the initial value is the same; indeed, the final value theorem applied in this case gives:

[3] Transfer function of adduction system for linear model elastic penstock with lumped parameter approximation n=1 and friction is in Appendix [5]

$$\Delta\bar{P}_m\,(\infty) = \lim_{s\to 0} s\frac{0.01}{s}\frac{1 - Z_p\tanh\,(sT_{ep}) - \phi_p}{1 + \frac{1}{2}Z_p\tanh\,(sT_{ep})} = 0.01(1 - \phi_p) \tag{6.13}$$

And the initial value theorem gives:

$$\Delta\bar{P}_m\,(0) = \lim_{s\to \infty} s\frac{0.01}{s}\frac{1 - Z_p\tanh\,(sT_{ep}) - \phi_p}{1 + \frac{1}{2}Z_p\tanh\,(sT_{ep})} = -0.02 \tag{6.14}$$

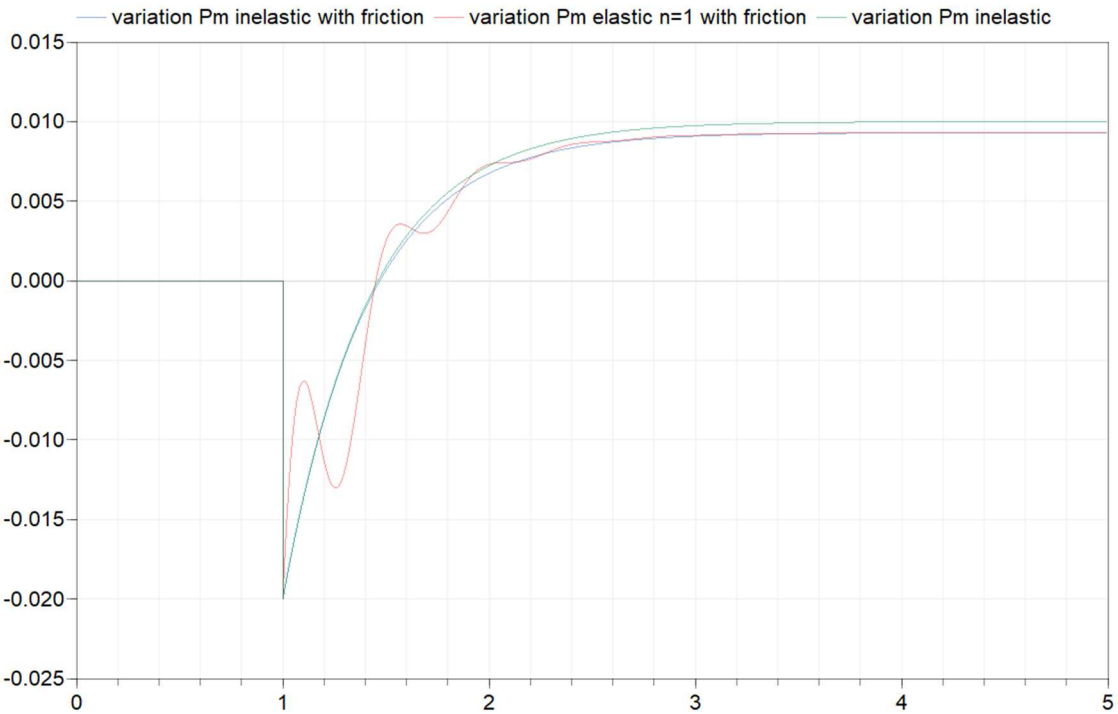

Figure 6-8 Variation of mechanical power[p.u.] in time[s] for step variation of amplitude $\bar{A}$ with friction losses

6.2 Linear model with surge tank effect

In this section, there are the results obtained for linear models with surge tank effect, with two distinctions: the case with non-elastic water columns and the one with elastic water column in the penstock and non-elastic water column in the tunnel.

6.2.1 Non-elastic water columns

The penstock is approximated with inelastic water column, and the only parameter needed is the water starting time T_w, which was previously computed. The dynamic of the tunnel is represented by water starting time T_{wc}:

$$T_{wc} = \frac{L_t}{A_t g}\frac{Q_0}{H_0} = 9.15 \text{ s} \tag{6.15}$$

The surge tank is identified by storage constant C_S:

$$C_s = \frac{A_S}{Q_0} H_0 = 170.69 \text{ s} \tag{6.16}$$

The natural period of surge tank T_S is:

$$T_S = 2\,\pi\sqrt{T_{wc} C_s} = \ \ 248.40 \text{ s} \tag{6.17}$$

The variation of mechanical power $\Delta\bar{P}_m$ is computed using (2.71):

$$G_a(s) = \frac{1 - \phi_p - Z_p T_{ep} s + \frac{G(s)}{Z_p} T_{ep} s - G(s)}{1 + \frac{1}{2}\phi_p + \frac{1}{2} Z_p T_{ep} s + \frac{1}{2} G(s) + \frac{G(s)}{Z_p} T_{ep} s} = \frac{-2.2629 s + 2.7022}{1.1315 s + 2.7022} \tag{6.18}$$

Figure 6-9 shows the time response of mechanical power $\Delta\bar{P}_m$ for a step variation of 0.01 p.u. at the gate. The transient interval of $\Delta\bar{P}_m$ behaves likes the case of inelastic penstock without surge tank effect in the transient time; but the steady state value is lower because

this model takes also in account the friction losses in pressure tunnel through the coefficient ϕ_c.

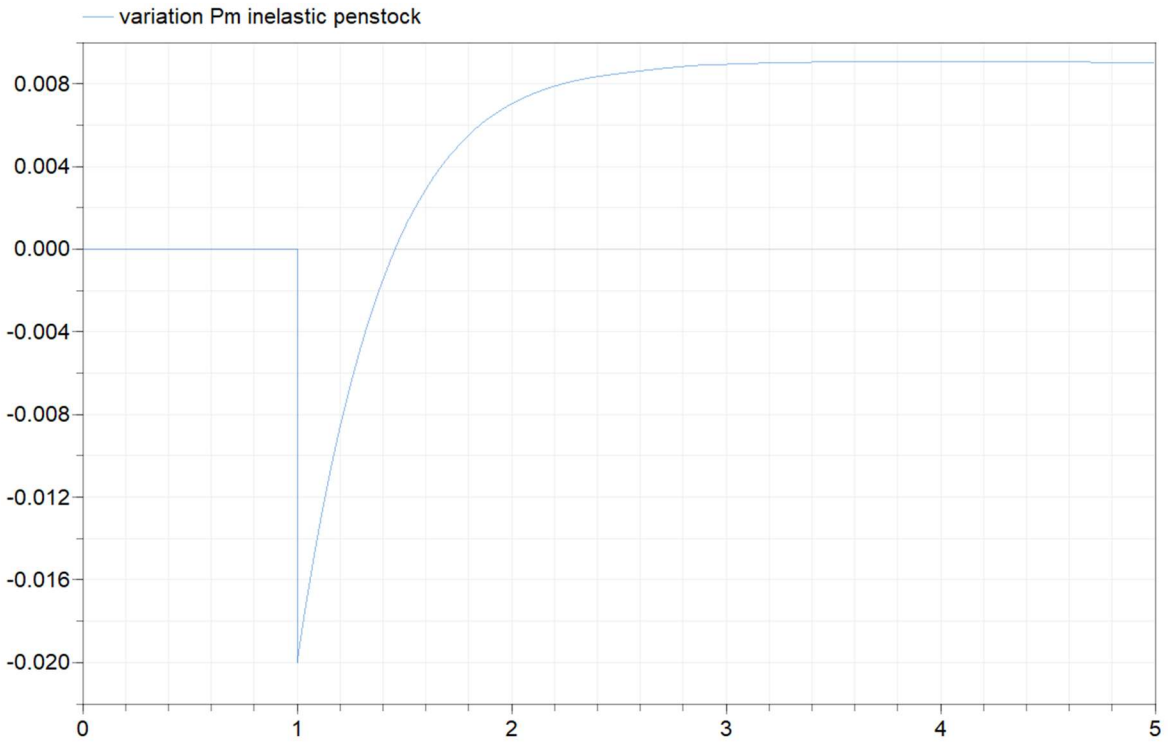

Figure 6-9 Variation of mechanical power[p.u.] in time[s] in case of surge tank effect with inelastic penstock

Figure 6-10 shows oscillations of $\Delta\bar{P}_m$ with period T_S around the steady state value after the first transient; while Figure 6-11 shows that the variation of mechanical power comes to a standstill after five times T_S.

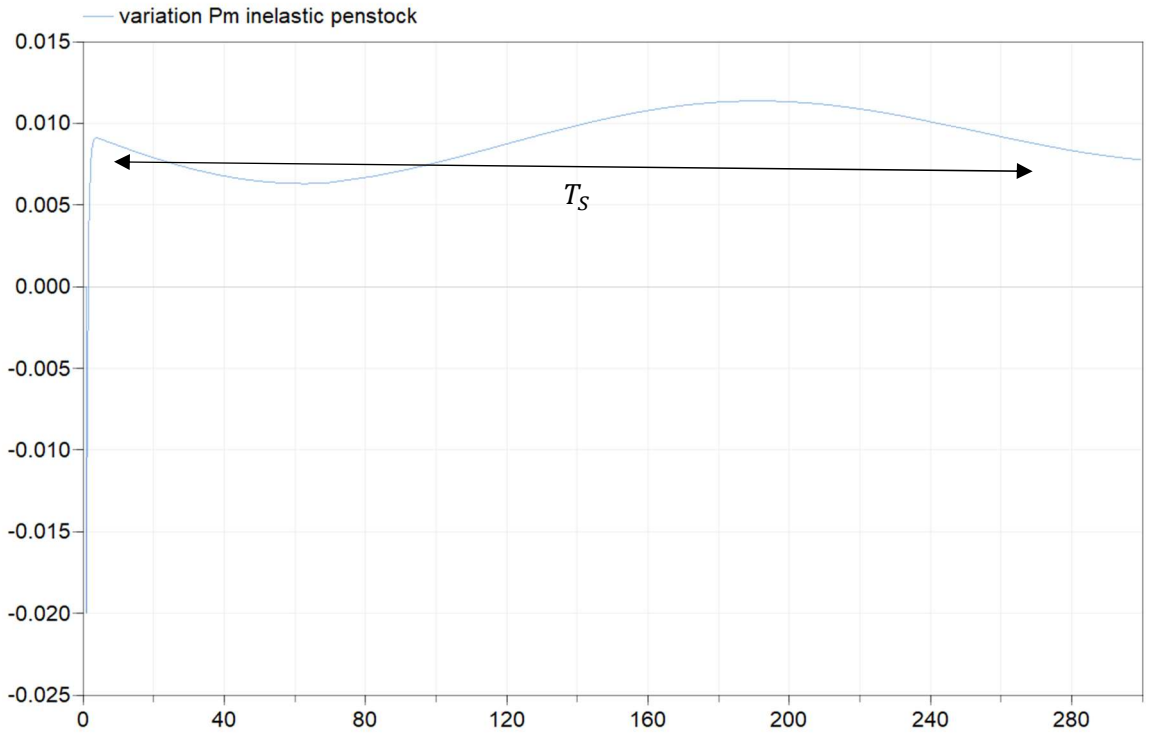

Figure 6-10 Oscillations of mechanical power[p.u.] in time[s] around steady state value

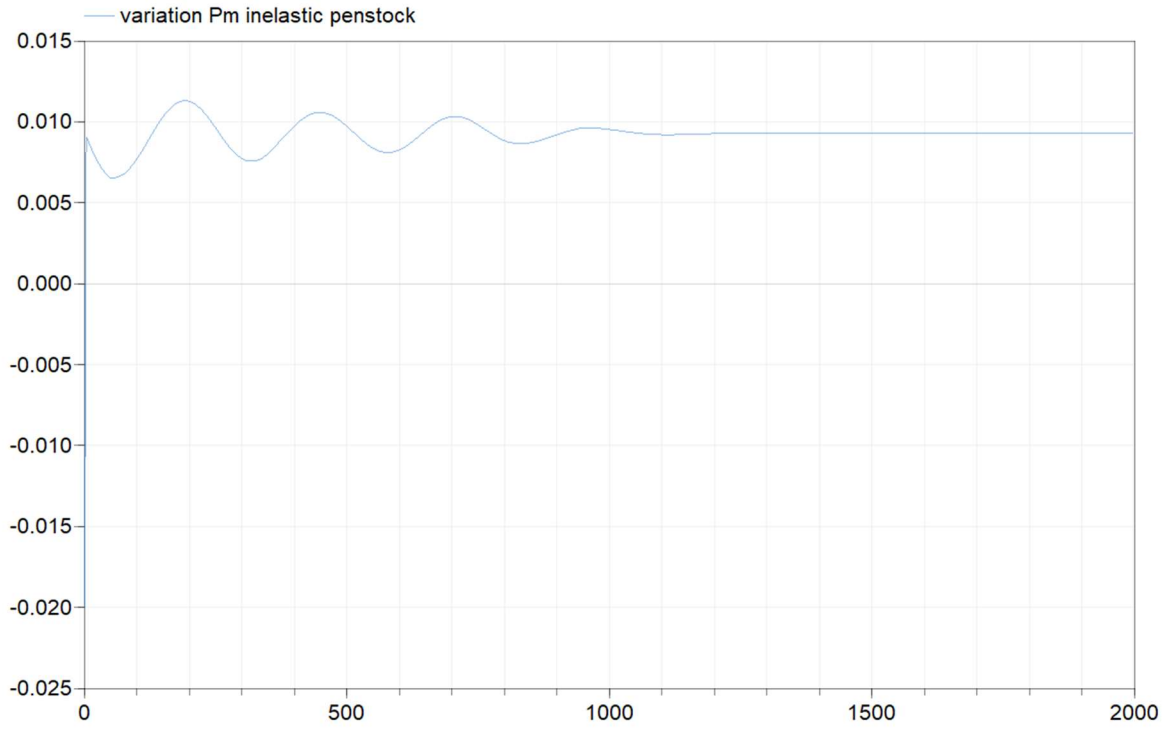

Figure 6-11 Damping of oscillations of mechanical power[p.u.] in time[s]

6.2.2 Elastic water column in the penstock and non-elastic water column in the tunnel

The elastic behavior of penstock is represented by elastic time T_{ep} (6.6) and normalized impedance of penstock Z_p (6.7) as for the model without surge tank effect.

The variation of mechanical power $\Delta\bar{P}_m$ has been computed through the adduction transfer function (2.70) with approximation of lumped parameter n=1[4].

The time response of $\Delta\bar{P}_m$ is shown in Figure 6-12: there are oscillations in transient time due to the propagation of elastic waves. Figure 6-13 shows that in the long term there are no differences with the inelastic case because the propagation of pressure waves and the correlated water hammer effect are fast phenomena.

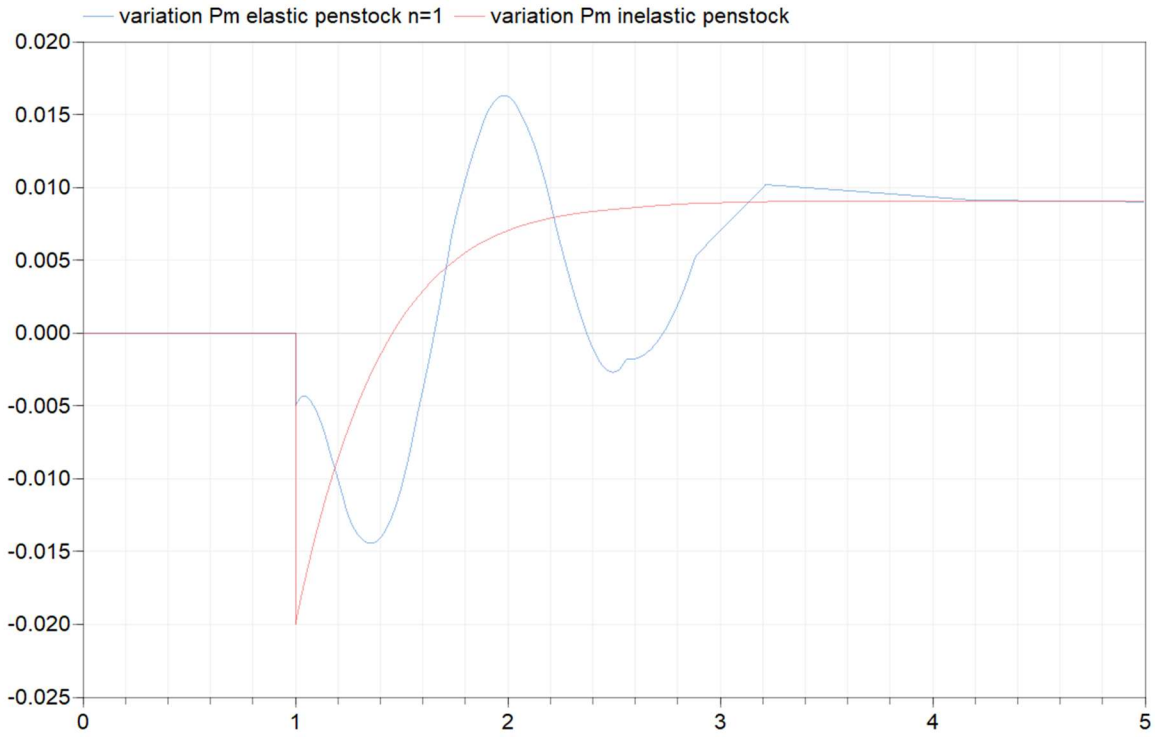

Figure 6-12 Variation of mechanical power[p.u.] in time[s] in case of surge tank effect with elastic penstock

[4] G_a is reported in Appendix [6].

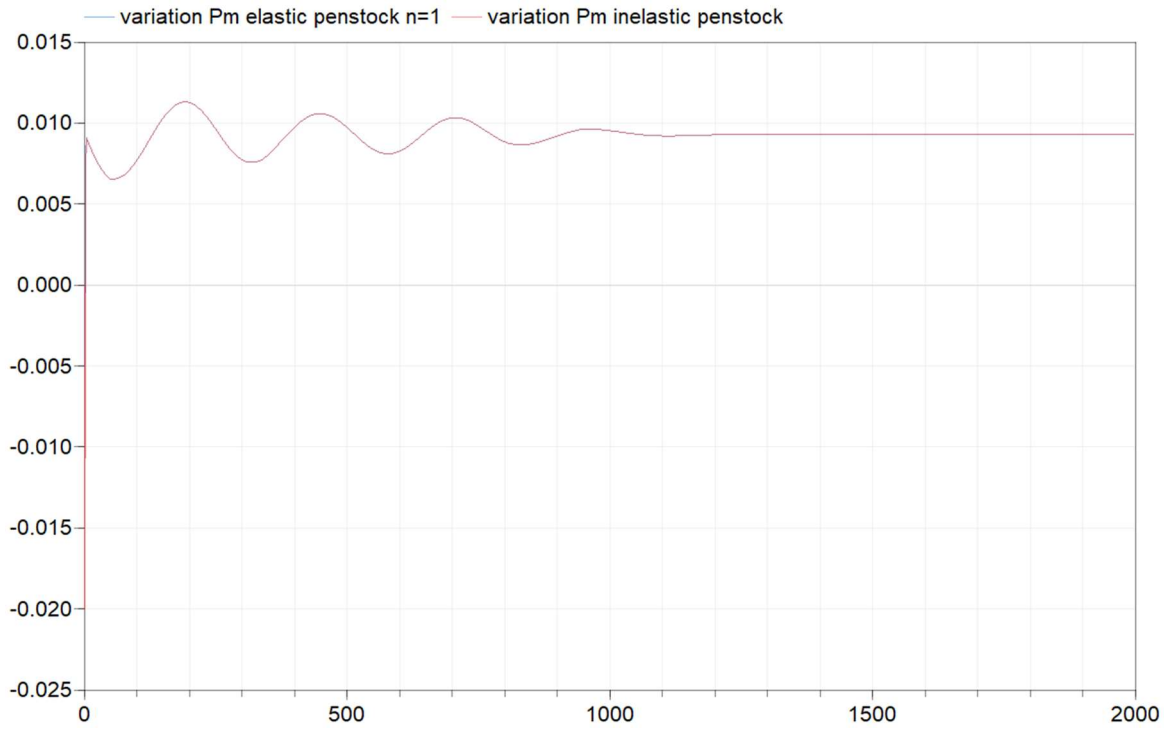

Figure 6-13 Damping of oscillation of mechanical power[p.u.] in time[s] with elastic penstock

6.3 Nonlinear model without surge tank effect

This section has examined the nonlinear model of the Susqueda Hydroelectric Power Station taking in consideration only the dynamics of penstock. The model chosen is the one of IEEE W. group 1992 in Figure 3-4, because the dynamics are more explicit rather than Kundur model allowing to observe singularly the variables.

The gate opening at no load $\bar{g}_{NL}$ is equal to 0.0778 p.u. and the gate opening at rated load $\bar{g}_{FL}$is 0.6766 p.u., hence the turbine gain function A_t is:

$$A_t = \frac{1}{g_{FL} - g_{NL}} = 1.67 \tag{6.19}$$

The no load speed $\bar{U}_{NL}$ is:

$$\bar{U}_{NL} = A_t g_{NL} (H_0)^{\frac{1}{2}} = 0.13\ p.u. \tag{6.20}$$

The initial real gate $\bar{g}$ is equal to 0.5 and the turbine self-regulation gain term D_t is considered null.

The transfer function of penstock dynamics has been approximated by lumped parameter, and need to be initialized determining the output, which is the head due to water flow $\overline{H}_{qss}$.

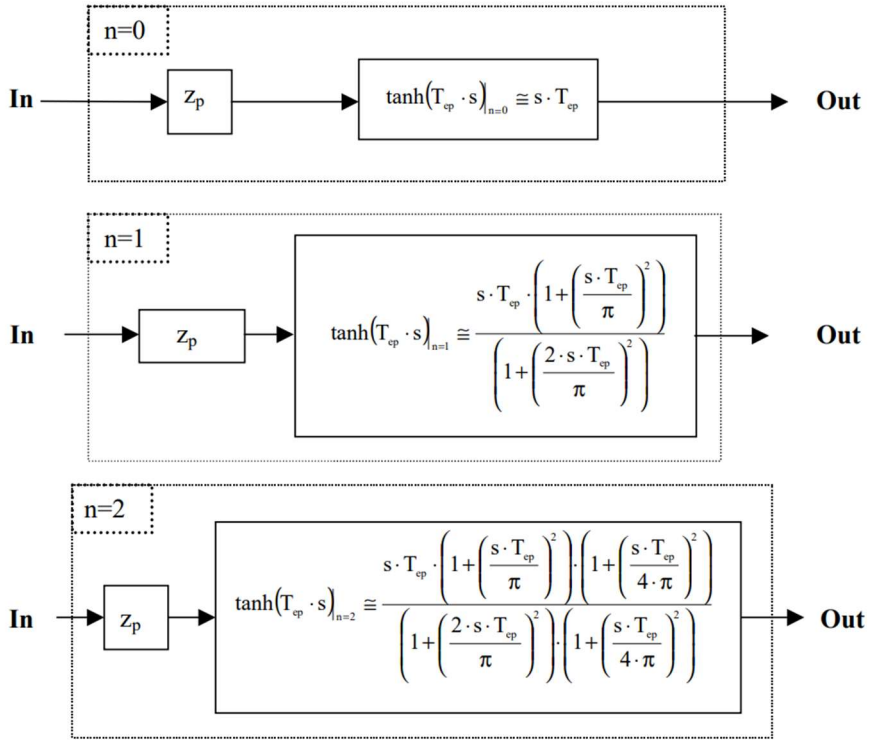

Figure 6-14 Representation of the block to calculate the approximation n=0, n=1 and n=2 of the hyperbolic tangent

Starting from the value at steady state of the waterflow speed $\overline{U}_{tss}$ (3.18):

$$\overline{U}_{tss} = \sqrt{\frac{1}{\frac{1}{\bar{g}^2} + \phi_p}} = 0.4971\ p.u. \tag{6.21}$$

through accurate computations, the initial steady state output of $\overline{H}_{qss}$is obtained equal to 0 p.u. for the cases n=0,1,2.

The time response of mechanical power $\bar{P}_{mec}$ has been analyzed for the cases n=0,1,2 after a step variation of 0.01 p.u. at time 1 second and is shown in Figure 6-15.

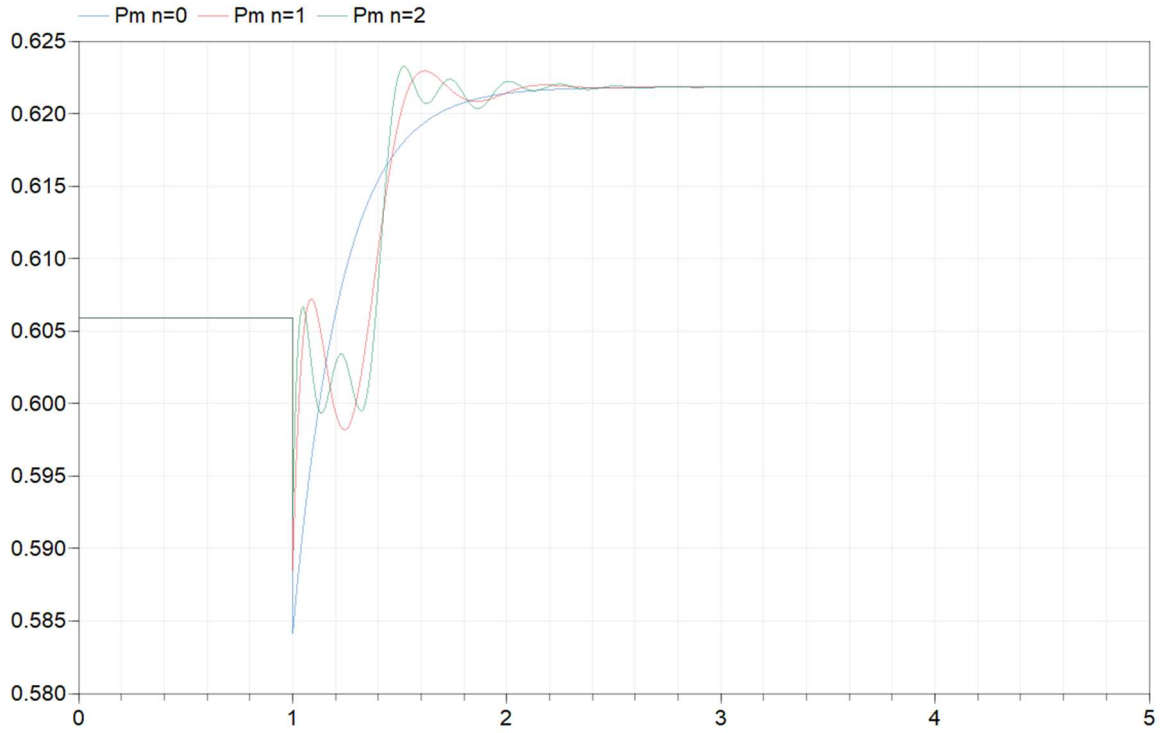

Figure 6-15 Mechanical power[p.u.] in time[s] in case of nonlinear model without surge tank effect

The initial steady state of mechanical power is:

$$\bar{P}_{mec} = A_t \bar{H}_{tss}(\bar{U}_{tss} - \bar{U}_{NL}) = 0.6058\, p.u. \tag{6.22}$$

Where $\bar{H}_{tss}$ is equal $\frac{\bar{U}_{tss}^2}{\bar{g}^2}$ so 0.9883p.u.

The final value of mechanical power $\bar{P}_{mec}$ is obtained repeating the computation of $\bar{H}_{tss}$ and $\bar{U}_{tss}$ for the new steady state with $\bar{g}$ equal to 0.51 p.u.. The values have been reported with the initial values in Table 6-2.

Table 6-2 Steady state variables

$\bar{g}$[p.u.]	$\bar{U}_{tss}$[p.u.]	$\bar{H}_{tss}$[p.u.]	$\bar{P}_{mec}$[p.u.]
0.5	0.4971	0.9883	0.6058
0.51	0.5069	0.9878	0.6217

$\bar{P}_{mec}$ has trends similar to the linear model, but the reached values are different: the linear adduction with initial gate of 0.5 p.u. provides mechanical power of 0.5 p.u., that after the variation of 0.01 p.u.at the gate decreases immediately to 0.48 p.u. and then increases to 0.51 p.u..

Figures 6-16 and 6-17 show the time response of available head $\bar{H}_t$ and water flow $\bar{U}_t$ for the nonlinear model with lumped parameter approximation with n=0,1,2. $\bar{H}_t$ and $\bar{U}_t$ have similar behavior to the linear model: the available head decreases and then tries to restore its initial value, but in the nonlinear case $\bar{H}_t$ reaches a lower steady state due to head losses in the penstock $\bar{H}_l$; $\bar{U}_t$ follows the step variation of gate increasing its value by almost 0.01 p.u..

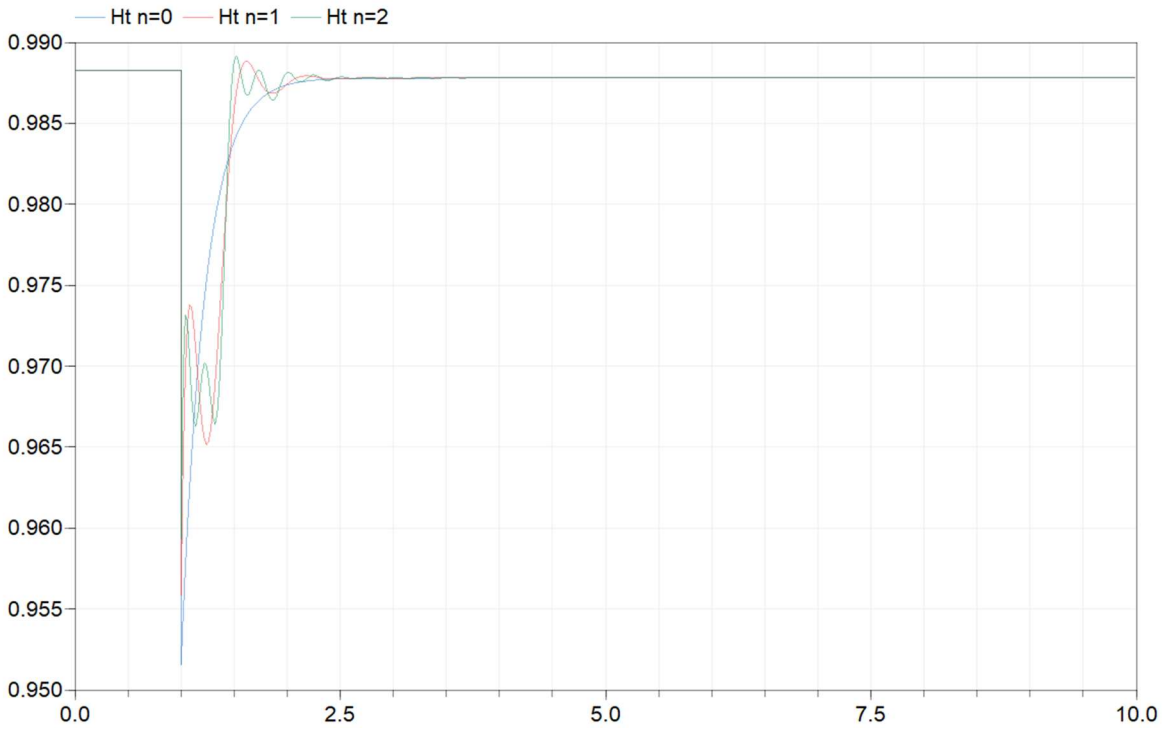

Figure 6-16 Available head in turbine[p.u.] in time[s] in case of nonlinear model without surge tank effect

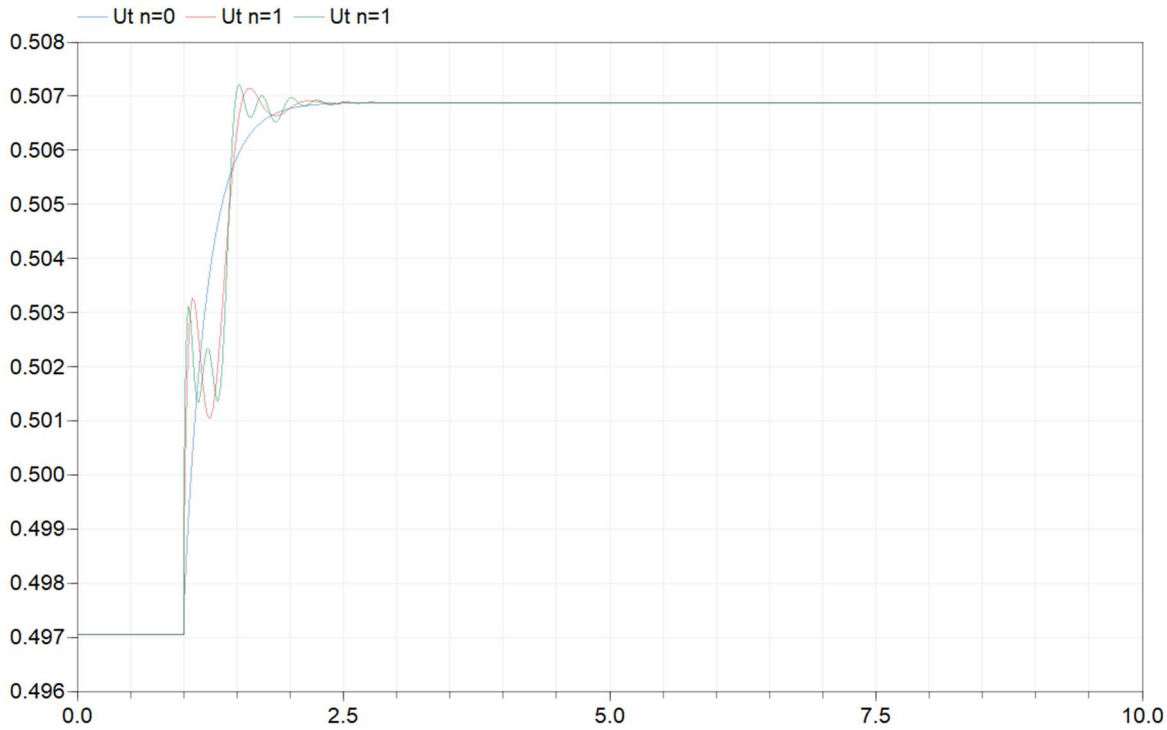

Figure 6-17 Water flow speed in turbine[p.u.] in time[s] in case of nonlinear model without surge tank effect

6.4 Nonlinear model with surge tank effect

In this section the nonlinear model of adduction system with surge tank effect of IEEE W. Group 1992 in Figure 3-5 has been analyzed.

The initialization of the three transfer functions has been done computing the steady state variables $\bar{U}_{tss}$ and $\bar{H}_{rss}$ in case of $\bar{g}$=0.5 p.u. through equations (3.29) and (3.28). The obtained values and $\bar{H}_{tss}$ -computed like previously by $\bar{U}_{tss}$- have been reported in Table 6-3 with also the final steady state variables with $\bar{g}$=0.51 p.u.

Table 6-3 Steady state at initial value and final value

$\bar{g}$[p.u.]	$\bar{U}_{tss}$[p.u.]	$\bar{H}_{tss}$[p.u.]	$\bar{H}_{rss}$[p.u.]
0.5	0.4970	0.9880	0.9998
0.51	0.5068	0.9875	0.9997

Through these values and accurate computations, the three transfer functions were initialized for these initial outputs:

- The penstock dynamic transfer function: $\bar{H}_{qss}$ equal to 0 p.u.;
- The surge tank transfer function with $\bar{H}_{rss}$equal to 0.9998 p.u.;
- The tunnel transfer function with $\bar{U}_{tss}$equal to 0.4970 p.u..

The time response of mechanical power $\bar{P}_{mec}$ is the same of the nonlinear model with only penstock for the first transient as shown in Figure 6-18. After reaching the new steady state value there are oscillations of period T_s (Figure 6-19) and then after 5 times T_s there is the damping (Figure 6-20).

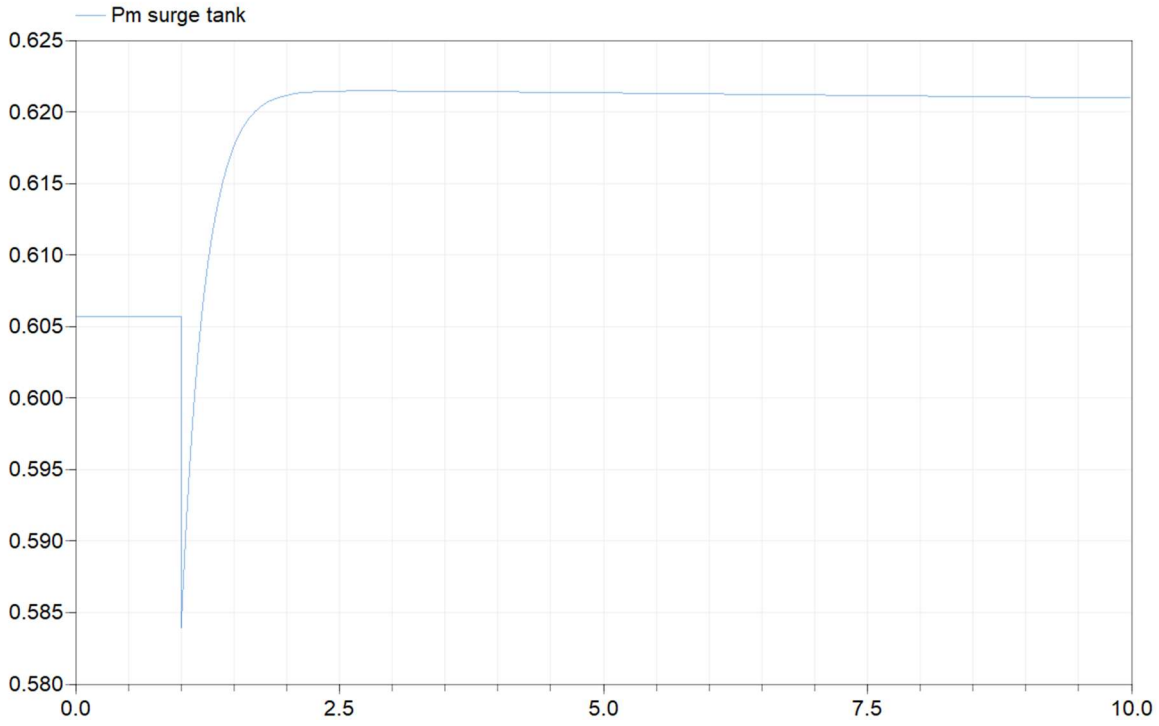

Figure 6-18 Mechanical power[p.u.] in time[s] in case of nonlinear model with surge tank effect

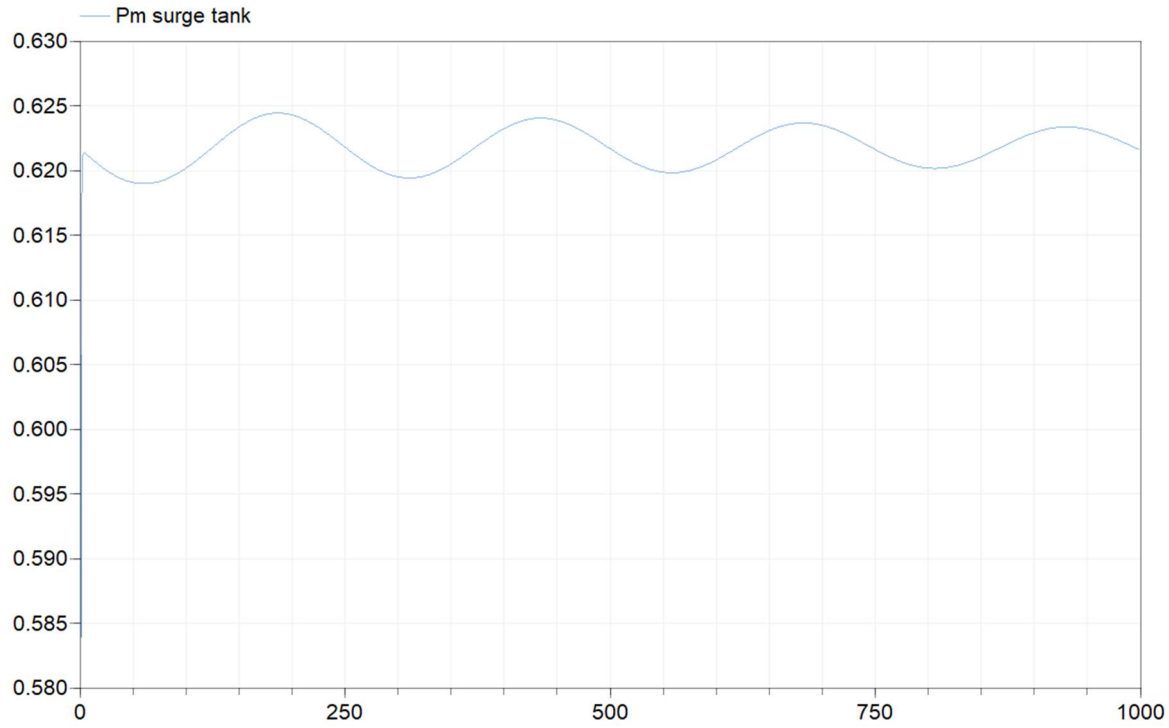

Figure 6-19 Mechanical power oscillation[p.u.] in time[s] in case of nonlinear model with surge tank effect

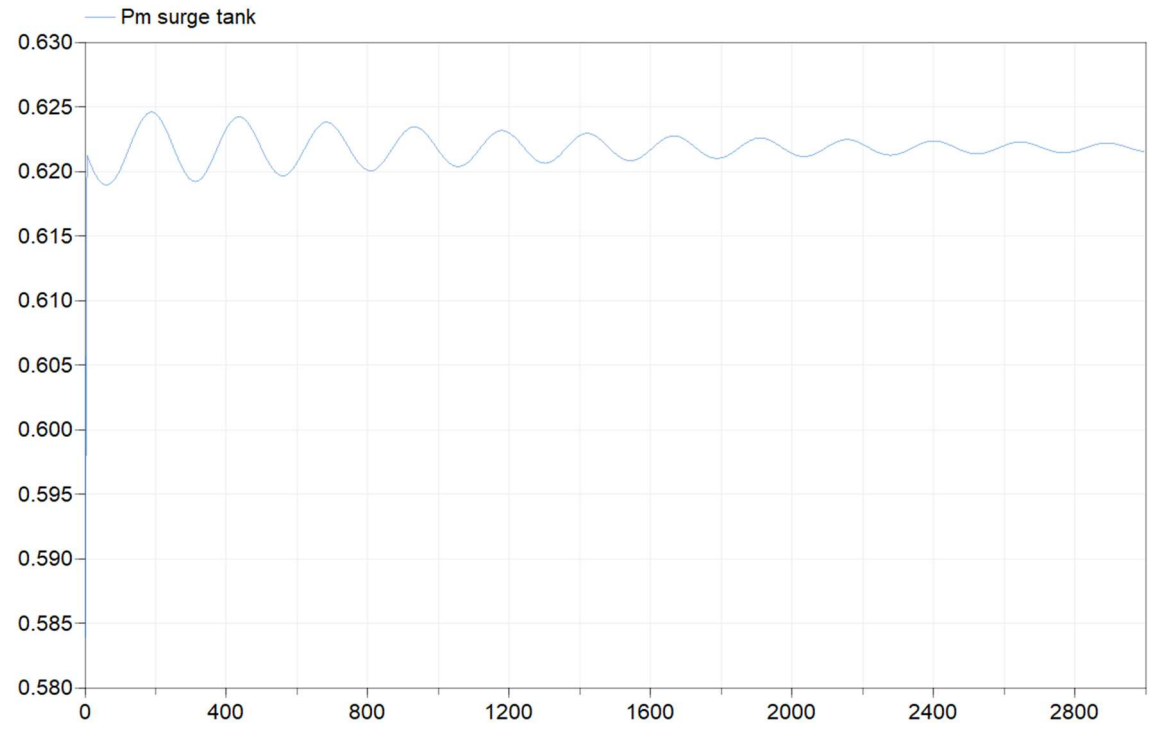

Figure 6-20 Mechanical power damping[p.u.] in time[s] in nonlinear model with surge tank effect

The physical phenomenon of power oscillation for long time period is the water mass oscillation in the surge tank and is represented by the time response of the head riser of surge tank $\bar{H}_r$ in Figure 6-21.

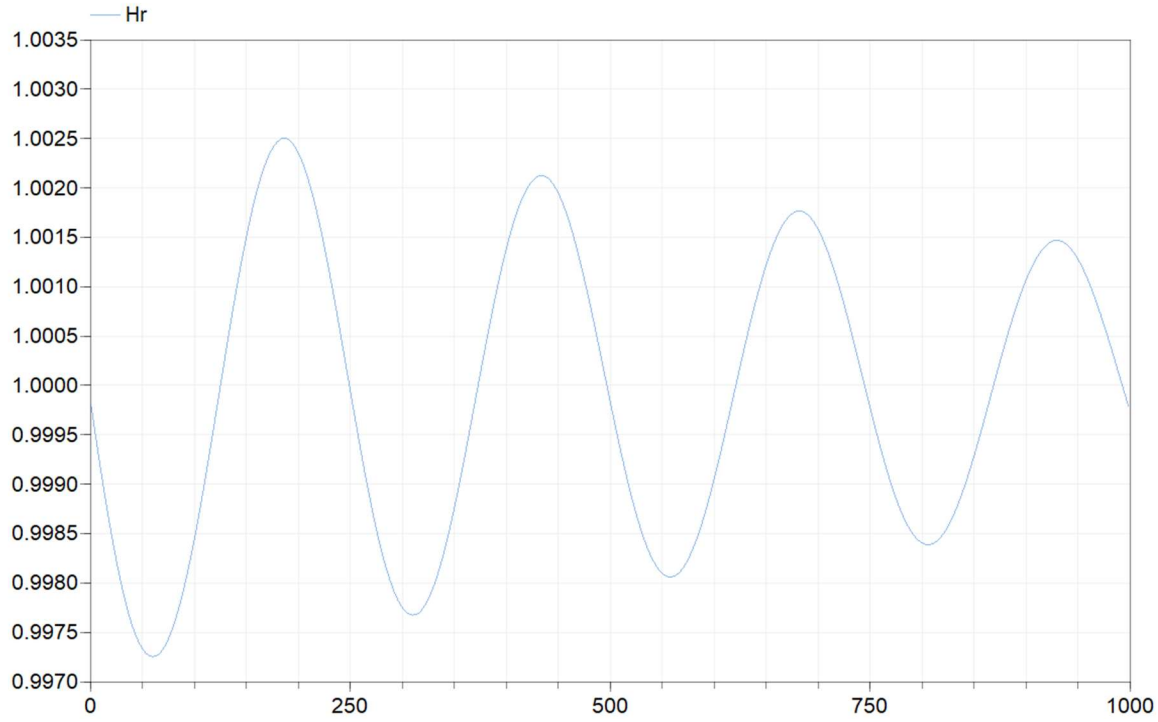

Figure 6-21 Head riser of surge tank [p.u.] in time[s] in case of nonlinear model

The propagation of elastic waves has been studied considering the penstock elastic with lumped approximation of hyperbolic tangent n=1.

Figure 6-22 shows that mechanical power $\bar{P}_{mec}$ for nonlinear model does not reach the steady state value of 0.6217 p.u. in the first 10 s: this happens because the dynamics of elastic penstock and water mass oscillation in the surge tank interfere. Starting from 0.610 p.u. $\bar{P}_{mec}$ oscillates around the final steady state value with period T_S (Figure 6-23); eventually the mechanical power reaches the final steady state (Figure 6-24).

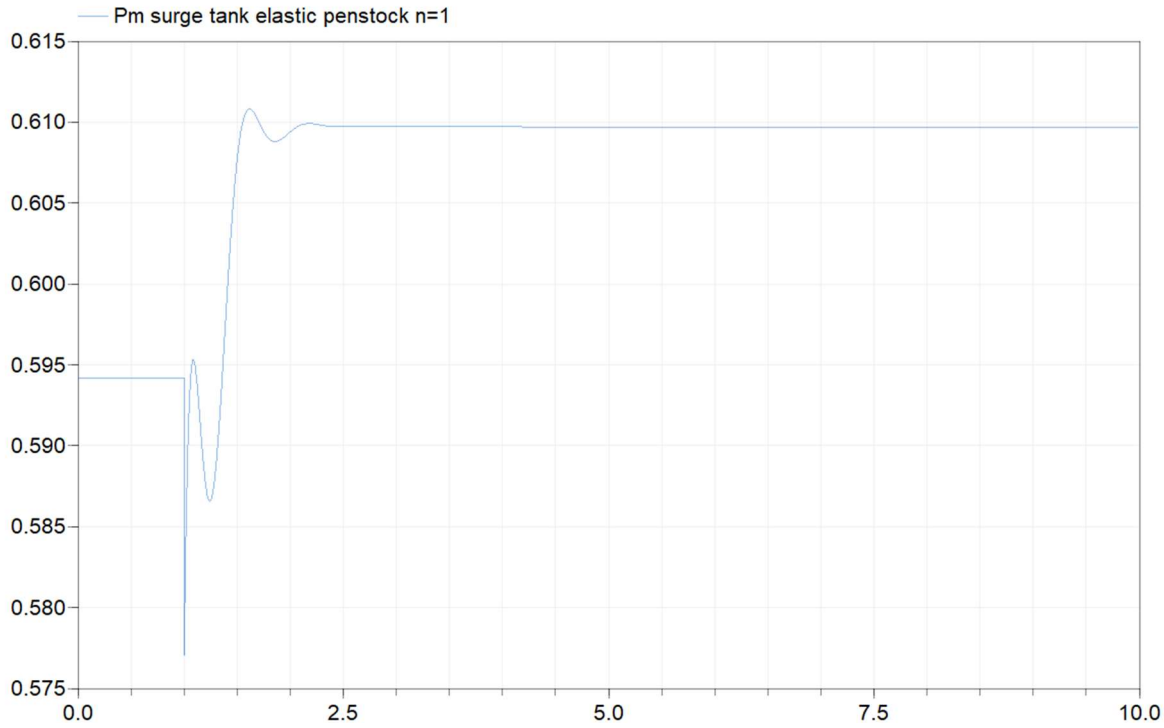

Figure 6-22 Mechanical power[p.u.] in time[s] in case of nonlinear model with surge tank effect and elastic penstock

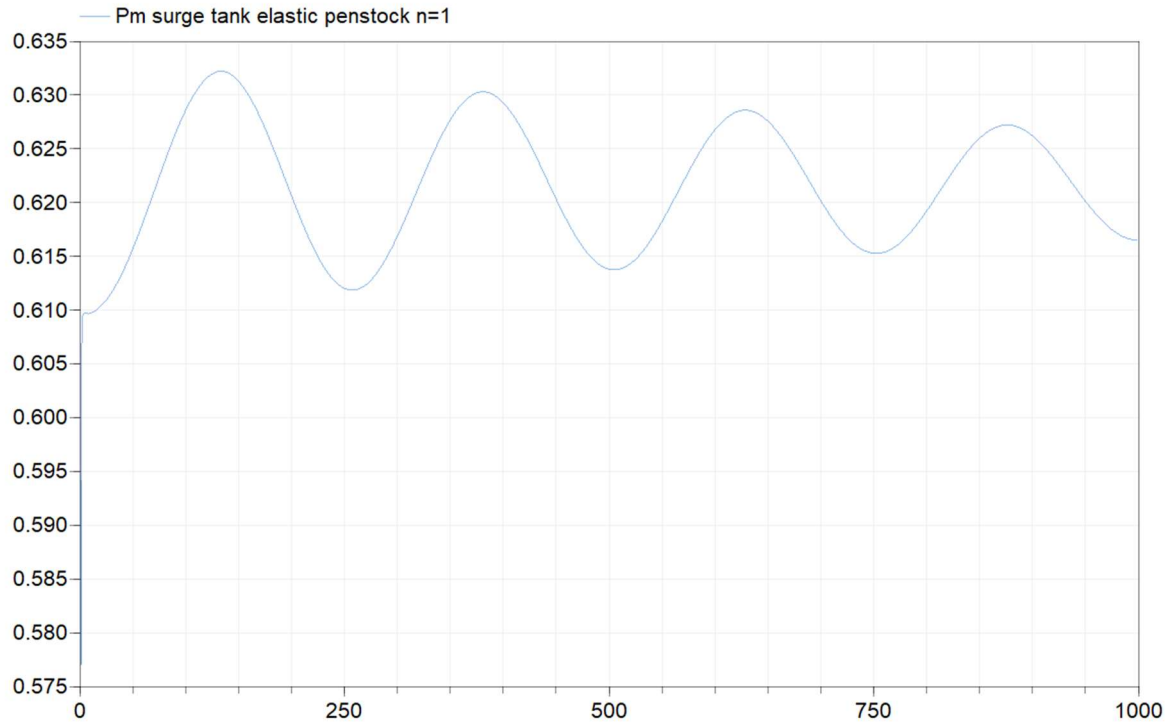

Figure 6-23 Mechanical power oscillations [p.u.] in time[s] in case of nonlinear model with surge tank effect and elastic penstock

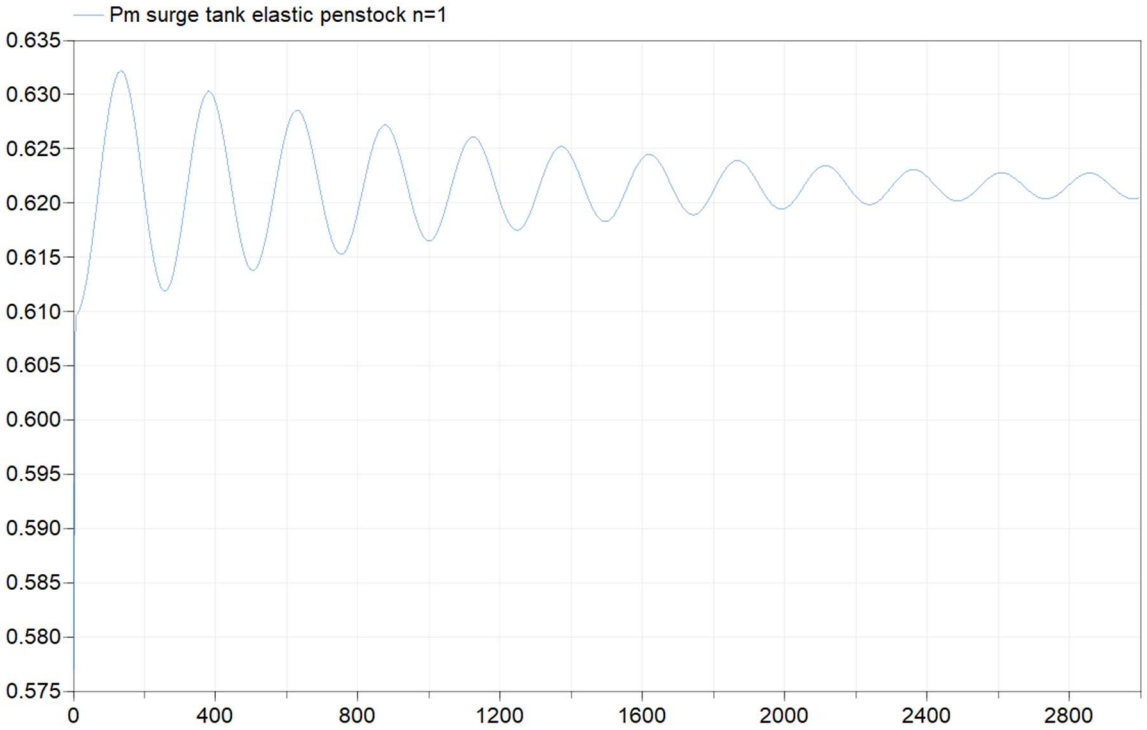

Figure 6-24 Mechanical power damping [p.u.] in time [s] in case of nonlinear model with surge tank effect and elastic penstock

Chapter 7
Dymola model of frequency control

This chapter focuses on the speed-governing system of hydraulic unit of the Susqueda power plant supplying an isolated load, and the tuning of PID speed governor has been realized through stability analysis.

Furthermore, Dymola models of frequency control with the variation of power load have been realized considering the effect of the Italian grid and the linear and nonlinear models of adduction system-analyzed in chapter 6.

7.1 Variation of frequency reference in frequency control

The control loop of frequency for isolated hydraulic unit is illustrated in Figure 7-1.

The aim is to tune the speed governor of the primary regulation in islanding operation for Susqueda power plant, which is simplified considering an inelastic penstock without surge tank. The same speed governor has been applied to the nonlinear model of Susqueda power plant.

Moreover, the effects of the water starting time T_w and mechanical starting time T_a in frequency control have been examined.

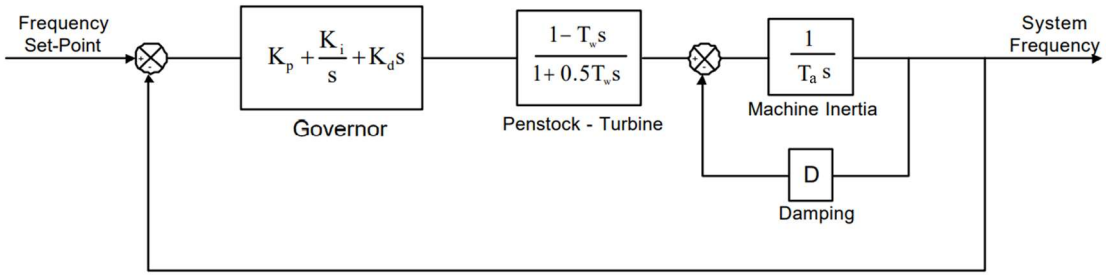

Figure 7-1 Frequency control loop for isolated hydraulic unit

7.1.1 Linear model with gain speed regulator

This analysis has considered only the proportional effect of the PID speed governor. The transfer function of speed regulator $G_r(s)$ is a gain with value equal to the reverse of the permanent droop b_p, so $G_r(s)=\frac{1}{b_p}$. [5]

(4.18) becomes:

$$\frac{1}{b_p}\,\frac{1-T_w s}{1+\frac{T_w}{s}s}\,\frac{1}{T_a s+D}+1=0 \tag{7.1}$$

The mechanical starting time T_a represents the generator: for hydroelectric unit the standard value is equal to 6 s. The load damping coefficient D is instead assumed null.

For the case study, (7.1) becomes:

$$2511 b_p s^2 + 6000 b_p s - 837 s + 1000 = 0 \tag{7.2}$$

For stability the roots of (7.2) must be in the left part of complex plant. In case of quadratic equation, a sufficient and necessary condition is that all the quadratic coefficients are positive. So,

$$\begin{cases} 2511 b_p > 0 \\ 6000 b_p - 837 > 0 \end{cases} \rightarrow b_p > 0.1395 \tag{7.3}$$

the result of the stability analysis affirms that the system is stable for values of b_p higher than 0.1395 p.u.. It is worth to notice that Terna value of permanent droop for hydro unit in islanding is 0.04 p.u., which determines an unstable system in this model. [13]

For critically damped, the discriminant of (7.2) must be zero to obtain negative real poles:

$$\left(6000 b_p - 837\right)^2 + 4 \cdot 2511 b_p \cdot 1000 = 0 \tag{7.4}$$

This equation has solution $b_p = [0.0141 ; 1.3809]$. The permanent droop of 0.0141 p.u. is less than he limiting value of stability $b_p$equal to 0.1395, so the solution for critically damped is having permanent droop of 1.3809 p.u..

The underdamped case is computed by choosing a permanent droop stable with discriminant of (7.2) higher than zero:

$$\begin{cases} b_p > 0.1395 \\ (6000b_p - 837)^2 + 4 \cdot 2511 b_p \cdot 1000 > 0 \end{cases} \tag{7.5}$$

One solution is b_p equal to 0.2 p.u..

Table 7-1 lists the permanent droops and the respective poles for the cases: underdamped, critically damped, undamped and unstable. For each case, the present study has analyzed the time response of the mechanical power $\bar{P}_{mec}$ and of the frequency $\bar{f}$ of the system after a step variation in frequency set point of 0.01 p.u. at time 1 second from steady state value of 1 p.u..

The transfer function of adduction system G_a is initialized by a null value of $\bar{P}_{mec}$, and the transfer function of the grid is initialized by 1 p.u., the frequency of the system at the steady state.

Table 7-1 Cases underdamped, critically damped, undamped and unstable

Cases:	$b_p[p.u./p.u.]$	Poles
Undamped	0.1395	[1.6896i, -1.6896i]
Critically damped	1.3809	[-2.0042, -0.1439]
Underdamped	0.2000	[-0.3614 + 1.3640i, -0.3614 - 1.3640i]
Unstable	0.0400	[2.9719 + 1.0601i, 2.9719 - 1.0601i]

Figure 7-2 shows the poles map for the 4 cases and complies with the stability theory of second order system in Figure 4-7.

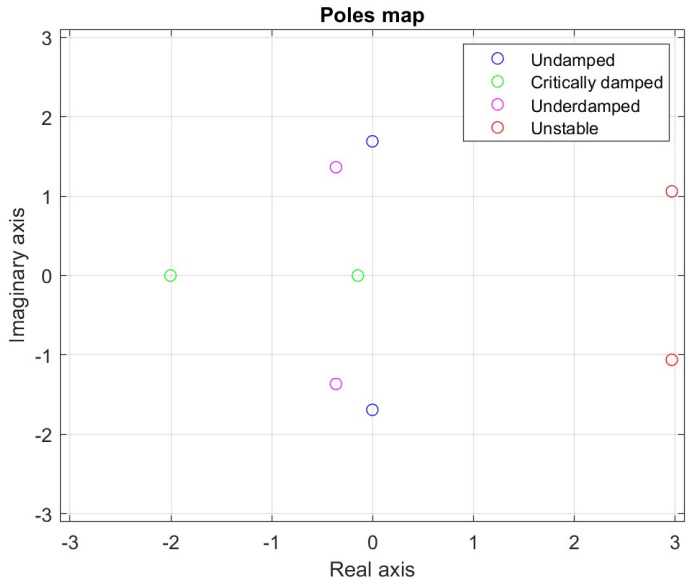

Figure 7-2 Poles map

The case with permanent droop b_p equal to 0.1395 p.u. is at the margin of stable system and is identified as undamped. The mechanical power $\bar{P}_{mec}$ after the perturbation should increase because the system must reach a value higher of frequency, but instead starts with a negative value a cause of the inertia of the water column. $\bar{P}_{mec}$ continues to increase and decrease with oscillations whose amplitude remains constant without stopping (Figure 7-3).

The period of undamped oscillation is computed:

$$T = \frac{\sqrt{2}\pi}{\left(\frac{1}{T_m T_w b_p}\right)^{\frac{1}{2}}} \tag{7.6}$$

For the study case T is 3.71 s.

The frequency of the system $\bar{f}$ starts from the steady state value of 1 p.u. and, after the perturbation, has the same trend of mechanical power (Figure 7-4).

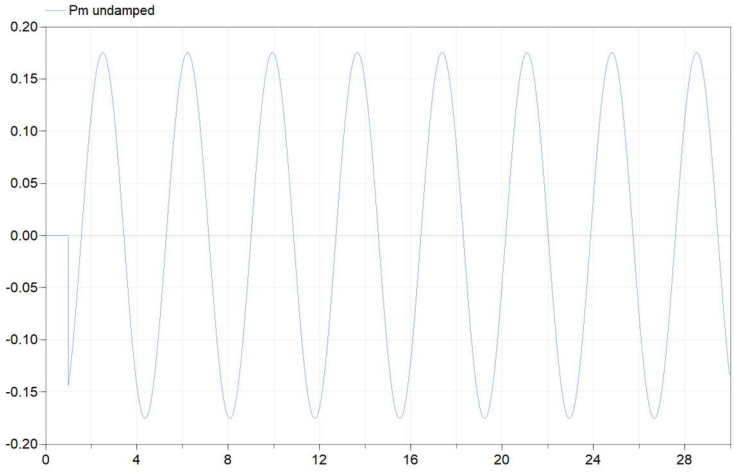

Figure 7-3 Mechanical power[p.u.] in time[s] undamped case

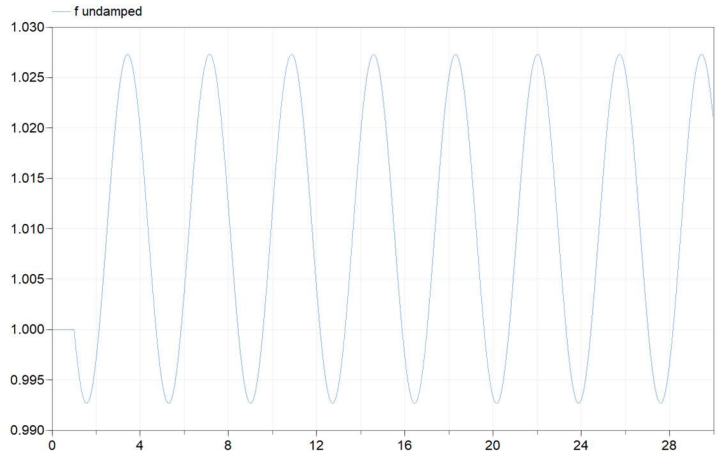

Figure 7-4 Frequency[p.u.] in time[s] in case undamped case

In the critically damped case, the frequency of the system reaches the new steady state of 1.01 p.u. quickly without oscillations (Figure 7-6). The mechanical power $\bar{P}_m$, starting with high negative value due to the inertia of water, increases and then goes to zero when the new steady state of the frequency is reached (Figure 7-5).

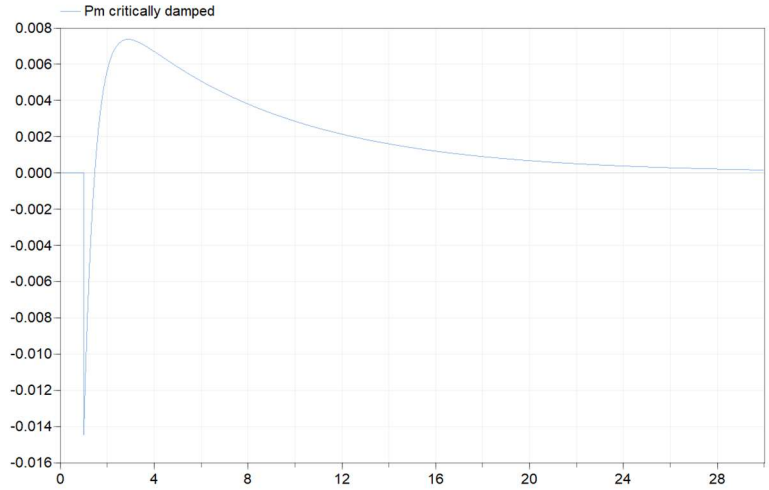

Figure 7-5 Mechanical power[p.u.] in time[s] in case of critically damped

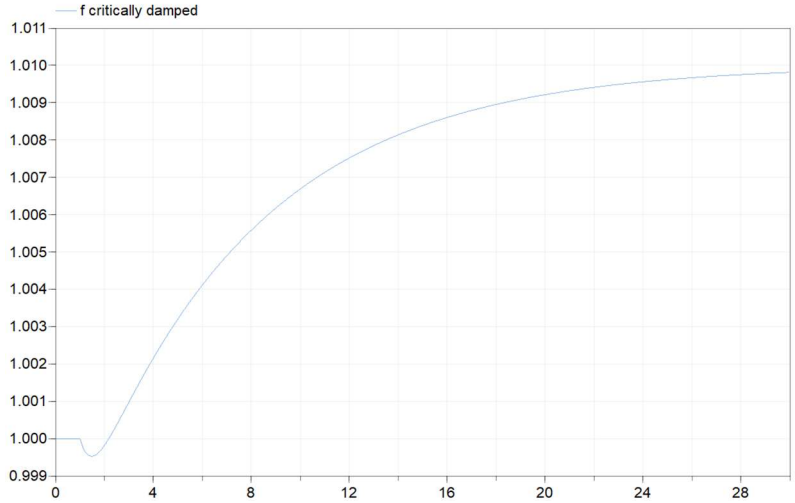

Figure 7-6 Frequency[p.u.] in time[s] in case of critically damped

The time response of $\bar{P}_m$(Figure 7-7) and of $\bar{f}$ (Figure 7-8) in underdamped case oscillates around the new steady state values and then converges respectively to 0 p.u. and 1.01 p.u..

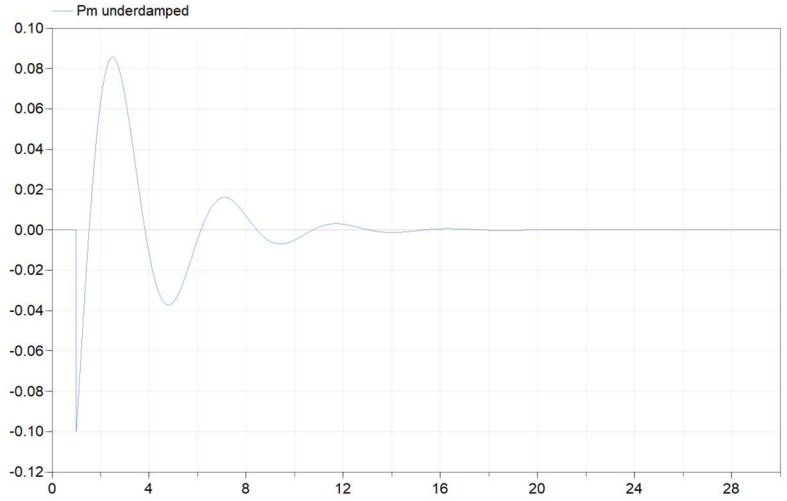

Figure 7-7 Mechanical power[p.u.] in time[s] in case of critically damped

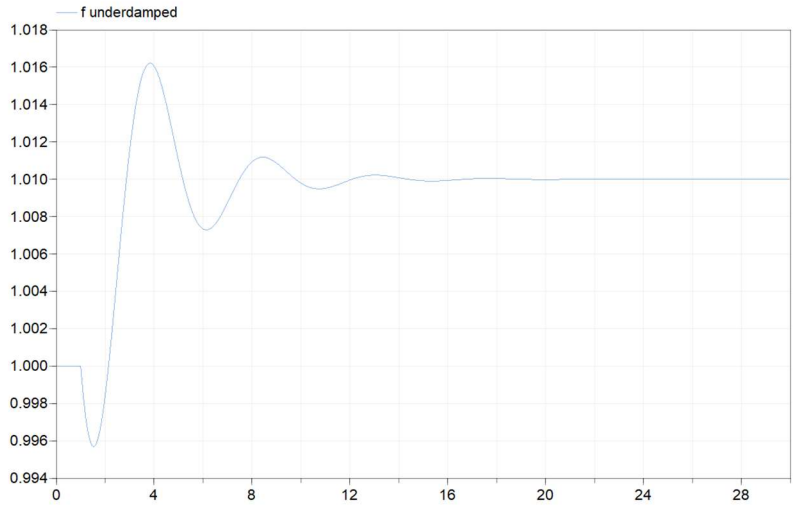

Figure 7-8 Frequency[p.u.] in time[s] in case of in case underdamped

The time response of mechanical power (Figure 7-9) and of frequency (Figure 7-10) for b_p equal to 0.04 p.u. is unstable and diverges.

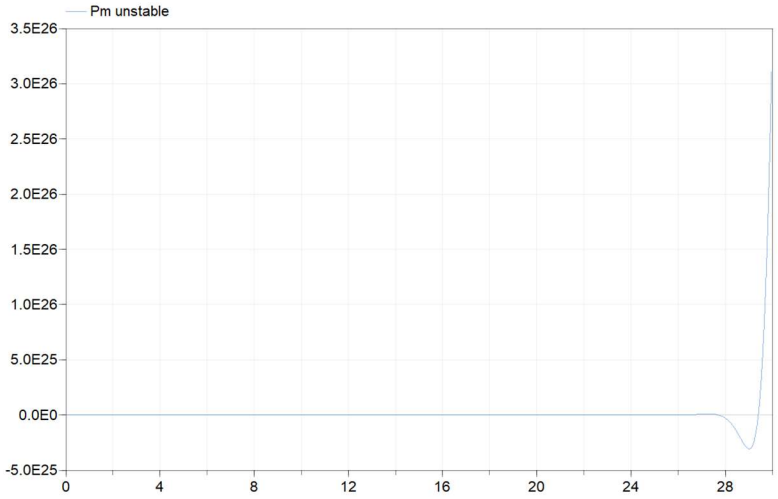

Figure 7-9 Mechanical power[p.u.] in time[s] in unstable case

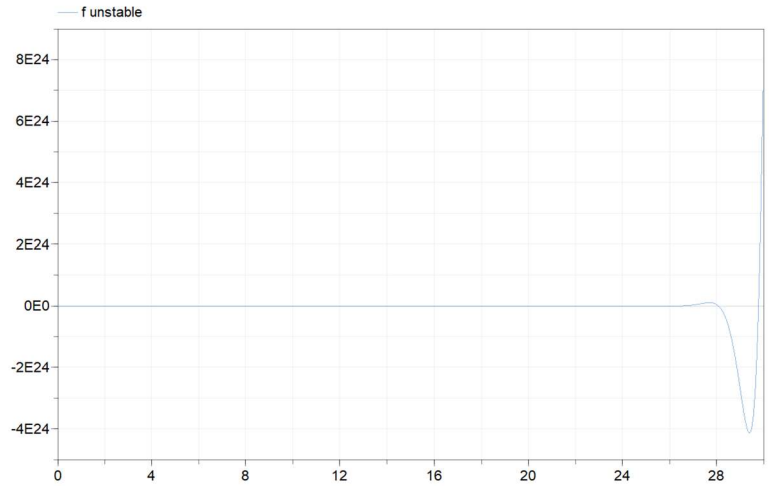

Figure 7-10 Frequency[p.u.] in time[s] in unstable case

7.1.2 Gain regulator nonlinear model

It is more complex to do stability analysis in case of nonlinear models, and the results would strongly depend on the initial point. Therefore, the behavior of the nonlinear model (Figure 3-4) of Susqueda power plant has been studied in the frequency control loop of Figure 7-1 using the same values of permanent droop obtained from the linear model in section 7.1.1..

Figures 7-11 and 7-12 show the time response of the mechanical power $\bar{P}_{mec}$ for respectively stable and unstable cases after a step variation in frequency set point of 0.01 p.u. at time 1 second from steady state value of 1 p.u..

The permanent droops b_p of 1.3809 p.u., 0.1395 p.u. and 0.2 p.u. identify stable cases also with nonlinear model of the penstock.

b_p equal to 0.04 p.u. still determines an unstable case: the value of mechanical power diverges and does it periodically because the non-linear solver of Dymola attempt to handle the problem.

In the nonlinear model, the value of b_p equal to 0.1395 p.u. determines an underdamped case and not undamped, as it was expected from the linear case.

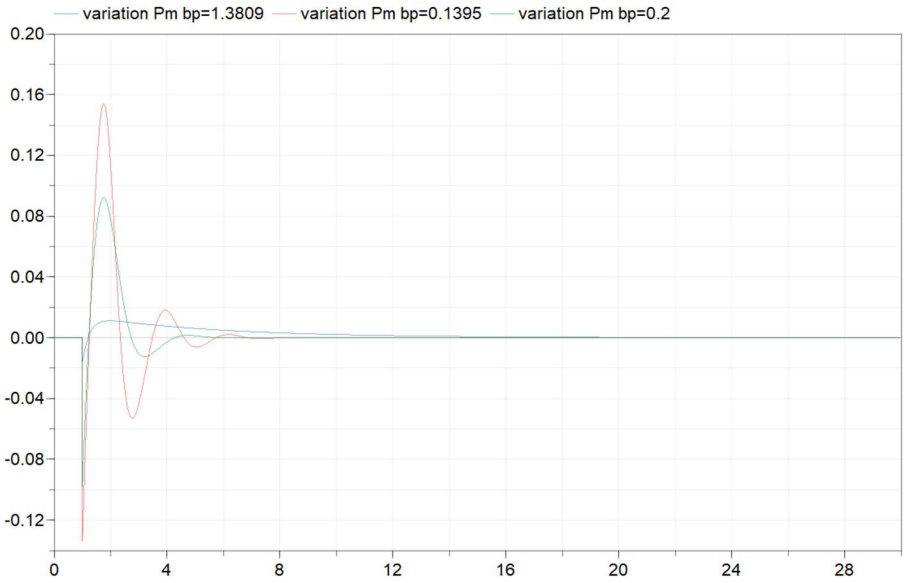

Figure 7-11 Mechanical power[p.u.] in time[s] for stable cases of gain regulator in nonlinear model

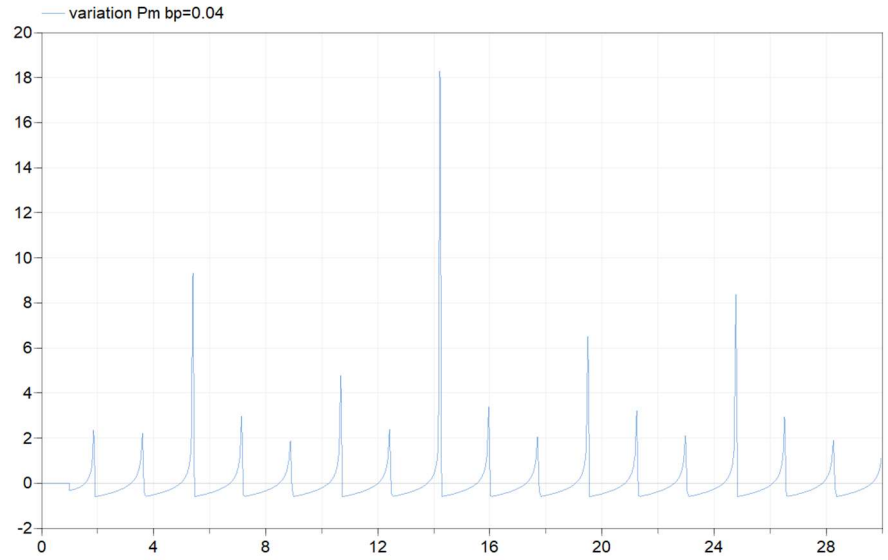

Figure 7-12 Mechanical power[p.u.] in time[s] for unstable of gain regulator in nonlinear model

7.1.3 The effect of T_w and T_a in regulation

The effect of water starting time T_w has been studied in three cases of linear model representing the Susqueda power plant. The speed regulator is a gain of value 0.884, that has been proved critically damped in section 7.1.1..

Table 7-2 Cases with different T_w

	Case 1	Case 2	Case 3
$T_w[s]$	0.83	2.76	5.52
$T_a[s]$	6	6	6

Increasing the water starting time, the delayed flow has more effects on hydraulic turbine and enhances the oscillations of the mechanical power (Figure 7-13) and of the frequency of the system (Figure 7-14). [14]

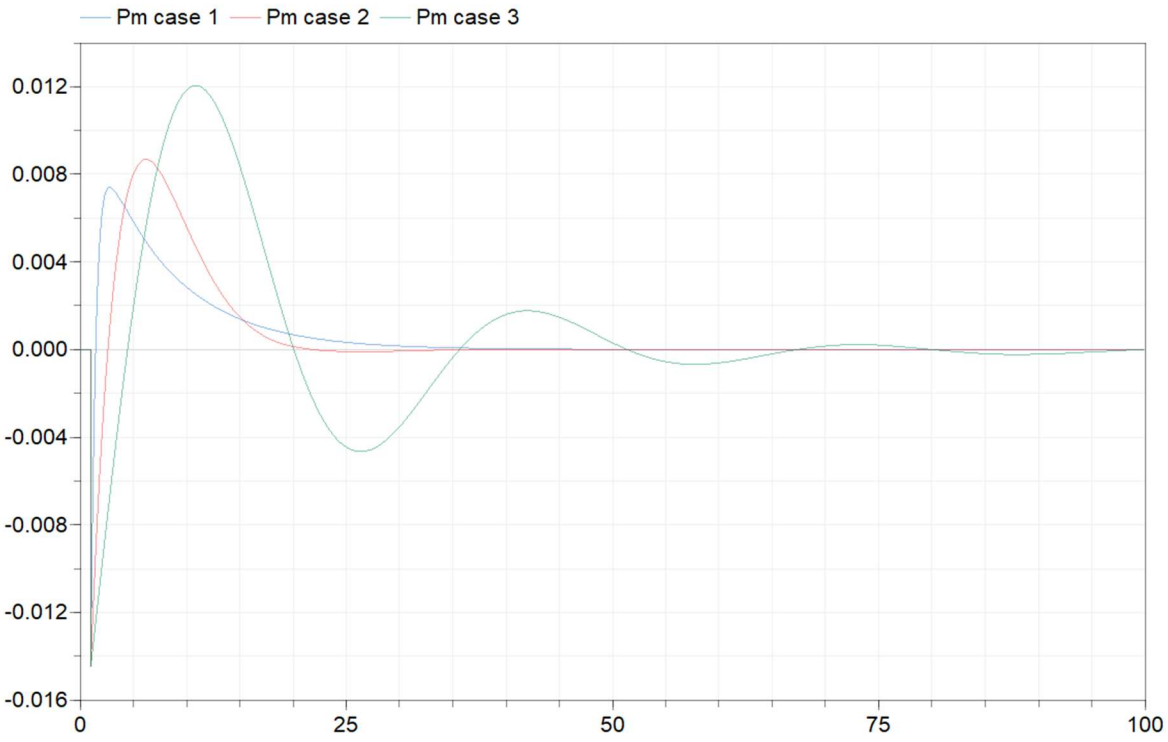

Figure 7-13 Oscillation of mechanical power[p.u.] in time[s] for three cases

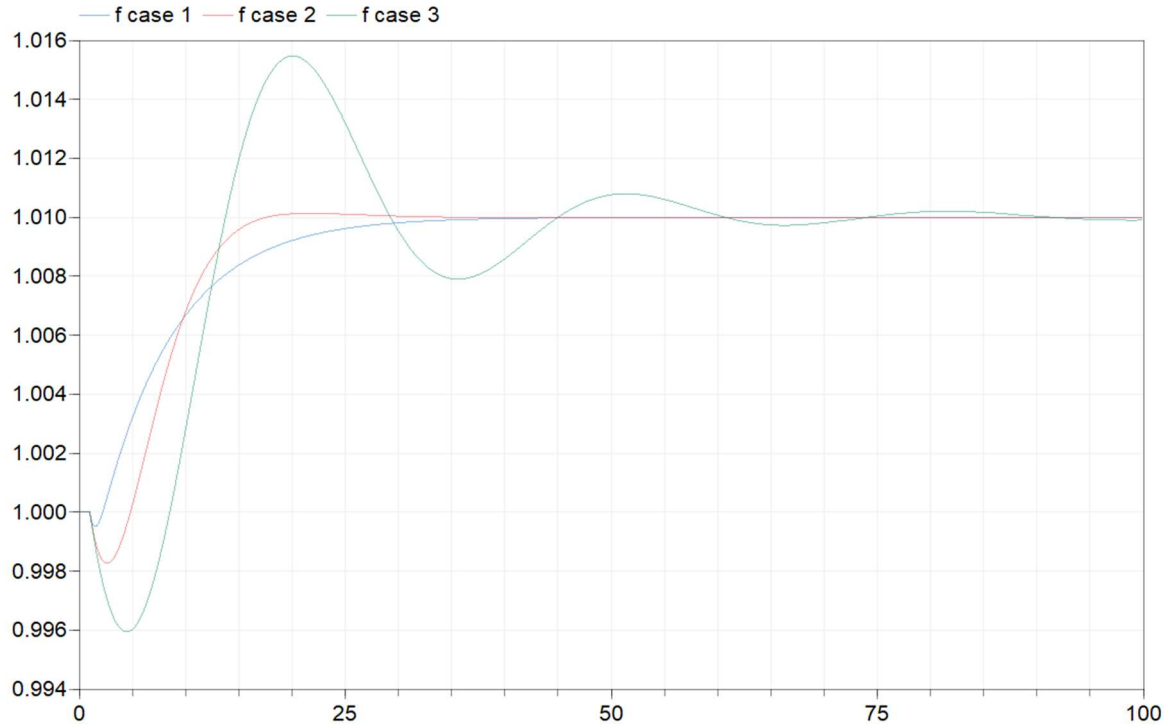

Figure 7-14 Frequency[p.u.] in time[s] of the system for the three cases

The oscillations due to T_w can be reduced acting on the mechanical starting time T_a.Three cases are studied with different values of T_a described in Table 7-3.

Table 7-3 Cases with different T_a

	Case 1	Case 2	Case 3
$T_w[s]$	0.83	0.83	0.83
$T_a[s]$	6	10	15

Increasing the value of T_a, the response in time of mechanical power $\bar{P}_m$ (Figure 7-15) and of the frequency of the system $\bar{f}$ (Figure 7-16) reduces deviation, but the time to reach the steady state increases. [14]

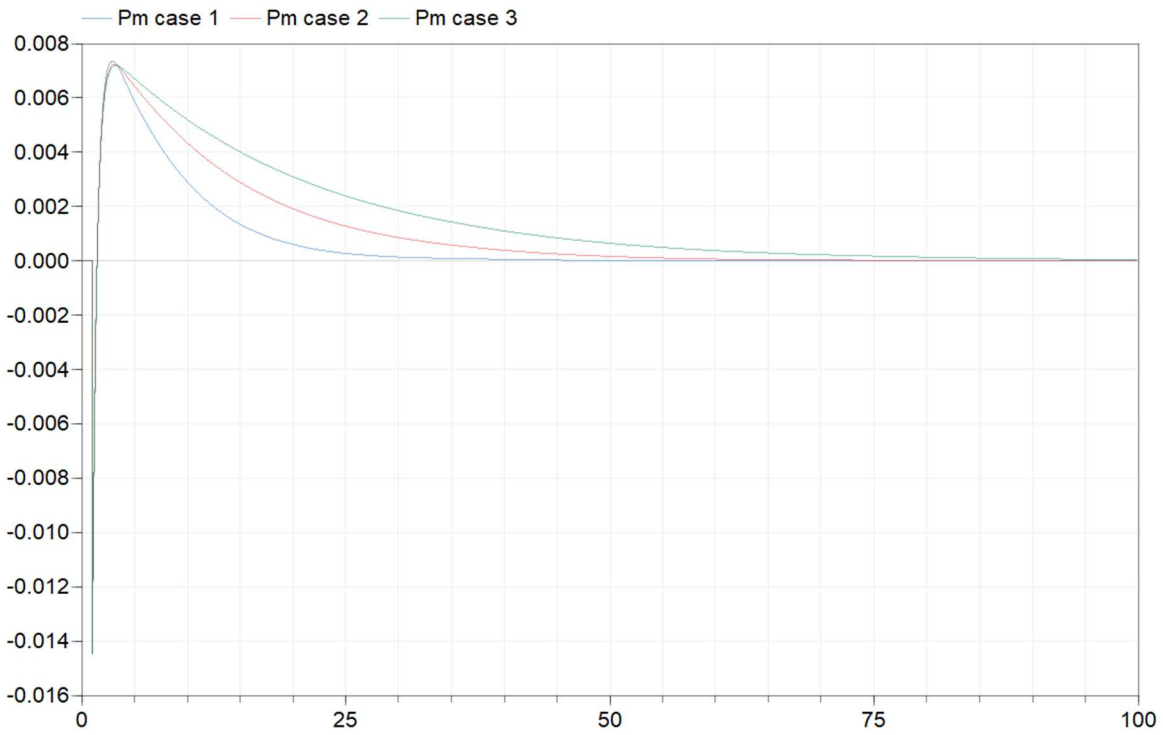

Figure 7-15 Mechanical power[p.u.] in time[s] for the three cases

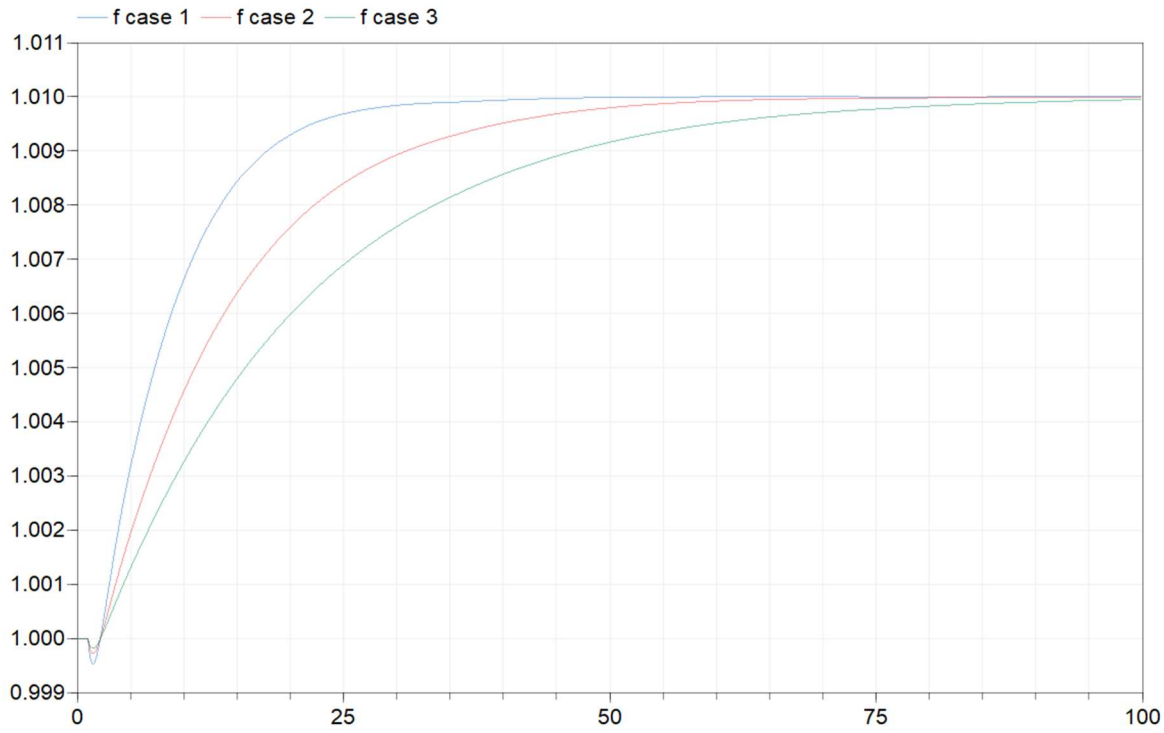

Figure 7-16 Frequency of the system[p.u.] in time[s] for the three cases

7.2 Variation of power load in frequency control

In this section, the Dymola models of frequency regulation have been realized with the Susqueda hydropower that oversees the variation of load power P_e inside the electrical grid (Figure 7-17). The analysis has been realized adding progressively more complex element in the adduction system and turbine block.

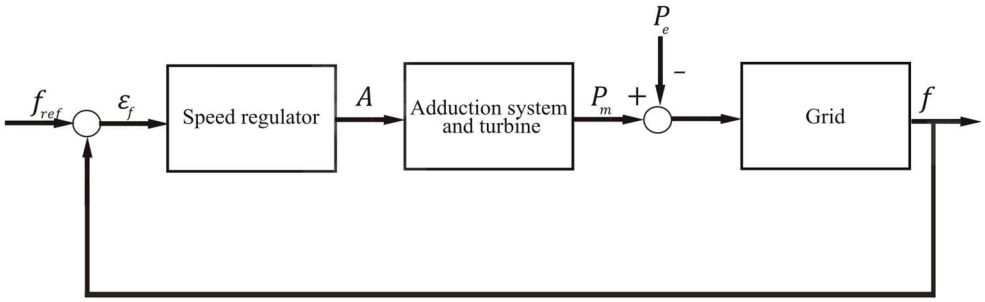

Figure 7-17 Control loop of frequency with grid

The reference grid is the one in the Italian blackout of 2003.The mechanical starting time T_a of the grid is computed as weighted average of mechanical starting time T_{ai} of the power plants-participating to regulation- with their rated power P_i as weight. At the time before the blackout, there were 1400 MW of hydroelectric powerplant and 19000 MW of thermal power plant; the standard values of T_a are 6 s for hydro unit and 10 s for thermal power plant. [15]

$$T_a = \frac{\sum P_i T_{ai}}{P_{tot}} = \frac{6\ s \cdot 1400MW + 10s \cdot 19000MW}{20400MW} = 9.72\ s \tag{7.7}$$

It has been hypothesized that the power plant of the case study represents 85 MW of 1400 MW of hydroelectric power plant.

The effects of the load regulating energy are assumed negligible; hence the grid block is represented by the transfer function:

$$G_{grid}(s) = \frac{1}{T_a s} = \frac{1}{9.72s} \tag{7.8}$$

7.2.1 Linear model of hydro unit in frequency regulation

This subsection focuses on the frequency regulation for linear model of hydroelectric power plant. The speed regulator is a gain equal to the reverse of the permanent droop of 0.20 p.u., which has determined an underdamped case in the analysis of subsection 7.1.1..

The frequency variation f and mechanical power $\bar{P}_{mec}$ have been analyzed firstly without the dynamics of penstocks: the transfer function of adduction system G_a has been assumed equal to 1.

The power load variation $\bar{P}_e$ is a step from 0 to 0.01 p.u. at 1 second, the time response of the frequency in Figure 7-18 shows that f decreases until the minimum value of 49.90 Hz (0.998 p.u.)-as expected from the chosen droop:

$$b_p = \frac{\Delta\bar{\mathrm{f}}}{\Delta\bar{P}} \rightarrow \Delta\bar{\mathrm{f}} = b_p \cdot \Delta\bar{P} = 2 \cdot 10^{-3}\,\mathrm{p.u.} \tag{7.9}$$

So

$$\bar{f} = 1\ \mathrm{p.u.} - \Delta\bar{\mathrm{f}} = 0.998\ \mathrm{p.u.} \tag{7.10}$$

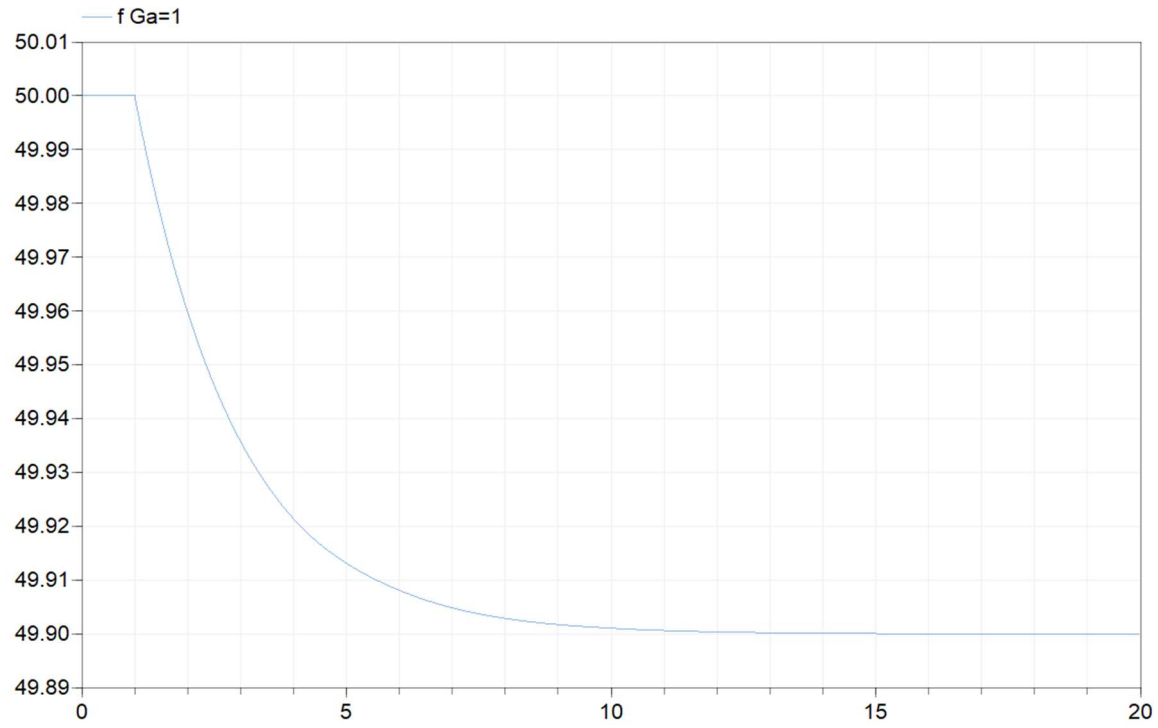

Figure 7-18 Frequency variation [p.u.] in time [s] in the case neglecting adduction system

Figure 7-19 shows the time response of mechanical power $\bar{P}_{mec}$: the variation of $\bar{P}_{mec}$ starts from 0 p.u., when there is no need to increase the power production because the balance of power is null; then, after the variation of power load $\bar{P}_e$ and the resulting negative accelerating torque, the mechanical power increases until reaches the value of $\bar{P}_e$ 0.01 p.u..

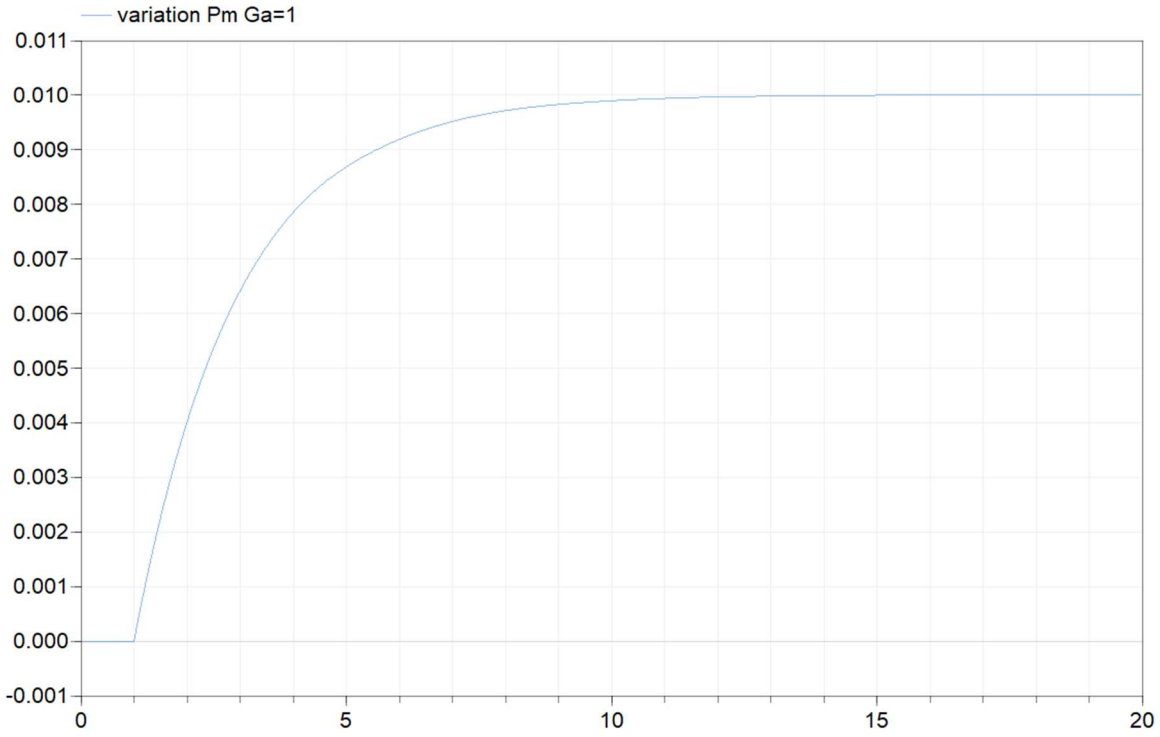

Figure 7-19 Mechanical power variation[p.u.] in time [s] in case of $G_a = 1$

The next step is to analyze the influence of linear adduction system in the frequency control without the effects of surge tank and propagation of pressure waves. The adduction transfer function for linear model is (6.2).

Figures 7-20 and 7-21 show oscillations respectively in mechanical power $\bar{P}_{mec}$ and frequency f due to the dynamics of inelastic penstock, represented by the water starting time T_w. It is worth to notice that $\bar{P}_{mec}$ has at first a negative variation due to water inertia and that the steady state values of f and $\bar{P}_{mec}$ are the same as the previous case.

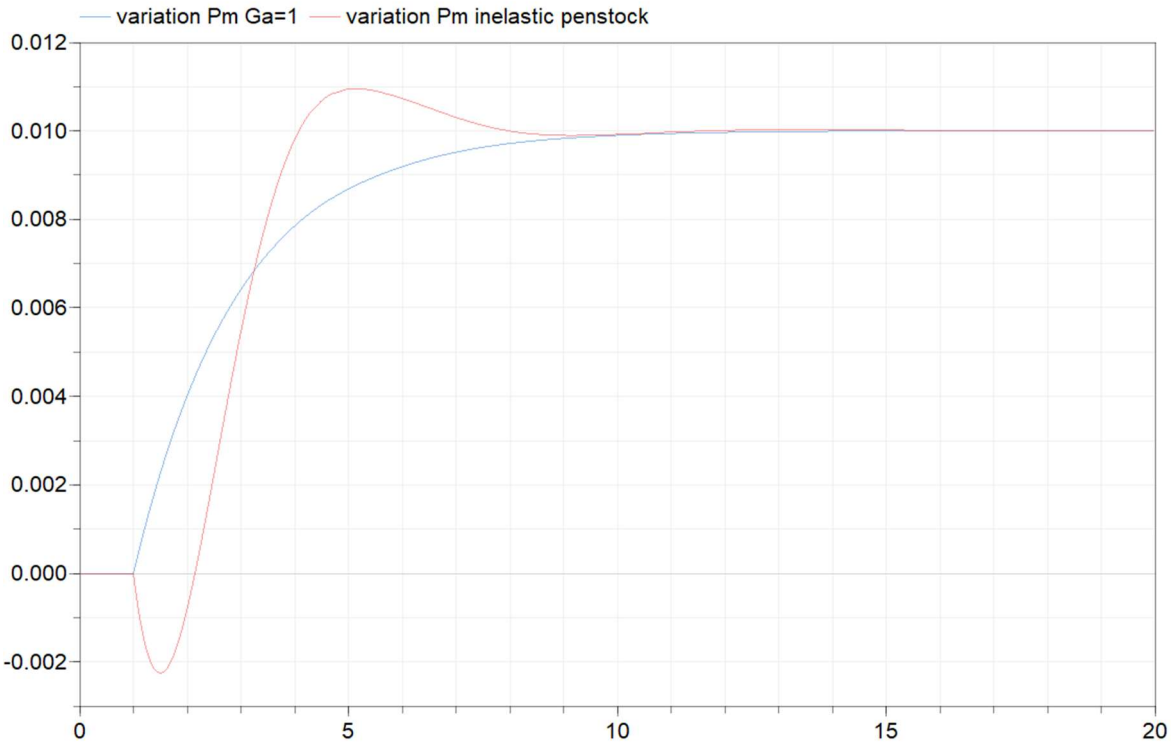

Figure 7-20 Mechanical power variation [p.u.] in time [s] in case of linear adduction with inelastic penstock

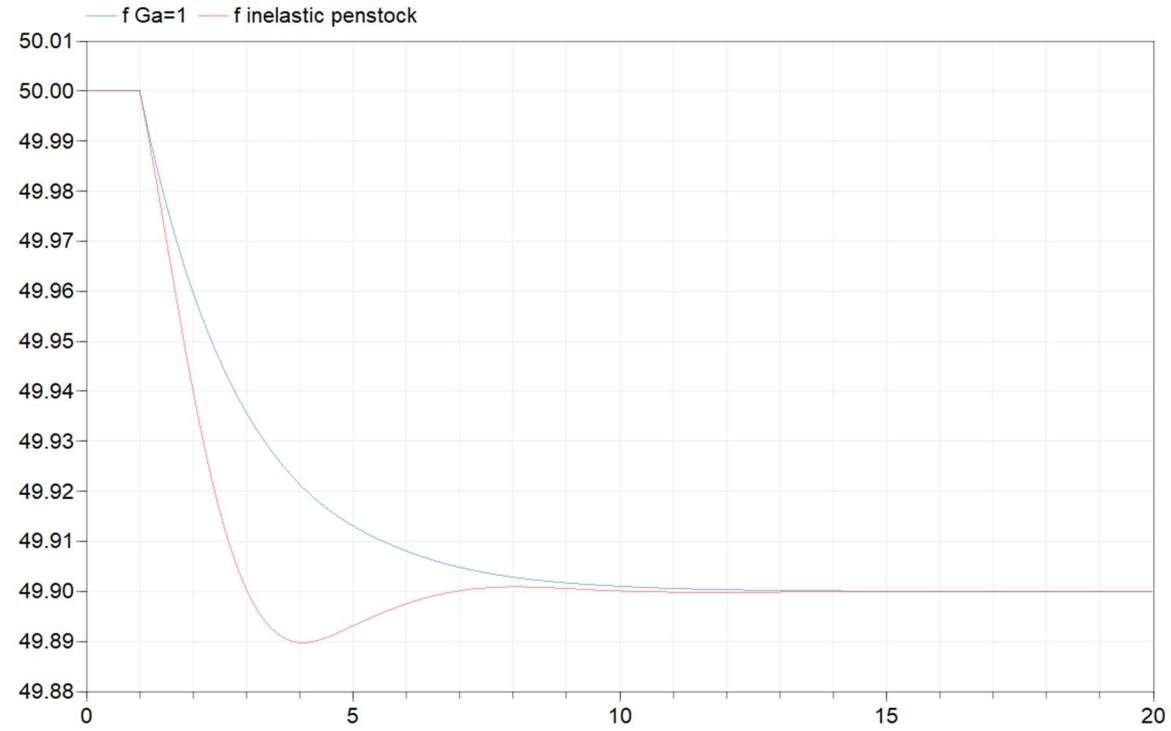

Figure 7-21Frequency[Hz] in time [s] in case of linear adduction with inelastic penstock

The propagation of elastic waves in the penstock has been approximated to lumped parameter with grade n=1 and n=2, and the time response of $\bar{P}_{mec}$ and of f is represented in

Figure 7-22 and 7-23. It is worth to note that the reached oscillations are higher, and that the approximation with grade n=1 and n=2 are equivalent: this hints that the approximation of hyperbolic tangent is good enough.

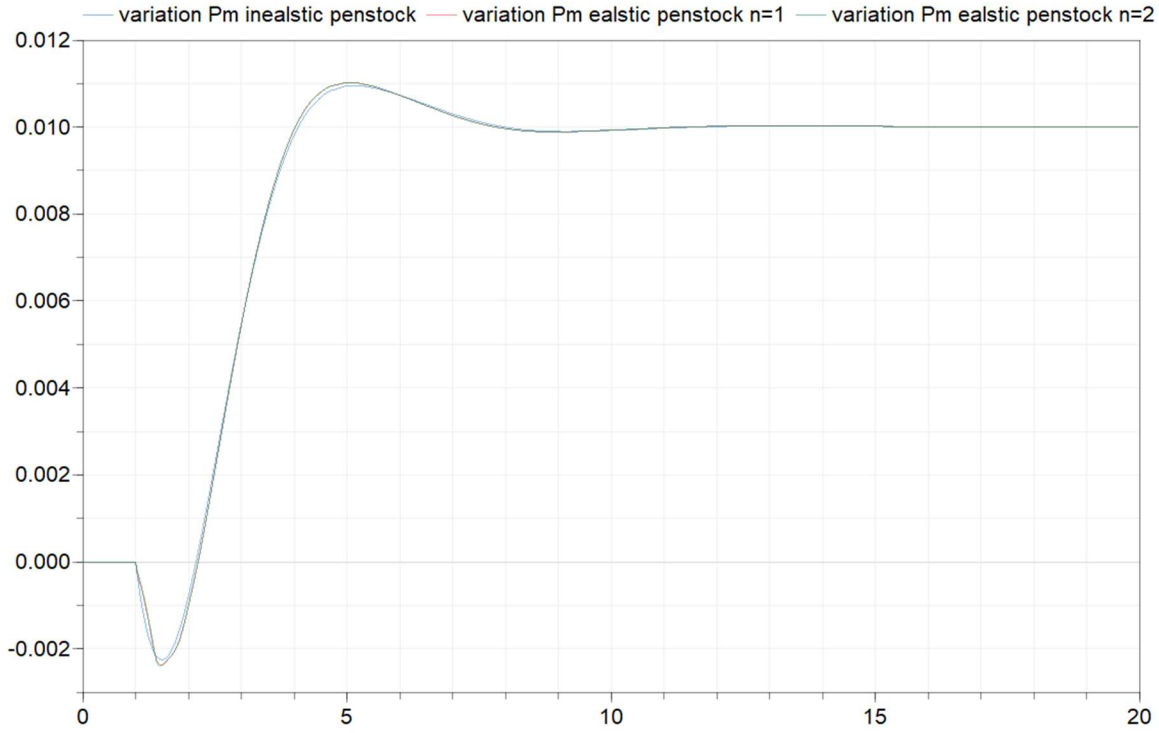

Figure 7-22 Mechanical power[p.u.] in time [s] in case of linear adduction with elastic penstock

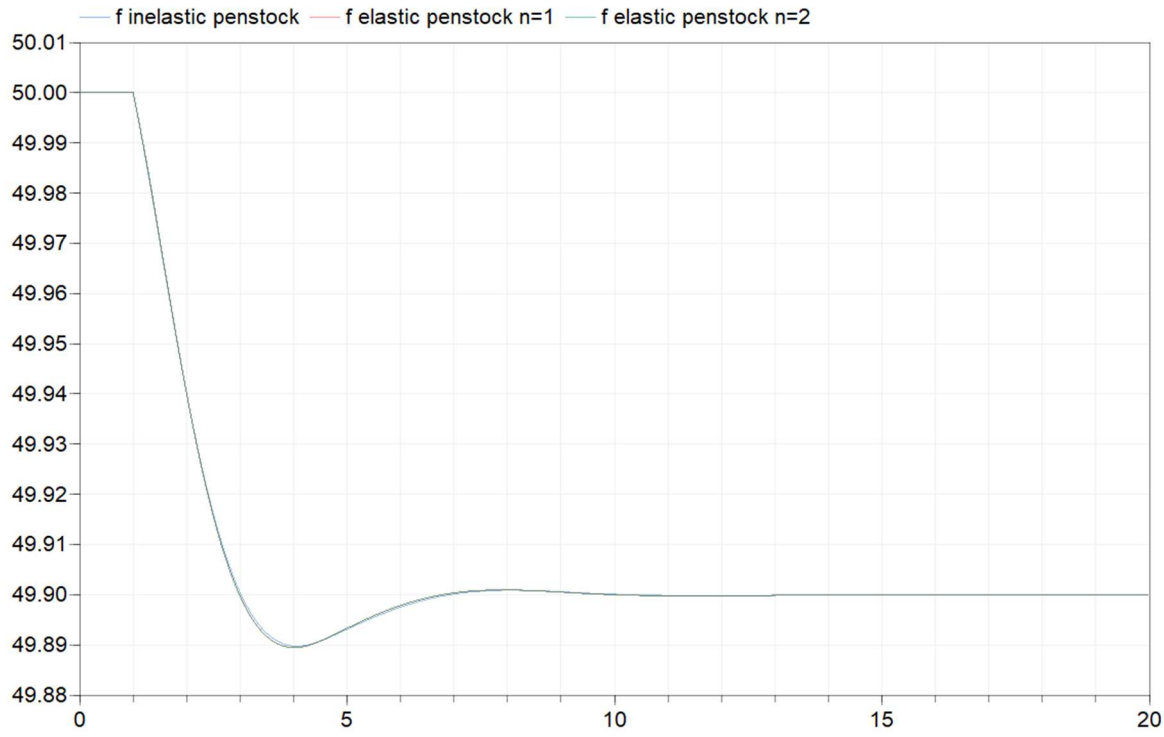

Figure 7-23 Frequency[Hz] in time[s] in case of linear adduction with elastic penstock

Figures 7-24 and 7-25 show the mechanical power $\bar{P}_{mec}$ and frequency f variation with surge tank effect. $\bar{P}_{mec}$ oscillates with surge tank period T_S around the steady state value of 1.01 p.u., and so does the frequency; but the oscillation increases instead of damping, so the system is unstable as mentioned in section 2.2.

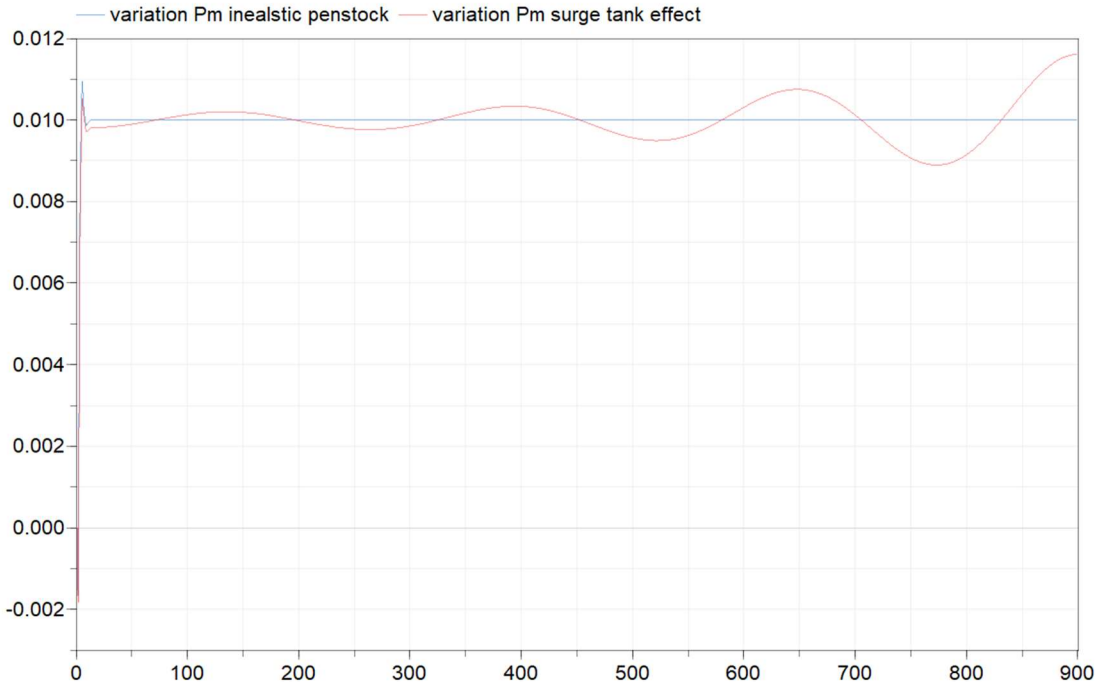

Figure 7-24 Mechanical power[p.u.] in time[s] in case of linear adduction with surge tank effect

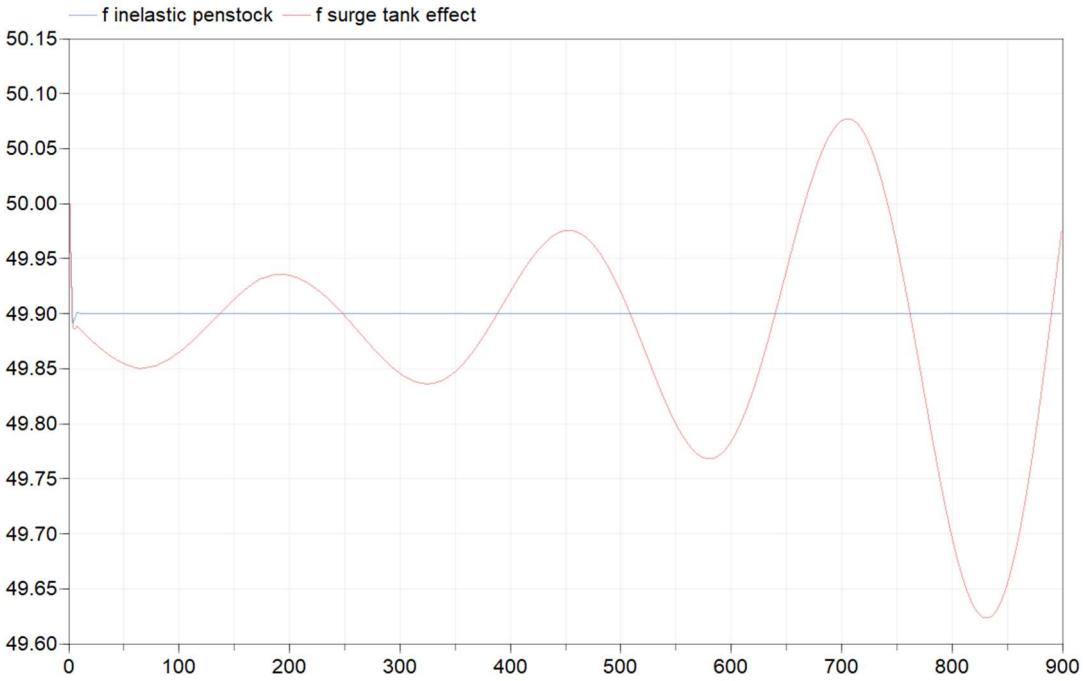

Figure 7-25 Frequency[Hz] in time[s] in case of linear adduction with surge tank effect

7.2.2 Nonlinear model frequency regulation

In this subsection, the frequency regulation has been studied adopting the nonlinear adduction scheme without surge tank effect analyzed in section 6.3. Like the previous subsection, the power load $\bar{P}_e$ is the disturbance with step variation of 0.01 p.u. at time 1 second.

Figures 7-26 and 7-27 show the time response of mechanical power $\bar{P}_{mec}$ and gate $\bar{g}$: the initial value of $\bar{P}_{mec}$ is 0.606 p.u. with the valve opened at 0.5 p.u., the final steady state is 0.616 p.u. with gate 0.506 p.u. equal to the value of power load $\bar{P}_e$.

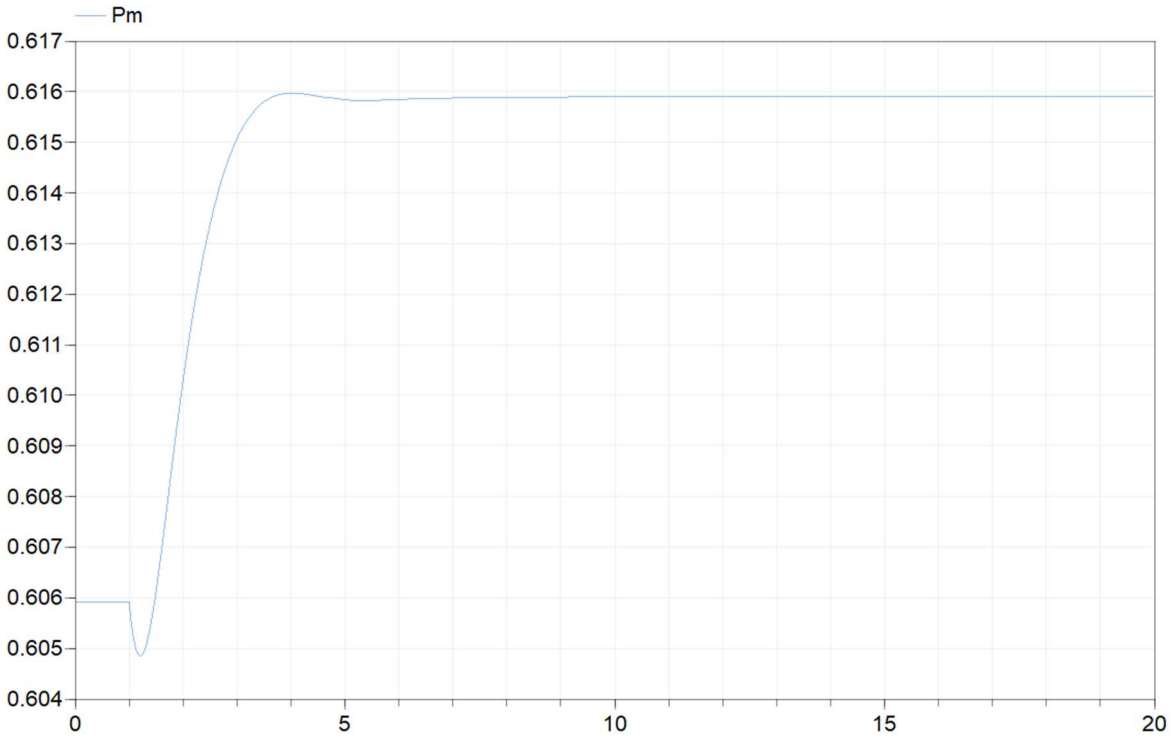

Figure 7-26 Mechanical power[p.u.] in time[s] in case nonlinear adduction

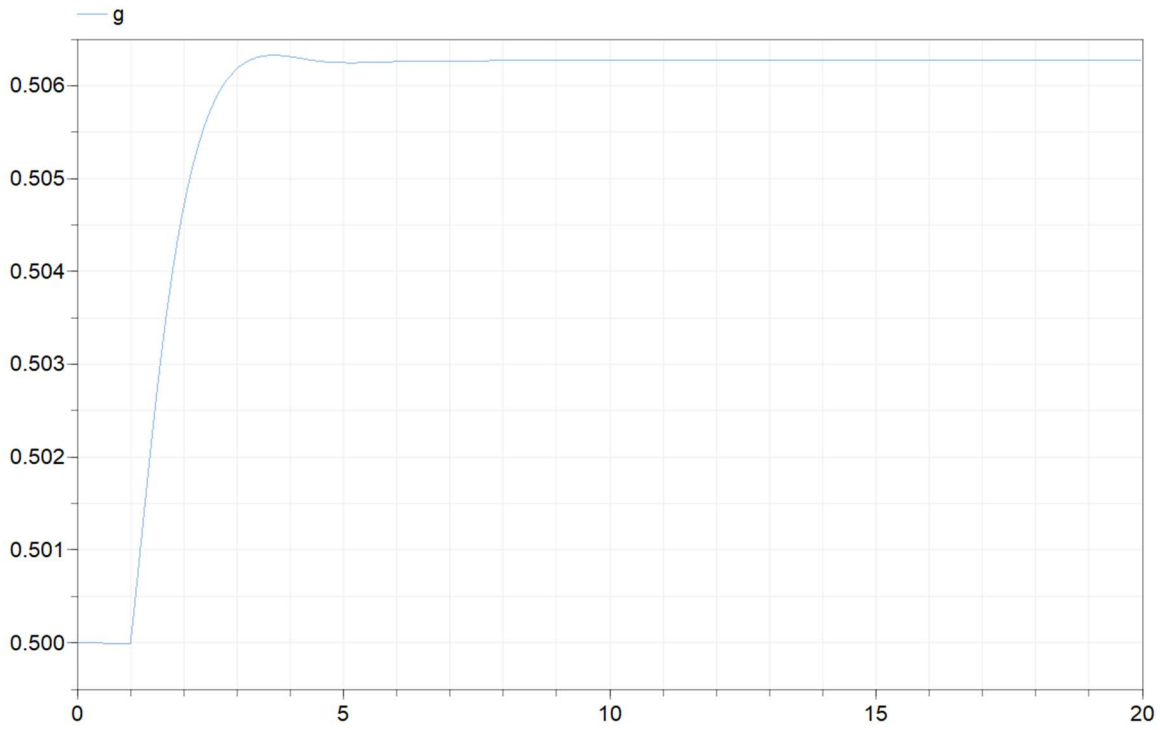

Figure 7-27 Gate opening[p.u.] in time[s] in case nonlinear adduction

The time response of the frequency is shown in Figure 7-28 and the steady state value is not 49.90 Hz but 49.937 Hz, hence nonlinearity does not satisfy the value expected for the frequency from droop computation in (7.10).

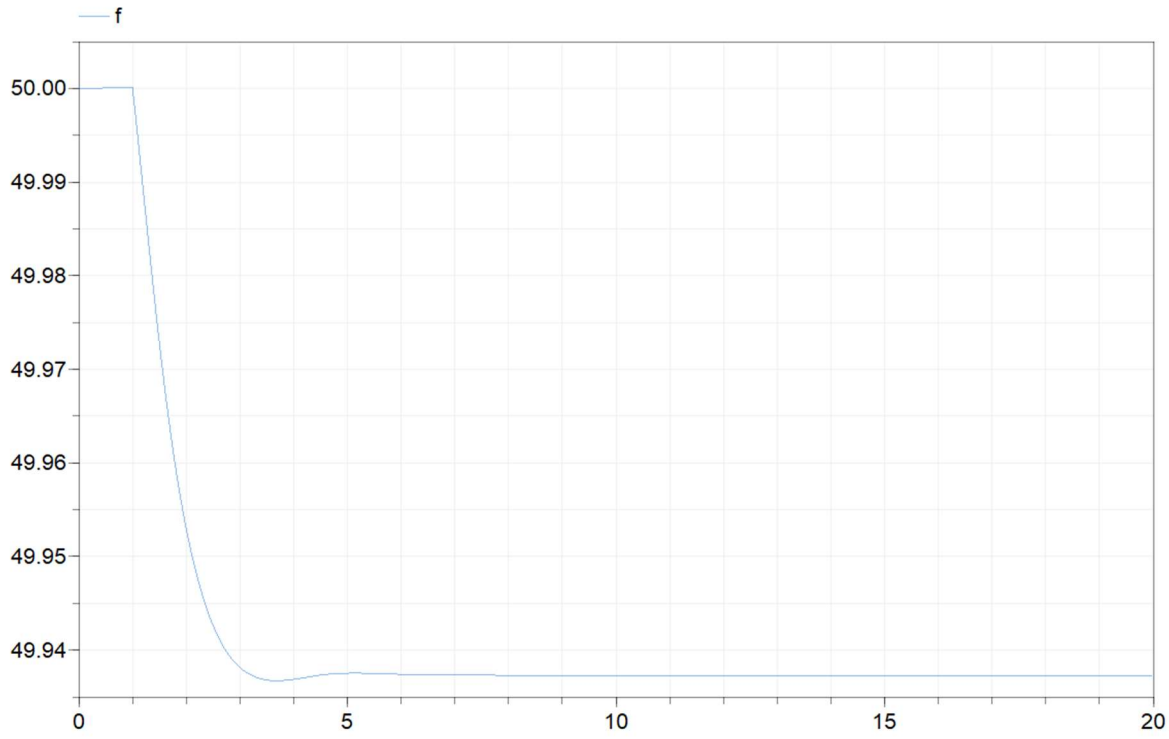

Figure 7-28 Frequency[Hz] in time[s] in case nonlinear adduction

Figure 7-29 is the time response of mechanical power $\bar{P}_{mec}$ with adduction system constituted by elastic penstock, the approximation of hyperbolic tangent has been realized with lumped parameter n=1 and n=2. It is worth to notice that elastic propagation in the penstock allows, in this case, to reach a minimum value of $\bar{P}_{mec}$ lower in amplitude and delayed.

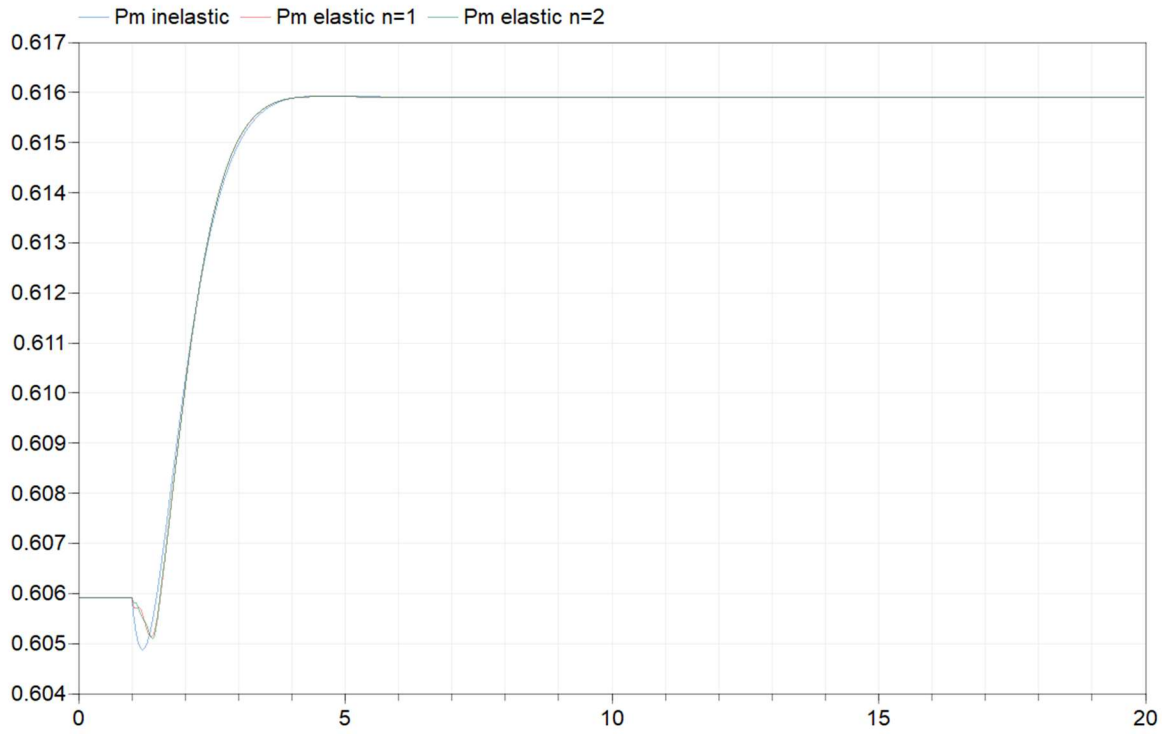

Figure 7-29 Mechanical power[p.u.] in time[s] in case of nonlinear adduction with elastic penstock

The scheme with surge tank effect of section 6.4, assuming inelastic water column in the penstock, has the same results in mechanical power $\bar{P}_{mec}$ and frequency f for the first few seconds of the nonlinear model without surge tank effect as shown by Figures 7-30 and 7-31.

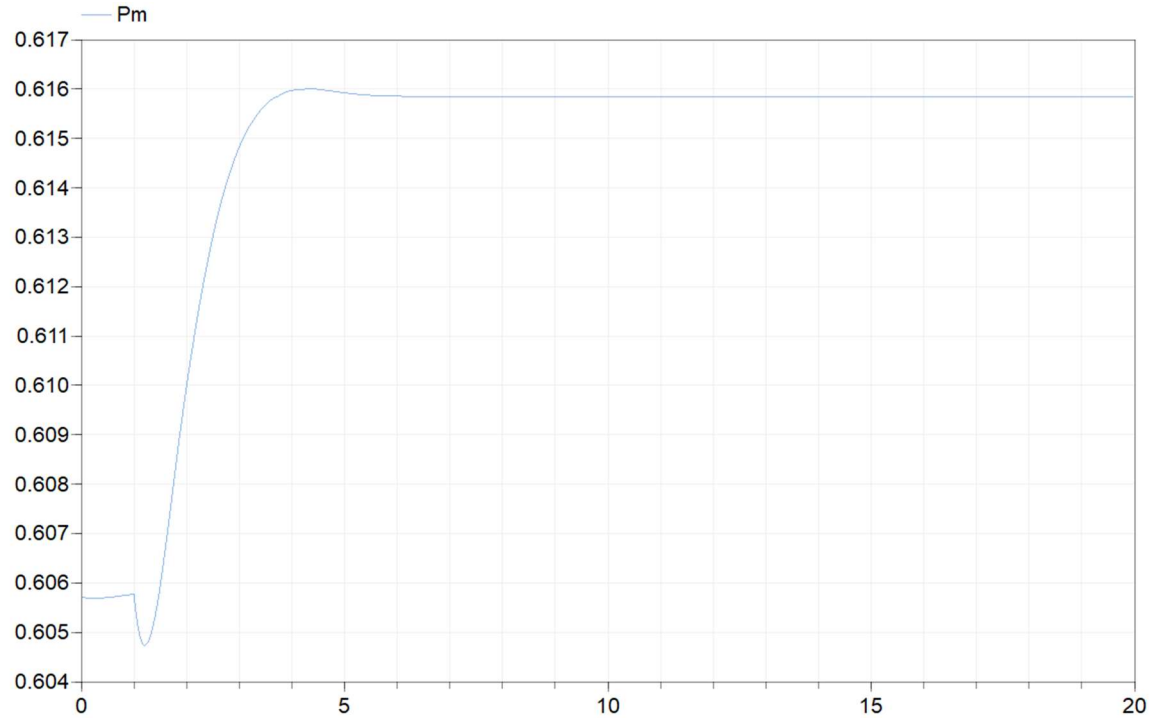

Figure 7-30 Mechanical power[p.u.] in time[s] in case of nonlinear adduction with surge tank effect

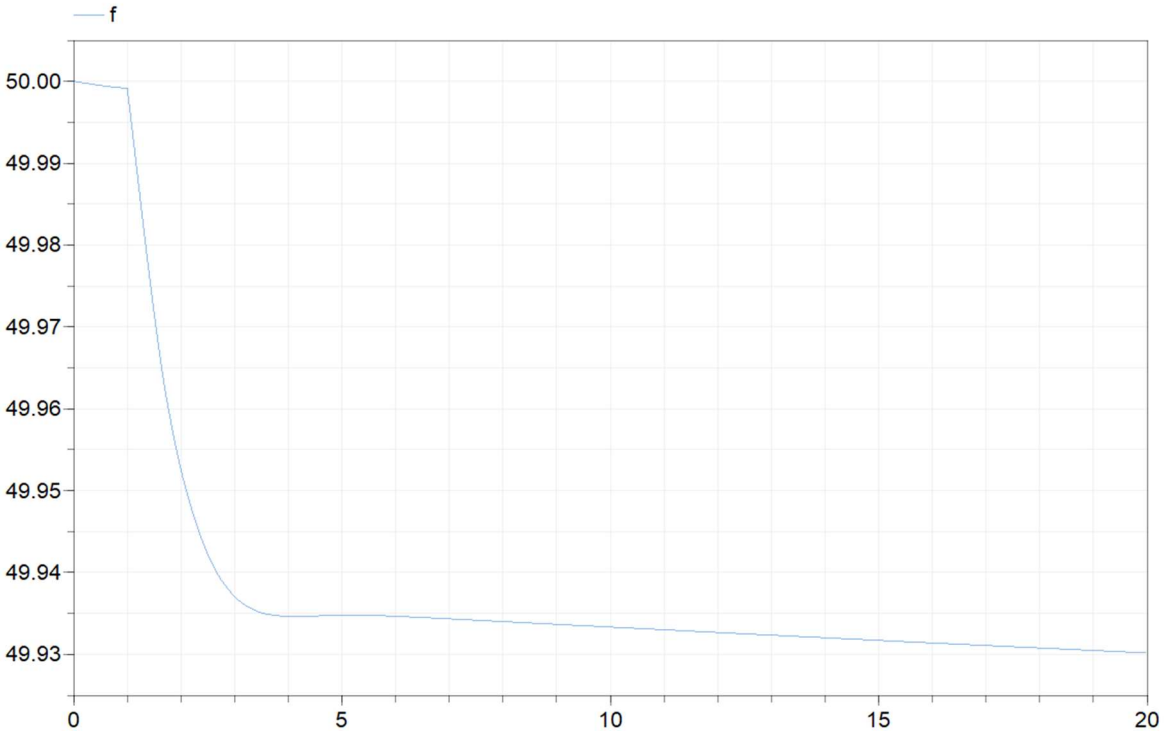

Figure 7-31 Frequency[Hz] in time[s] in case of nonlinear adduction with surge tank effect

Figures 7-32 and 7-33 show that the nonlinear model with surge tank has oscillation in $\bar{P}_{mec}$ and f in long term with period T_s.

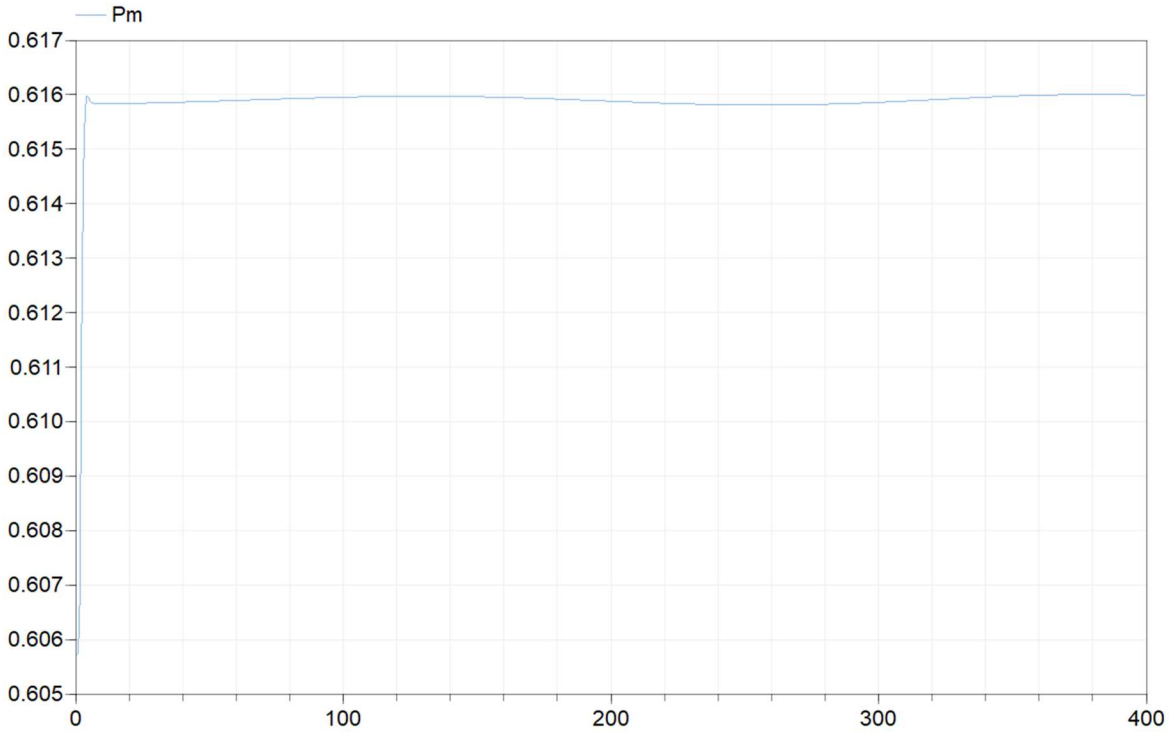

Figure 7-32 Mechanical power oscillations[p.u.] in time[s] in case of nonlinear adduction with surge tank effect

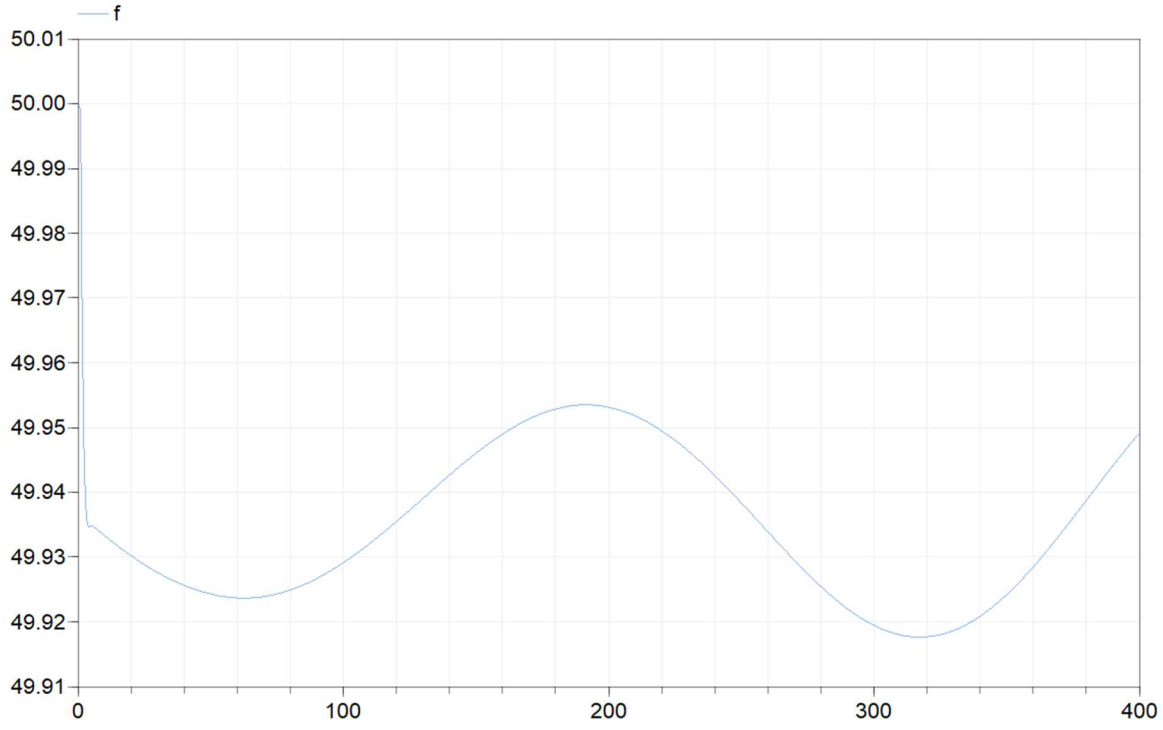

Figure 7-33 Frequency oscillations[Hz] in time[s] in case of nonlinear adduction with surge tank effect

7.3 Frequency regulation with nuclear reactor in the grid

In this section, the primary frequency regulation realized by the hydroelectric powerplant has been studied in presence of baseload nuclear power in the Italian grid-represented by block (7.8).

The hydroelectric power plant is the nonlinear model of Susqueda power plant with surge tank effect and elastic penstock approximated through lumped parameter n=1. The hydro unit starts at steady state with gate opened at 50%, so mechanical power is 0.606 p.u., as reported in Table 6-2, which is equivalent to 51.5 MW.

The speed governor of hydro unit is a gain equal to the reverse of the permanent droop of 0.20 p.u., as in section 7.2.

The nuclear power plant is composed of IRIS, which has been modelled in the thesis project group of Nuclear Section of DENG in Dymola (Figure 7-34). IRIS is a SMR that was developed by an international consortium, led by Westinghouse, involving so many companies, research centers and universities, including Politecnico di Milano. IRIS is a light water reactor, PWR type, with a thermal power output of 1 GW and an electric output of 335 MW. The fuel enrichment is around 4.95 % and it is usually UO2 even if it can be loaded also using MOX. The reactor is designed to have a half core refueling every three years and the planned life is 60 years. [16]

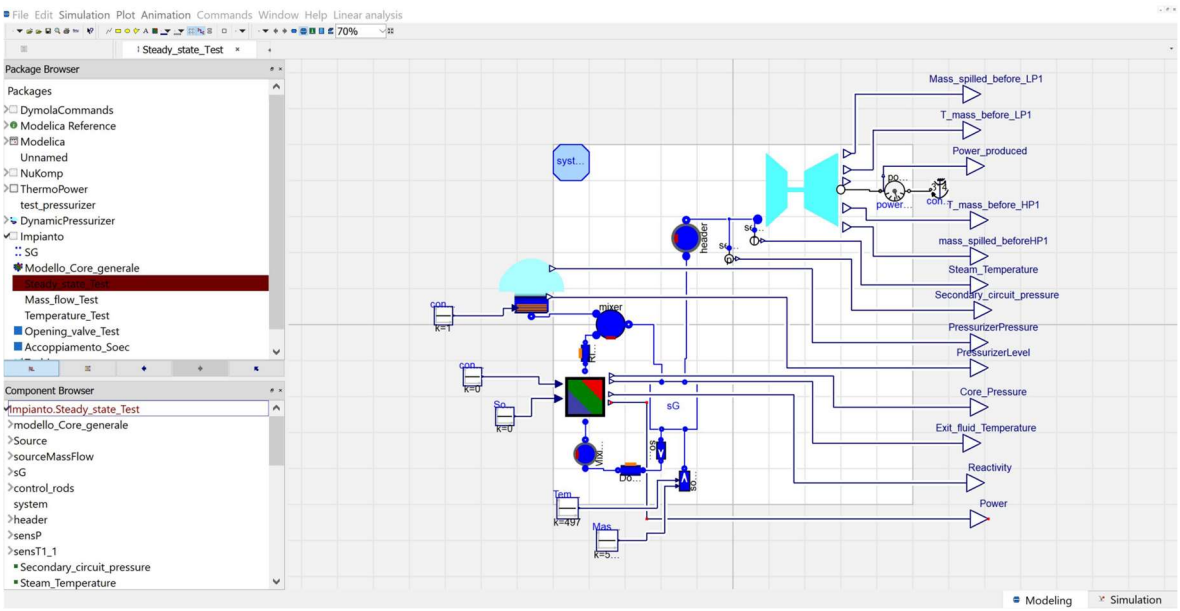

Figure 7-34 Dymola model of IRIS [16]

The electrical power time response for the Dymola model of IRIS is shown in Figure 7-35 and IRIS is producing 335 MW of electrical power.

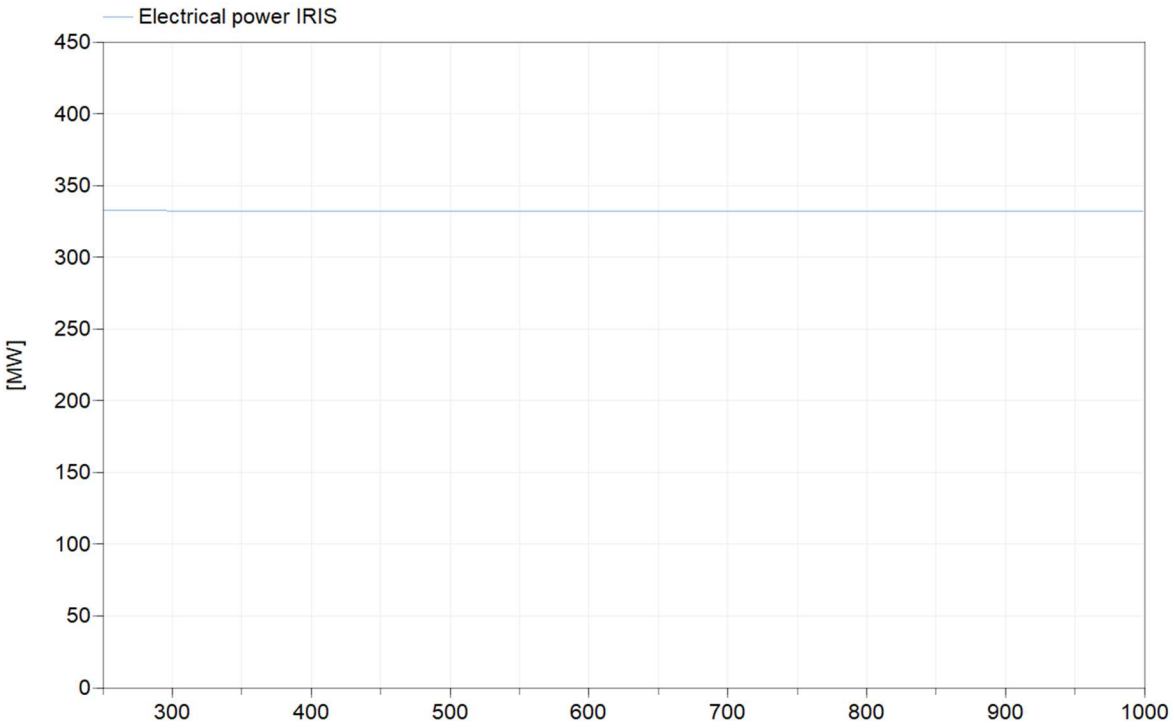

Figure 7-35 Power[MW] in time[s] in IRIS

The frequency regulation has been studied for variation of power load of 1 MW at time 300s in the grid as section 7.2. The mechanical power $\bar{P}_{mec}$ (Figure 7-36) oscillates before and after the power load variation for surge tank effect; and after 300 s, $\bar{P}_{mec}$ increases its value to 0.6175 p.u., equivalent to 52.5 MW, with a settling time of 25 s.

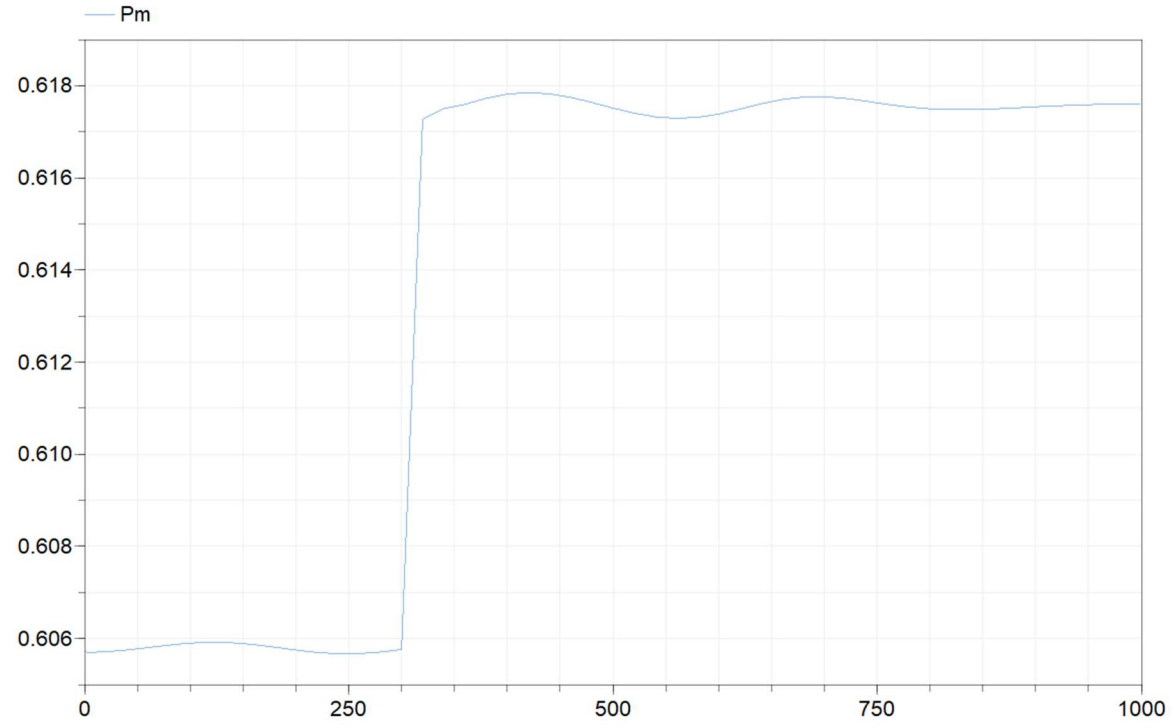

Figure 7-36 Mechanical power[p.u.] in time[s] of hydro unit

The frequency of the grid (Figure 7-37) is oscillating around 50 Hz before the disturbance, then decreases and oscillates around 49.925 Hz.

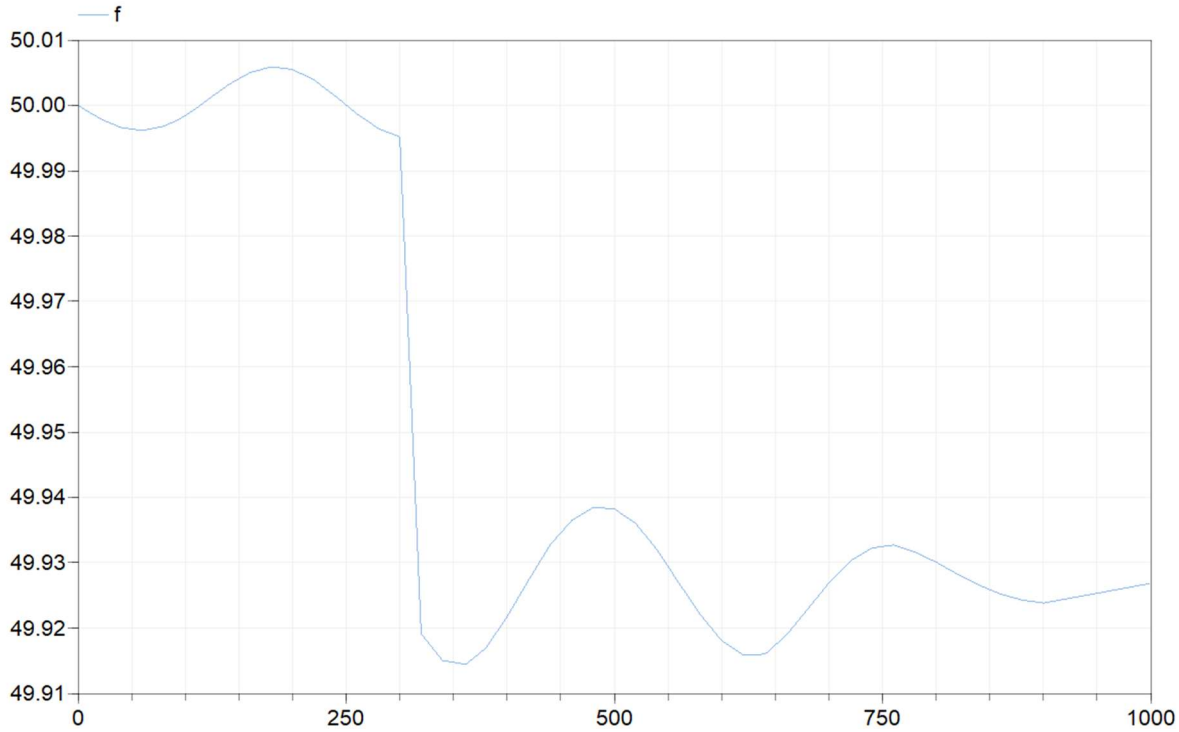

Figure 7-37 Frequency of the grid [Hz] in time[s]

Chapter 8
Conclusions

The aim of this thesis work is the modelling of the hydroelectric power plant dynamics inside frequency regulation and is part of thesis group project of Nuclear Section of DENG on modelling in Dymola. These models have been realized taking singularly the dynamics of adduction system, speed regulator and grid, and are all consistent with a progressive increase of accuracy.

The importance of the dynamics inside the penstock has been explored:

- The mechanical power has initial negative behavior at the opening of the gate due to water inertia;

- For very long penstocks, the wave travel time of the water column becomes significant, and the reflected pressure waves in the water column cause the preceding treatment of water start time to be no longer valid.

The circuit of penstock-surge tank has been analyzed: the mechanical power is affected by long term oscillations because the water level in the surge tank begins to oscillate with the natural period following a change in the turbine flow.

The nonlinear models of IEEE have been developed to allow to deal with large variation in frequency and power output. Furthermore, these models are more explicit in the dynamics of the penstock, tunnel, and surge tank.

Dymola models of regulation have been implemented starting from stability analysis, and the time responses of the mechanical power and of the grid frequency highlight the importance of the adduction system of hydroelectric power plant inside the frequency control loop.

The thesis work has shown how these models of regulation are interconnectable with other power plant models on Dymola, in fact the frequency regulation of hydro power plant has been realized with presence of baseload power of IRIS in the grid.

The models realized are the first of thesis group project on hydropower: there is more focus on the adduction system of the plant rather than on regulation. Hence, there are future

developments to increase the accuracy of regulation models; some suggestions on what to work on can be:

- Implementing Dymola models of hydroelectric power plant using speed regulator with transient droop;
- Taking into consideration the dependency of the power load on the frequency;
- Realizing Dymola models with also secondary regulation.

Appendix

[1]

Transfer function of adduction system for linear model elastic penstock with lumped parameter approximation n=1:

N={[-5.6573]; [2.7022e+1];[-1.2864e+3];[1.5361e+3]}

D={[2.8286];[2.7022e+1];[6.4322e+2];[1.5361e+3]}

[2]

Transfer function of adduction system for linear model elastic penstock with lumped parameter approximation n=2:

N={[-4.2430];[3.6029e+1];[-4.8241e+3];[2.0482e+4];[-8.7759e+5];[1.0479e+6]}
D={[2.1215];[3.6029e+1];[2.4121e+3];[2.0482e+4];[4.3880e+5];[1.0479e+6]}

[3]

Transfer function of volumetric flow for linear model elastic penstock with lumped parameter approximation n=1:

N={[2.7022e+1];[0];[1.5361e+3]}
D={[2.8286];[2.7022e+1];[6.4322e+2];[1.5361e+3]}

[4]

Transfer function of available head for linear model elastic penstock with lumped parameter approximation n=1

N= {[-5.6573];[0];[-1.2864e+3];[0]}
D= {[2.8286];[2.7022e+1];[6.4322e+2];[1.5361e+3]}

[5]

Transfer function of adduction system for linear model elastic penstock with lumped parameter approximation n=1 and friction:

N= {[-1.4143e+1];[6.4345e+1];[-3.2161e+3];[3.6580e+3]}
D={[7.0716];[6.9158e+1];[1.6080e+3];[3.9316e+3]}

[6]

Transfer function linear model with surge tank elastic grade n=1:

N={[-3.8703e+1];[1.7609e+2];[-8.8019e+3];[1.0012e+4];[-6.6090e+1];[6.3977]}
D={[7.7405e+1];[1.8927e+2];[4.4010e+3];[1.0763e+4];[3.4786e+1];[6.8870]

Bibliography

[1] R. Marconato, Electric power systems vol.2 Steady-state behaviour controls, short circuits and protection systems, CEI, 2004.

[2] A. Berizzi e M. M., «Slides of "Regolazione della frequenza",notes of course “Modellistica delle macchine e degli impianti"».

[3] ENTSO-E, «UCTE OH –Policy 1: Load-Frequency Control and Performance,» 2009.

[4] Gatta, «La regolazione della velocità dei generatori sincroni e della frequenza,» in *Impianti elettrici*, Esculapio , 2014.

[5] Kundur, Power System Stability and Control, McGraw-Hill Education, 1994.

[6] IEEE, «IEEE Guide for the Application of Turbine Governing Systems for Hydroelectric Generating Units,» *IEEE Std 1207-2011 (Revision to IEEE Std 1207-2004) ,* pp. 1-139, 2011.

[7] M. H. Chaudhry, Applied Hydraulic Transients, Springer, 2013.

[8] Ó. D. Quiroga, «Modelling and nonlinear control of voltage frequency of hydroelectric power plants,» 2000.

[9] IEEE, «Dynamic Models for Turbine-Governors in Power System Studies,» 2013.

[10] IEEE, in *Working Group Prime Mover and Energy Supply ,"Hydraulic turbine and turbine control models for system dynamic studies"in IEEE Transactions on Power Systems*, Feb. 1992, pp. vol. 7, no. 1, pp. 167-179.

[11] Naghizadeh, S. Jazebi e B. Vahidi, «Modeling Hydro Power Plants and Tuning Hydro Governors as an Educational Guideline. International Review on Modelling and Simulations.,» 2012.

[12] Dynasim AB, «Dymola, Dynamic Modeling Laboratory. User's Manual,» 2004.

[13] Terna, «Partecipazione alla regolazione di frequenza,» 20-07-2008 .

[14] M. Giangi, «Master thesis "Dynamic Modelling of Virtual and Real Inertia Systems in Green Microgrids",» 2021.

[15] A. Berizzi, «seminar "Regolazione di frequenza" course of "Modellistica degli impianti elettrici"».

[16] P. Croce, «Master degree thesis "Preliminary simulations for nuclear power plant cogeneration",» 2020-2021.